



**FATIGUE EFFECTS OF LASER SHOCK
PEENING MINIMALLY DETECTABLE
PARTIAL-THROUGH THICKNESS SURFACE
CRACKS**

THESIS

David L. A. Eisensmith, Captain, USAF
AFIT-ENY-MS-17-M-259

**DEPARTMENT OF THE AIR FORCE
AIR UNIVERSITY**

AIR FORCE INSTITUTE OF TECHNOLOGY

Wright-Patterson Air Force Base, Ohio

DISTRIBUTION STATEMENT A
APPROVED FOR PUBLIC RELEASE; DISTRIBUTION UNLIMITED.

The views expressed in this document are those of the author and do not reflect the official policy or position of the United States Air Force, the United States Department of Defense or the United States Government. This material is declared a work of the U.S. Government and is not subject to copyright protection in the United States.

AFIT-ENY-MS-17-M-259

FATIGUE EFFECTS OF LASER SHOCK PEENING MINIMALLY
DETECTABLE PARTIAL-THROUGH THICKNESS SURFACE CRACKS

THESIS

Presented to the Faculty
Department of Aeronautical Engineering
Graduate School of Engineering and Management
Air Force Institute of Technology
Air University
Air Education and Training Command
in Partial Fulfillment of the Requirements for the
Degree of Master of Science in Aeronautical Engineering

David L. A. Eisensmith, B.S.M.E. & A.A.S.

Captain, USAF

March 2, 2017

DISTRIBUTION STATEMENT A
APPROVED FOR PUBLIC RELEASE; DISTRIBUTION UNLIMITED.

AFIT-ENY-MS-17-M-259

FATIGUE EFFECTS OF LASER SHOCK PEENING MINIMALLY
DETECTABLE PARTIAL-THROUGH THICKNESS SURFACE CRACKS

David L. A. Eisensmith, B.S.M.E. & A.A.S.
Captain, USAF

Committee Membership:

Anthony N. Palazotto, PhD
Chair

Kristina M. Langer, PhD
Member

Thomas J. Spradlin, PhD
Member

Stephano Coratella, PhD
Member

Abstract

Laser Shock Peening (LSP) has evolved as a viable alternative to other surface treatments (shot peening, burnishing, etc.) which induce beneficial residual stress into structural components. Fatigue life improvements have been recognized by the aerospace industry. Aerospace engineers are inherently risk adverse due to component failures having potentially catastrophic consequences. With fatigue causing an estimated 55% of aircraft structural component failure, fatigue life benefits of LSP cannot be neglected. Aircraft service life extensions compound fatigue issue, especially for non-economically feasible replace components. In-service components may have surface flaws below current inspection limits. Aerospace engineers are concerned with LSP application over an existing crack causing unintended detrimental consequences.

To address this concern, two differing types of LSP (circular and square spot shapes) were applied over a partial-through thickness surface fatigue crack of 0.25" (6.35 mm), in 7075-T651 aluminum. The crack length is the minimal detection limit of surface scanning eddy current. Specimens were fatigued under constant amplitude cyclic loading. Baseline specimens fatigue limit was 49, 048 cycles. Peened specimens survived to run-out exhibiting no crack growth when examined with an optical microscope, utilizing marker banding techniques. The result is more than 2000% increase in fatigue life.

Acknowledgments

First and foremost, I want to thank my wife, LaTanya, and son, Bennett, for there love, support, and patients given over the past year and half! I would not be where I am today without you. I will never be able to repay you for the sacrifice you both make for me. I love you both!

Dr. Palazotto, Thank you for your advisement, support, and belief in me while at AFIT. Your encouragement and support as a mentor and friend will not be forgotten.

To the staff at AFRL/RQVS, Dr. Kristina Langer, Dr. Thomas "TJ" Spradlin, Dr. Stefano Coratella, Mr. James "Jim" Harter and Mr. Michael Wipperman; Thank you for your trust, support, guidance, mentorship and friendship over the past year. I have learned a tremendous amount of information and know that our continued work together will be informative and challenging but most likely enjoyable. Additionally, I would like to thank you for investing in my education with research funding and my attendance of the 6th Int'l Conference on Laser Peening and Other Related Phenomena. It was extremely educational, allowed for networking with world leaders in the field, and an overall a great experience in South Africa.

I would like to thank the following people for their support, guidance, and knowledge: University of Cincinnati's Dr. S.R. "Manny" Mannava and his graduate student, Metal Improvement Company's Dr. Lloyd Hackel and his team, Canadian Neutron Beam Center's Dr. Michael Gharghour, and Hill Engineering's Dr. Adrian DeWald. I look forward to working with you all in the near future.

David L. A. Eisensmith

Table of Contents

	Page
Abstract	iv
Acknowledgments	v
List of Figures	ix
List of Tables	xiii
I. Introduction	1
1.1 Chapter Overview	1
1.2 Objective	2
1.3 Motivation	2
1.4 Assumptions	3
1.5 Methodology	5
1.6 Overview	6
II. Background	7
2.1 Chapter Overview	7
2.2 Fracture Mechanics	7
2.3 Residual Stress	14
2.4 Residual Stress Measurement Techniques	15
2.4.1 Incremental Hole Drilling	16
2.4.2 Diffraction Techniques	17
2.5 Load Shedding	20
2.6 Marker Banding	22
2.7 Laser Shock Peening	25
2.8 Summary	28
III. Research Methodology	29
3.1 Chapter Overview	29
3.2 Specimen Machining	29
3.3 Starter Notch Formation	30
3.4 Initial Pre-Cracking	33
3.5 Final Thickness Machining	34
3.6 Pre-Crack Shape Formation	38
3.7 Marker Band Development	39
3.8 Laser Shock Peening	41
3.8.1 Laser Energy and Number of Application Determination	42
3.8.2 General LSP Parameters	43

	Page
3.8.3 Sample Mounting Fixture	45
3.8.4 LSP Application Process	46
3.9 Fatigue Testing	52
3.10 Residual Stress Measuring	54
3.10.1 Circular Spot Laser Peening Residual Stress Measurement Techniques	54
3.10.2 Square Spot Laser Peening Residual Stress Measurement Techniques	57
3.11 Fractography	58
3.12 Summary	59
IV. Results and Discussion	60
4.1 Chapter Overview	60
4.2 Initial Crack Shape Investigation	60
4.3 Specimen Crack Shape Results	62
4.4 Does the presence of a minimal detection level surface crack affect the Laser Shock Peening Process?	64
4.4.1 Circular Spot Laser Residual Stress Profile	64
4.4.2 Square Spot Laser Residual Stress Profile	69
4.5 Does the presence of a minimal detection level surface crack prior to LSP application cause detrimental effects to the fatigue life?	73
4.5.1 Stress Intensity Factor Inspection	79
4.6 Variations Between Circular and Square spot Laser Peening Results	83
4.7 Summary	84
V. Conclusions and Recommendations	85
5.1 Chapter Overview	85
5.2 Conclusions	85
5.2.1 Does the presence of a minimal detection level surface crack affect the Laser Shock Peening Process?	85
5.2.2 Does the presence of a minimal detection level surface crack prior to LSP application cause detrimental effects to the fatigue life?	86
5.2.3 Will the two previous objectives be effected if two different cross-section laser systems are used, circular and square?	87
5.3 Recommendations and Discussions	87
5.4 Future Research	88

	Page
Appendix A. Test Specimen Drawings	90
Appendix B. Material Certification of Manufacturing Process, (AA 7075-T651)	93
Appendix C. Ablative Tape of Single Application of Circular Spot Laser Peening Process	95
Appendix D. Specimen Machining and Numbering	96
Bibliography	98

List of Figures

Figure		Page
1.1	Crack dimension assumptions	4
2.1	Fracture Modes.....	8
2.2	Semielliptical Surface Crack	9
2.3	Semielliptical Surface Crack Shape	9
2.4	Typical fatigue crack growth	13
2.5	Typical Strain Gage used for Incremental Hole Drilling	16
2.6	Incremental Hole drilling method of calculating Residual Stress.	16
2.7	Radiation Diffraction	17
2.8	Neutron Diffraction Gage Volume	20
2.9	Load Shedding Characterization	21
2.10	Marker Band.....	22
2.11	Marker Banding Explanation	24
2.12	Characterization of LSP process	26
2.13	Typical LSP residual stress profile	27
3.1	Specimen Manufacturing.....	30
3.2	Stress Orientation Directions in each Sample	30
3.3	Ball End Mill with Full Radius Tip	31
3.4	Starter Notch Representation.....	32
3.5	Laser profilometer scan data of starter notch	32
3.6	MTS Load cell with traveling microscope attached	34
3.7	Through Thickness Material Grain Structure	36
3.8	Grain Structure Showing Final Material Thickness	37

Figure	Page
3.9	Fractured Surface Showing the Marker Band Experimentation. 39
3.10	Fractured surface showing the Marker Band. 41
3.11	Energy Level Test Samples 43
3.12	Circular Spot Laser Peening Cross-Section 43
3.13	Square Spot Laser Peening Cross-Section 44
3.14	Circle Spot Laser Peening Fixture 46
3.15	Square Spot Laser Peening Fixture 46
3.16	Circular Spot Laser Peening Path for Each Sequence 47
3.17	Robotic Arm Used to Relocate Sample in Beam’s Path 48
3.18	All Circular Spot Laser peening sequence patterns showing the offset for each..... 49
3.19	Circular Spot Laser Application Offset..... 50
3.20	Square Spot Laser peening patterns for each application..... 51
3.21	Square Spot Laser Application Offset 52
3.22	Cyclic Applied Load Depiction 53
3.23	Residual Stress Measurement Areas for Hole Drilling 55
3.24	Residual Stress Measurement Areas for Neutron Diffraction 56
3.25	Neutron Diffraction Gauge Volume Representations 56
3.26	Unpeened Residual Stress Measurement Area for X-Ray Diffraction 57
3.27	Peened Residual Stress Measurement Area for X-Ray Diffraction 57
3.28	Optical microscope with integrated XY measuring table. 58
4.1	Test samples for crack shape investigation 61

Figure	Page
4.2	Crack Ratio vs. Crack Depth 62
4.3	Neutron Diffraction RS Results 65
4.4	Neutron Diffraction Residual Stress Results 66
4.5	Hole Drilling Results for Circular spot Laser Peened Region 67
4.6	Hole Drilling Results for unPeened Region 67
4.7	Circular spot Laser Peened RS Comparison in LSPed Area. (Shear stress shown for completeness.) 68
4.8	Circular spot Laser Peened RS Comparison in Unpeened Area. (Shear stress shown for completeness.) 69
4.9	Residual stress data measured by X-ray diffraction..... 70
4.10	Hole Drilling Results for Square spot Laser Peened Region. Shear stress shown for completeness.) 71
4.11	Hole Drilling Results for UnPeened Region. (Shear stress shown for completeness.) 71
4.12	Square Spot Laser Peened RS Comparison in LSPed Area 72
4.13	Square Spot Laser Peened RS Comparison in Unpeened Area 73
4.14	Fractured surface showing marker bands 75
4.15	Unpeened specimen with marker band illustration overlay..... 75
4.16	Unpeened specimen showing marker band. 76
4.17	Square Spot Laser Peened Specimen showing no signs of fatigue growth after peening. 77
4.18	Circular Spot Laser Peened specimen showing no signs of fatigue growth after peening 77
4.19	Fracture surface of a laser peened specimen 78

Figure		Page
4.20	Profile of specimen showing bending due to LSP application.....	79
4.21	Depiction of angle Phi.....	80
4.22	Plot of Stress Intensity (K) spanning full crack tip.....	81
4.23	Crack Growth Rate Curve.....	82

List of Tables

Table		Page
3.1	Specimen Process Flow	29
3.2	Incremental Load Shedding	34
3.3	Marker Band Sequence	40
3.4	Circular spot laser parameters	44
3.5	Square spot laser parameters	45
4.1	Specimen Fatigue Results	61
4.2	Specimen Crack Shape Measurements (Only reported in British units)	63
4.3	Specimen Fatigue Results (Note: Specimens 5/4 and 4/3 were not cleaved)	74
4.4	Specimen Deformation Post-LSP	79
4.5	Parameters used to generate K vs. Crack Face Position plot See Figure 4.21 for explanation of angle ϕ (* Estimated Values)	80

FATIGUE EFFECTS OF LASER SHOCK PEENING MINIMALLY
DETECTABLE PARTIAL-THROUGH THICKNESS SURFACE CRACKS

I. Introduction

1.1 Chapter Overview

Laser Shock Peening (LSP) has evolved over the past 40 years to become a viable alternative to other forms of surface treatments (shot peening, burnishing, etc.) that induce beneficial residual stress in structural components. These residual stress have many potential benefits but increasing the fatigue life of structural components by retarding the initiation and/or growth of cracks [1] is of greatest concern for aerospace application. Prior studies have shown these benefits in new material but not previously fatigued material, which can contain surface defects at or below the detectable limit of current inspection techniques. The research presented here explores the effects of LSP on the fatigue life of an aircraft grade structural aluminum alloy (AA 7075-T651) in a generic geometry and loading. LSP is applied over a known partial-through thickness surface crack having a surface crack length at the minimal detectable limit (which is 0.25" (6.35mm)) for the nondestructive inspection (NDI) technique of surface scan eddy current (SSEC) [2]. This chapter will discuss the objectives for research, the motivation, background, assumptions, and briefly discuss the methodology that will be used for this research.

1.2 Objective

This research was focuses on better understanding the fatigue effects of laser shock peening as applied over a preexisting partial-through thickness surface crack. The primary question driving this research is “Does LSP cause unintended detrimental consequences if inadvertently applied over a flaw?” This question drives the objectives of this thesis:

- Does the presence of a minimally detectable surface crack affect the Laser Shock Peening Process?
- Does the presence of a minimally detectable surface crack prior to LSP application cause detrimental effects to the fatigue life?
- Will the two above questions be effected if two different cross-sectional laser systems are used, circular and square? (common cross sections in the industry)

1.3 Motivation

Failure of an aerospace structural component can have catastrophic consequences resulting in loss of life and aircraft. Findaly et al. [3] estimated that 55% of aircraft structural components fail due to fatigue. This issue is compounded when airframe service lives are extended, which is becoming more commonplace. Some examples of aircraft life extensions are: Lockheed Martin currently attempting to extend the F-16 Fighting Falcon from the current flight hour limit of 8000 to 12000 flight hours [4], the United States Air Force is reportedly extending the B-52 bomber to 2040 [5], and the F-35 Joint Strike Fighters current service life extension program is attempting to extend use to 2070 [6].

Aerospace engineers have various tools at their disposal to deal with aircraft service life extension

- proactive and/or reactive component replacement
- assumption of risk (possible aircraft service retirement if certain components fail)
- additional structural reinforcements
- surface treatments

Surface treatments can be most beneficial when structural components replacement is not cost-effective. Many surface treatments that induce beneficial residual stresses into the material are available, but the limitations of application method, cost, accessibility, amongst many others are limiting factors for most organizations. There is a fatigue life benefit due to those induced residual stresses, however, some can be more effective than others. Laser Shock Peening has proven to induce large compressive residual stresses much deeper than most, which can lead to improved fatigue life performance [7].

As stated previously, the complexity of many aircraft structures do not allow for a cost effective replacement of many structural components requiring LSP application in-situ, which may have undetected flaws present. Aging aircraft engineers are concerned with the unintended consequences of the LSP application over these undetected flaws/cracks.

1.4 Assumptions

Aircraft components that have been in service will have accumulated many fatigue cycles throughout the life of the aircraft. Each aircraft platform and subsequent component is different, and thus each spectrum will be unique to that aircraft and component. To simplify this complexity, a tension-tension fatigue test will be conducted. This type of testing will allow for an initial investigation of the issue.

Fatigued aircraft components are assumed to have a certain type and size of flaw for initial damage tolerance calculations. This initial flaw size is determined by the type of inspection used at that location, accessibility of the inspection area, amongst many other factors. This thesis will assume that the inspection method will be a surface scan eddy current (SSEC), a common non-destructive inspection (NDI) technique used for surface flaws. Additionally, it is assumed that the inspection area has a radius of curvature less than 1.0", is in a fully accessible area, and would be accomplished by manually scanning using a pencil probe by a qualified NDI technician. These assumptions garner an assumed surface crack length ($2c$) of 0.250" (6.35mm) and an assumed crack depth (a) of 0.125" (6.175 mm) (Figure 1.1) [2]. This crack length will be referred to in this thesis as the minimal detectable limit. These values, as defined in The USAF Structures Bulletin EN-SB-08-012, Revision C, are an empirical, statistically determined limit in which there is a 90% probability of detection at a 95% confidence in that detection [2].

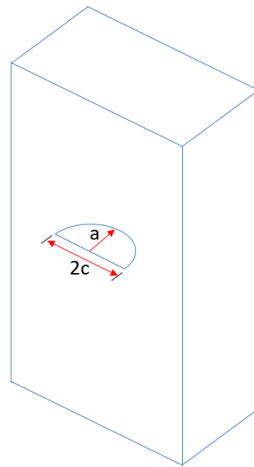


Figure 1.1. Crack dimension assumptions

It is assumed the material is homogeneous. The research material (AA 7075-T651) used was purchased from a single manufacture and was provided with a certification showing the chemical composition and specification that the material was manufac-

tured to (AMS-QQ-A-250/12 Rev A).

The LSP application process has many process controls to maintain consistent parameters. It is assumed that each type of laser (NdCr-YAG, Nd-YAG, etc.) provides desired power, repeatedly for each impact and application. A few of the lasers parameters can be monitored and adjusted via daily inspections, but conditions can change throughout the day affecting laser performance. Each peening type (circular/square) was conducted under the supervision of experienced personnel, and each peening type followed their own internal processes and quality control to limit variations.

Representative residual stress measurements were taken for each of the two types of peening (square and circular laser spot shapes) in two key areas. The key points were measured, inside the peened area and at an area away from the peened area. It is assumed that the residual stress (RS) profile in the peened area remote from the edges of the peened area will have a similar profile. Likewise, it was assumed that the RS profile outside of the peened areas have similar RS profiles as that measured.

1.5 Methodology

Multiple specimens were wire EDMed (electrical discharge machining) from 0.685" (17.4 mm) certified AA 7075-T651 plate to 16" x 4" (406.4 mm x 101.6 mm) (Appendix A). A starter notch was then cut into the center of one side of the plate to ensure a crack would initiate and propagate from a consistent and controlled position. Samples were then placed into an MTS load frame and fatigued in tension-tension until a crack was grown to 0.300" (7.62 mm). This length allowed for surface material removal required to remove starter notch while leaving a sub-minimal detectable crack length. The specimens were again placed into an MTS load frame and fatigued until the minimally detectable crack length of 0.25" (6.35 mm) was reached. Eight of the twelve pre-cracked specimens were then laser peened.

Three specimens were peened using a circular spot LSP process, consisting of two sets of applications, each containing four offset sequences (further explanation in Chapter II). Five specimens received the square spot LSP process, accomplished by a different vendor, with peening parameters similar to the circular spot laser parameters. The square spot LSP process consisted of two offset layers (further explanation in Chapter II). LSP was only applied on the cracked surface, covering a 2" x 2" (50 x 50 mm) square area in the center of the plate with the crack approximately centered in the peened area. RS measurements were made in both peened and unpeened specimens with roughly the same crack length prior to the peening process.

Following the peening process, all specimens including those not peened, were mounted in the MTS load frame and fatigued either to failure or to run-out (one million cycles), under constant amplitude cyclic loading. The growth of the surface crack was monitored and measured with a traveling microscope. Periodically, the cyclic loading was interrupted to apply a marker band. The marker band was accomplished by reducing the load amplitude and varying the load ratio of the loading creating a unique surface feature on the fractured surface. The results of the unpeened and two peening strategies are compared to understand the effects of LSP on fatigue cracks as they relate to the objectives of this research.

1.6 Overview

- Chapter II: Discussion of the theory presented in the literature
- Chapter III: Outlines testing methodology used for this research
- Chapter IV: Presents the results and discussion
- Chapter V: Summarizes the results, draws conclusions, and discusses recommendations for future research

II. Background

2.1 Chapter Overview

This chapter will discuss the theory used to conduct and evaluate the information received from this research. A basic understanding of engineering is required prior to fully comprehending the topics discussed. Some items provide a brief overview of the topic, without delving too deeply. The reason for this is that those topics and their use are not the direct objective of this research but a tool that was used within.

2.2 Fracture Mechanics

Fracture mechanics is the study of crack propagation through a material [8]. In linear elastic fracture mechanics, solid mechanics is used to understand and predict crack growth based on the relationships of the materials resistance to crack extension, geometry, and the applied loads. Various applied loads can cause crack propagation but they can all be differentiated by one, or any combination of the following three modes: Mode I, also known as the opening mode, is the result of a force normal to the crack plane being applied to opposite sides of the crack face; Mode II, known as the in-plane shearing or sliding mode, is generated by opposing forces acting in parallel to the crack plane and perpendicular to the crack front; Mode III, defined as the out-of-plane shearing or tearing mode, is generated as a result of opposing forces acting in parallel to the crack plane but perpendicular to the crack face. All three modes are depicted in Figure 2.1. The primary mode of failure was Mode I for this work, thus any further discussions will only reflect applications to this mode of failure.

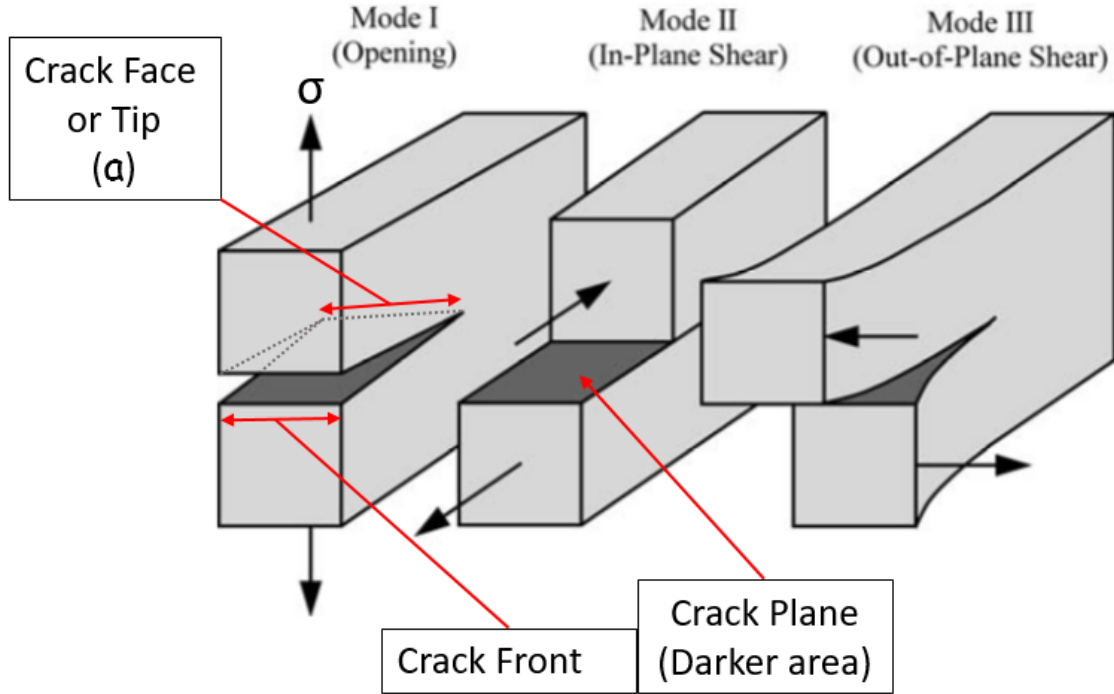


Figure 2.1. The three modes of loading that can be applied to a crack [8].

The tip of every crack can be treated as a singularity at which the greatest stress will be concentrated. The quantity used to gauge this singularity is the stress intensity factor, K . In a conventional crack the stress intensity is given by Equation 2.1. In equation 2.1, σ is the applied stress, a is the crack length, and β is a geometry correction factor. However, for a semi-elliptical surface crack shown in Figure 2.2 has a stress intensity factor calculated by Equation 2.2a, which utilizes the subsequent equations. Note that Equation 2.2a is only valid when $a \leq c$. Anderson provides a solution for K_I when $a/c > 1$, however none of the specimens met this condition, thus the equations are not presented here [8]. The subscripts indicate which fracture mode (I, II, or III) the stress intensity is being related to. This research is only concerned with Mode I fracture thus the subscripts will be dropped in subsequent sections.

$$K_1 = \sigma\beta\sqrt{\pi a} \quad (2.1)$$

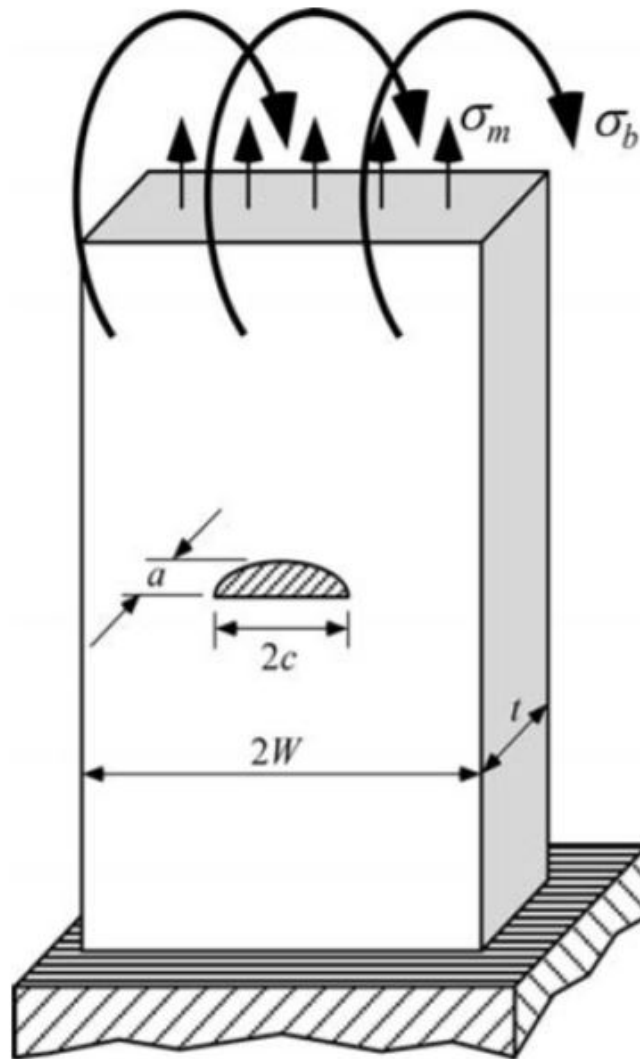


Figure 2.2. Semielliptical Surface Crack [8].

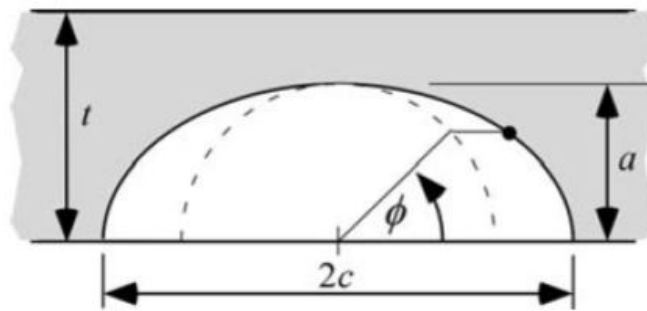


Figure 2.3. Semielliptical Surface Crack Shape [8].

$$K_1 = (\sigma_m + H(\sigma_b) + \sigma_{RS}) \sqrt{\frac{\pi a}{Q}} F\left(\frac{a}{c}, \frac{a}{t}, \frac{a}{W}, \phi\right) \quad (2.2a)$$

$$Q = 1 + 1.464\left(\frac{a}{c}\right)^{1.65} \quad (2.2b)$$

$$F = [M_1 + M_2\left(\frac{a}{t}\right)^2 + M_3\left(\frac{a}{t}\right)^4] f(\phi) f(w) g \quad (2.2c)$$

$$M_1 = 1.13 - 0.09\left(\frac{a}{c}\right) \quad (2.2d)$$

$$M_2 = -0.54 + \frac{0.89}{0.2 + \frac{a}{c}} \quad (2.2e)$$

$$M_3 = 0.5 - \frac{1.0}{0.65\frac{a}{c}} + 14\left(1.0 - \left(\frac{a}{c}\right)^{24}\right) \quad (2.2f)$$

$$f(\phi) = \left[\left(\frac{a}{c}\right)^2 \cos^2(\phi) + \sin^2(\phi)\right]^{\frac{1}{4}} \quad (2.2g)$$

$$f(w) = \left[\sec\left(\frac{\pi c}{2W} \sqrt{\frac{a}{t}}\right)\right]^{\frac{1}{2}} \quad (2.2h)$$

$$g = 1 + \left[0.1 + 0.35\left(\frac{a}{t}\right)^2\right] (1 - \sin(\phi))^2 \quad (2.2i)$$

$$H = H_1 + (H_2 - H_1)(\sin(\phi))^P \quad (2.2j)$$

$$P = 0.2 + \frac{a}{c} + 0.6\left(\frac{a}{t}\right) \quad (2.2k)$$

$$H1 = 1 - 0.34\frac{a}{t} - 0.11\frac{a}{c}\left(\frac{a}{t}\right) \quad (2.2l)$$

$$H2 = 1 + G1\left(\frac{a}{t}\right) + G2\left(\frac{a}{t}\right)^2 \quad (2.2m)$$

$$G1 = -1.22 - 0.12\left(\frac{a}{c}\right) \quad (2.2n)$$

$$G2 = 0.55 - 1.05\left(\frac{a}{c}\right)^{0.75} + 0.47\left(\frac{a}{c}\right)^{1.5} \quad (2.2o)$$

Equation 2.2b, Q, is a conversion factor for a non-semicircular shaped crack. F (Equation 2.2c) is a conversion factor to account for edge effects. H (Equation 2.2j) is a bending multiplier used to convert surface bending stress to in-depth bending stress. All other equations support equation 2.2c. Note that the angle ϕ does not directly represent the physical angle from the center of the crack to point of interest (reference 4.21) [8]. Additionally, the stresses shown in equation 2.2a are; σ_M = Membrane (tensile) stress, σ_b = Bending stress, σ_{RS} = Residual Stress. The residual stress component was added to Anderson's equations and is the measured residual stress at a specific area. When that area is substantially small it can be considered a point. This will be discussed further in Section 2.4.

When the stress intensity, K, reaches a critical limit the material will fail. However, when load is applied cyclically the critical stress intensity does not need to be reached for crack growth to happen. ΔK (Equation 2.3) is used in Paris Law (Equation 2.4) to define the rate of crack growth [8].

$$\Delta K = K_{max} - K_{min} \quad (2.3)$$

$$\frac{da}{dN} = C\Delta K^m \quad (2.4)$$

In Paris Law, the values of C and m are empirically determined constants and N is the number of cycles. Paris's law assumes that as the variation in stress intensity (ΔK) increases, so too does the rate of crack growth. This behavior is shown in Figure 2.4 , which is a plot of da/dN vs. ΔK (log-log scale plot). The full length of the plot is not linear but the curve can be broken down into three regions. The curve in Region I shows that there must be a certain (Δ)K reached for crack growth to occur, typically referred to as the threshold and is asymptotic in nature. Region II, or Paris's regime, of the curve is linear in nature (in log-log scale), while, Region III is asymptotic, showing that when (Δ)K approaches a critical stress intensity factor for the material K_{IC} , unstable crack growth will occur until failure.

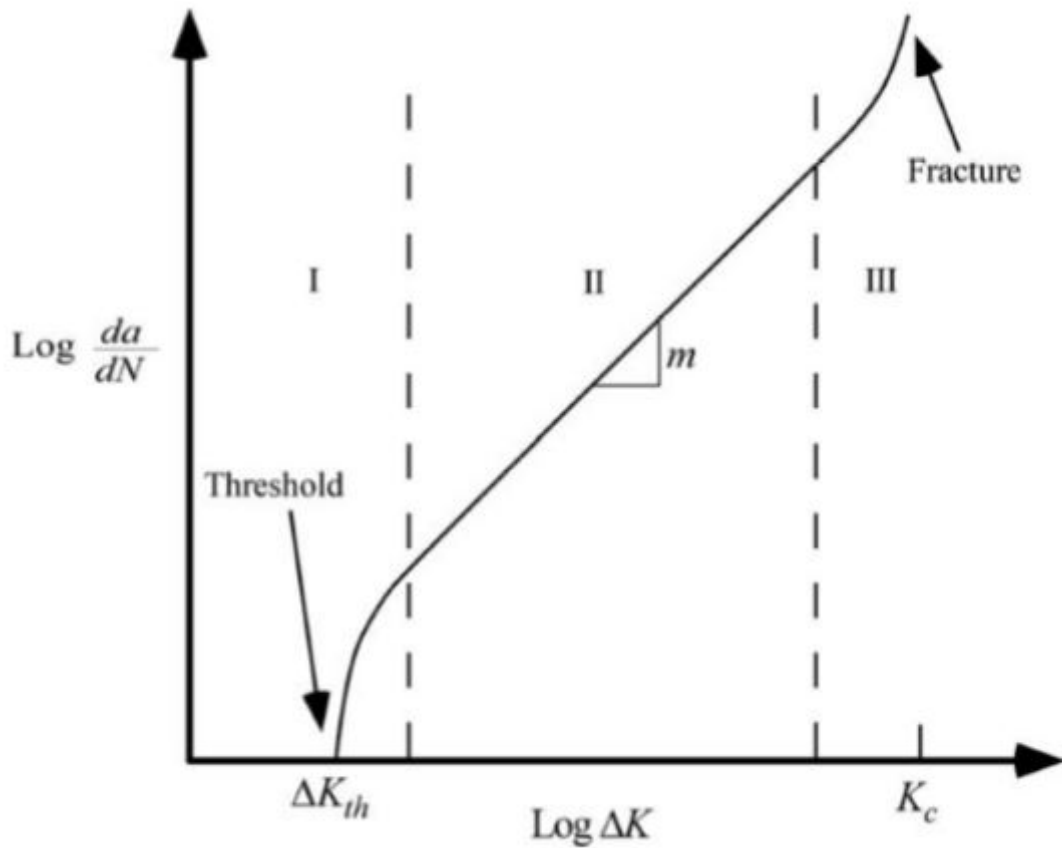


Figure 2.4. Typical fatigue crack growth behavior in metals [8].

It is widely expected that Paris's Law (Equation 2.4) sufficiently describes Region II in Figure 2.4 [8]. The only way to alter the crack growth rate, da/dN , for this region is to either alter the crack size or alter the applied load to the material. In fatigued specimens under constant cyclic load, like the work conducted here, the crack length is the only variable. The rate of crack growth will increase as the crack length increases until the point of transition to Region III. Many researchers are still developing models and equations to characterize and combine all three regions into a single equation[9], [10], [11], [12], [13], [14], [15].

2.3 Residual Stress

Residual stress (RS) is defined as “that stress which would exist in an elastic solid body if all the external load (forces, couples, and applied stresses), acceleration, and gravitation were removed” [16]. However, RS is derived from elastic strain measurements because strain can be directly observed: stress is a calculated value. The generalized Hookes Law for 3-dimensional stress is defined in Equation 2.5, where E is the modulus of elasticity, ν is Poissons ratio, and ϵ is the measured strain in the indicated directions (x, y, z).

$$\sigma_{\alpha} = \frac{E}{(1 + \nu)} \left[\epsilon_{\alpha} + \frac{\nu}{1 - 2\nu} (\epsilon_x + \epsilon_y + \epsilon_z) \right], \alpha = (x, y, z) \quad (2.5)$$

In simple engineering models, the method to describe the shapes of cracks in material typically assumes that the material’ elastic properties are homogeneous and isotropic [16]. Elastically isotropic means that the internal RS are uniform. If the material acts in this way and the stresses remain elastic, then the stress intensity factor calculated by Equation 2.5 would be applicable [8]. However, all material even the so called “stress relieved” materials, possess internal RS. RS is present in any mechanical structure due to many different causes. They can be induced into the material by:

- Material Production (Casting, Rolling, Forging)
- Manufacturing processes (Welding, Machining, Heat Treatments, surface treatments)
- Environmental conditions (Thermal Gradients and restraint)
- System engineering (unaccounted transfer of loadings) [17]

These RSs will vary throughout the material/component. This gradient of stress can be transposed over the applied stress to recalculate the stress intensities, however, the internal stresses are not usually known. When tensile RS is aligned with the applied loads the stress intensity at that point will be increased, causing crack growth under a lower external applied force. However, compressive RS will result in a higher external applied load to generate the same amount of crack growth. This unknown RS field can cause a crack to propagate through the material in a manner atypically compared to the component without RS present. Therefore, the semicircular shape prediction is no longer valid.

One method used to determine the crack shape as it propagates is to fatigue the specimens and mark the fracture surface at known intervals. After component fracture the markings can be inspected and crack growth and shape can be discovered. If the material and component manufacturing techniques are properly controlled, the crack shape and growth rate can be predicted in the future. In this work, marker bands are being utilized to this effect.

2.4 Residual Stress Measurement Techniques

As mentioned in the preceding section; measuring RS is not possible, the residual strain is measured and then converted into residual stress through the use of Hookes Law (Equation 2.5) For the purposes of clarity, all discussions within this work will discuss measuring residual stress with the pretense that it is the act of measuring strain and converting it to stress. There are many different and established methods of measuring residual stress, each having their advantages and disadvantages. All methods can be categorized as nondestructive, destructive, or semi-destructive. Only the methods used for this experiment will be discussed in the following subsections. They are incremental hole-drilling, X-ray diffraction, and neutron diffraction.

2.4.1 Incremental Hole Drilling

Incremental hole-drilling is the “most widely used general-purpose technique for measuring residual stresses in materials” [17]. This method involves drilling a small hole through a strain gage rosette and into the material where the measurement is desired. (Figure 2.6) This method is very popular because there is an ASTM standard test method, E837, that covers the method from material preparation to data acquisition.

The method is called incremental hole-drilling because the hole being drilled is accomplished in incremental steps. A typical step of drilling depth is 0.001” (0.025mm). The drilling causes the material surrounding the hole to relax. This relaxation is then measured by the attached strain gages. The strain measurements are assumed to be an in-plane stress due to the very small increment of drilling depth. A proprietary calculation is accomplished to calculate the average RS over the volume of material removed. The stepping process allows for subsurface measurements to be accomplished to a depth of roughly the radius of the hole being drilled. If the investigation of RS is only to be near the surface, the hole will not protrude very deep, which may be within damage tolerances for an in-service component. This is why this method is categorized as a semi-destructive measurement technique.

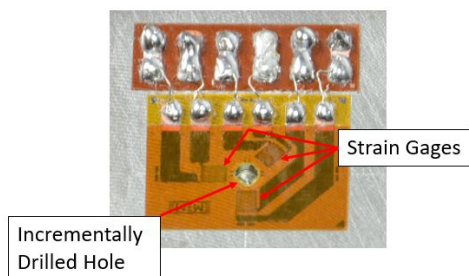


Figure 2.5. Typical Strain Gage used for Incremental Hole Drilling [18].

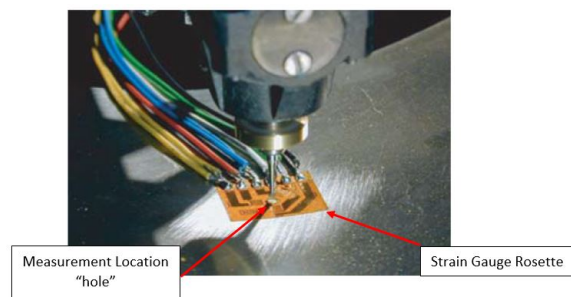


Figure 2.6. Incremental Hole drilling method of calculating Residual Stress.

2.4.2 Diffraction Techniques

“Diffraction methods exploit the ability of electromagnetic radiation to measure the distance between atomic planes in crystalline or polycrystalline, materials” [19]. When RS stress is present in a material, the crystallographic planes will displace, closer in compression and further apart when in tension. When the radiation is directed towards a crystalline material the radiation interacts and diffracts off of the atomic lattices or crystallites. Certain diffraction angles coincide with crystalline planes creating a strong emission of radiation which can be explained by Bragg's Law (Equation 2.6). (reference Figure 2.7 for further explanation and depiction of parameters of Bragg's Law)

$$\lambda = 2d\sin(\theta) \quad (2.6)$$

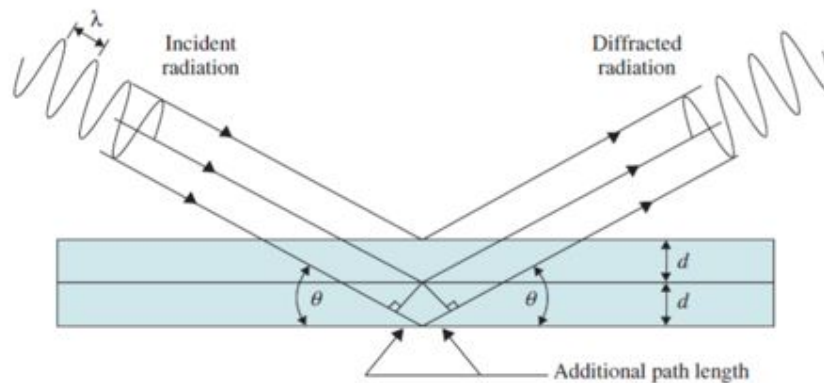


Figure 2.7. Radiation diffraction with a crystal structure d = spacing between lattice planes, θ = Bragg angle, and λ = wavelength of radiation [19]

In diffraction stress measurement techniques either the wavelength of the radiation or the diffraction angle is known and the other is measured. Solving Bragg's Law for “ d ” will provide the lattice spacing of the crystalline structure. When comparing this spacing to an unstressed portion of the same material and inserting this into Hooke's Law 2.5, the RS can be determined.

2.4.2.1 X-ray Diffraction with Layer Removal

The radiation for a table top X-ray diffraction (XRD) stress measuring technique is generated from an X-ray tube that when energized produces X-rays with wavelengths ranging from 0.7 to 2 Angstroms. Typical table top XRD devices generate radiation that penetrates the first few atomic layers of the materials surface on the order of 0.001" (0.025mm) in depth, which is why this technique is characterized as a nondestructive technique to measure surface residual stress [19].

The XRD stress measurement is an average of the stress over the sampled volume. Due to physics of the XRD method and that the radiation cannot penetrate deep into the material, only a two dimensional stress field can be measured. Additionally, due to the thin penetration, the assumption that the normal stress on the surface is zero is valid [19]. This measurement area is dictated by the grain structure of the material. There must be an adequate number of grains per measurement area to ensure reliable data.

To analyze the RS within the material requires the removal of material to allow the XRD to access it. Layer removal is accomplished by the use of electropolishing. The process removes small increments on the order of 10s of microns. Once each layer is removed a RS measurement is taken. This process can be repeated to a substantial depth, which is why XRD with layer removal is considered a destructive method to measure RS.

2.4.2.2 Neutron Diffraction

Neutron diffraction requires a nuclear reactor producing high-energy neutrons that penetrate the material and diffract off of the crystalline structure, where their diffraction angle is measured. The wavelength and direction of the neutrons is defined by passing a multiple wavelength neutron beam through a single crystal. Various crystals

can be used to direct a single wavelength of neutrons towards the material. Again, the angle and wavelength can be plugged into Braggs Law (Equation 2.6) to determine the lattice spacing [19].

The measurements received from neutron diffraction are typically the three primary stress tensors. It can not measure shear stresses, due to the way it method measures strain. Luckily, the primary type of stress in the material used in this experiment is not shear stress. The stress measurements garnered from neutron diffraction are an average, similar to XRD, over a gage volume. The gage volume is determined by the intersection of the incident and diffracted beams. (Figure 2.8) The scattering vector, Q , is the direction of stress measurement. The specimen can be positioned such that the scattering vector and stress can be measured for all three directions. Cadmium masks are used to control the gage volume size because cadmium absorbs neutrons. Due to the physics of how the neutrons react with the material, neutron diffraction has the ability to determine RS inside a material. For example, in aluminum measurements can be taken at a depth of nearly 10" (287 mm) [19]. Of the three methods discussed here, neutron diffraction is the only method that is completely nondestructive, while being able to provide RS measurements through the material.

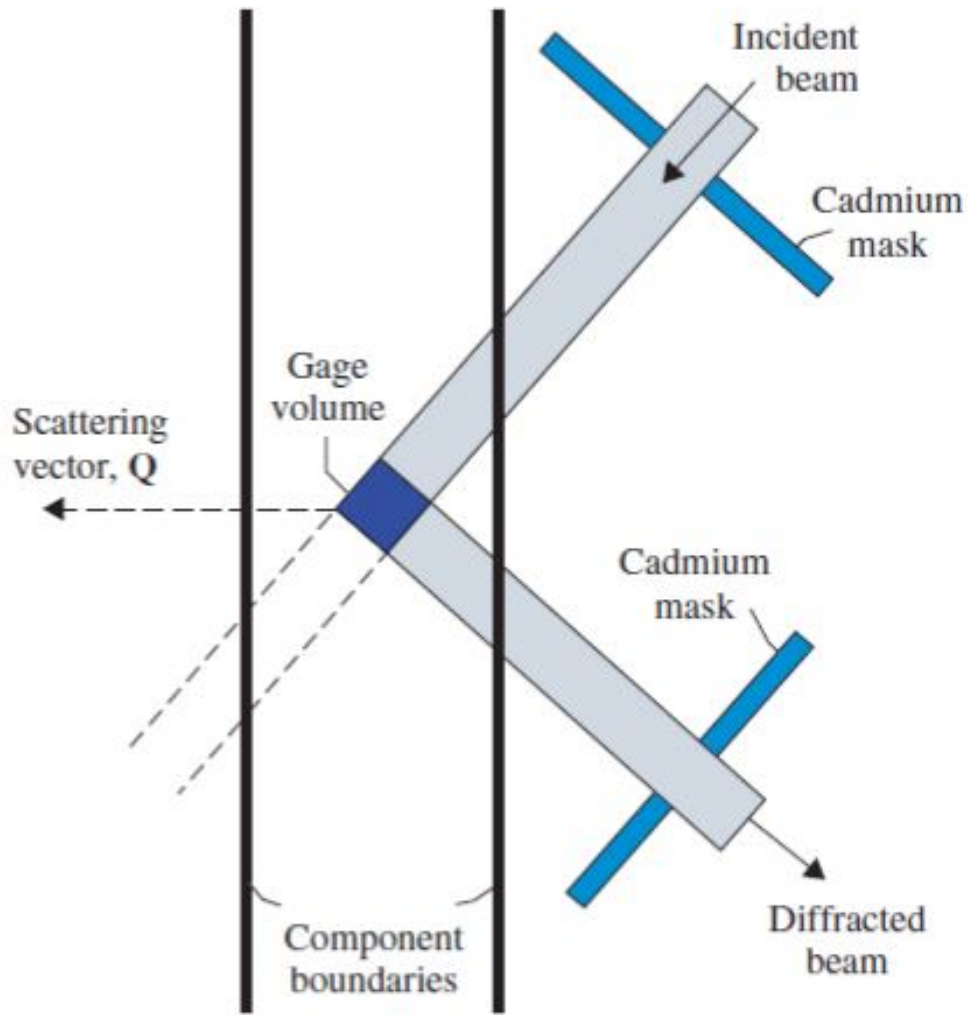


Figure 2.8. The gage volume is the bisector of incident and diffracted beams. Q , scattering vector is direction of stress measurement [19].

2.5 Load Shedding

Load shedding is the process of decreasing the applied load on a specimen in a controlled manner to maintain a constant ΔK at the crack tip. The purpose is to keep the stress intensity at the crack tip above the threshold limit, such that the crack will propagate and reduce the effects of localized strain hardening on crack growth. (2.9)

When a crack propagates, there is a portion of material radiating from the crack tip that yields. The size of the plastically deformed region is directly proportional

to the stress intensity, K [8]. Typically this plastically deformed region is on the order of hundred-thousandths of an inch or micrometers. Load shedding maintains a relatively uniform plastically deformed region from the previous step so that it will not interfere with the crack growth of interest.

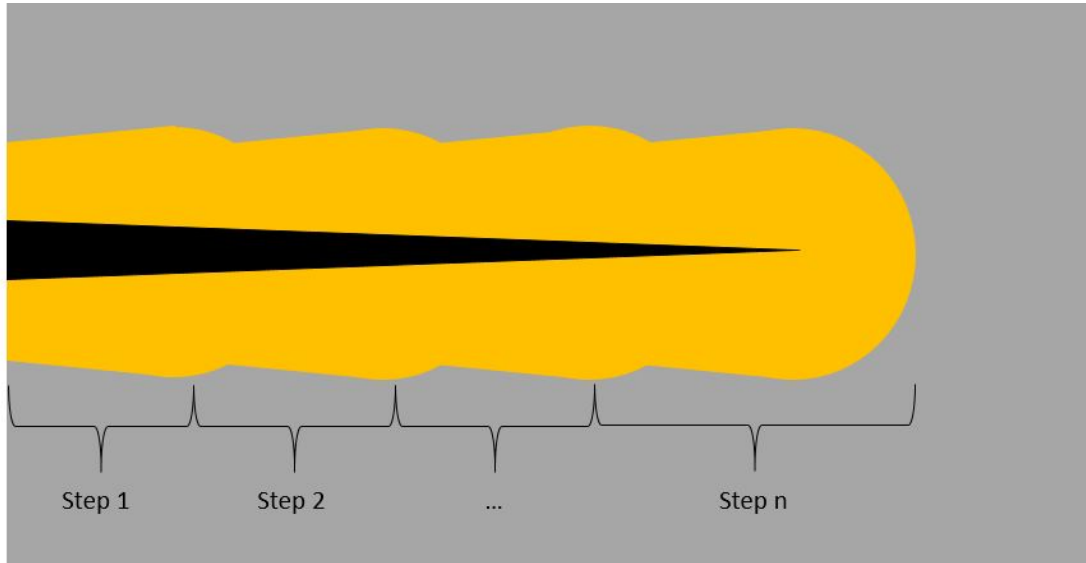


Figure 2.9. Load Shedding characterization. Orange area represent plastically deformed/strain hardened area with crack propagation. (Not to scale)

2.6 Marker Banding

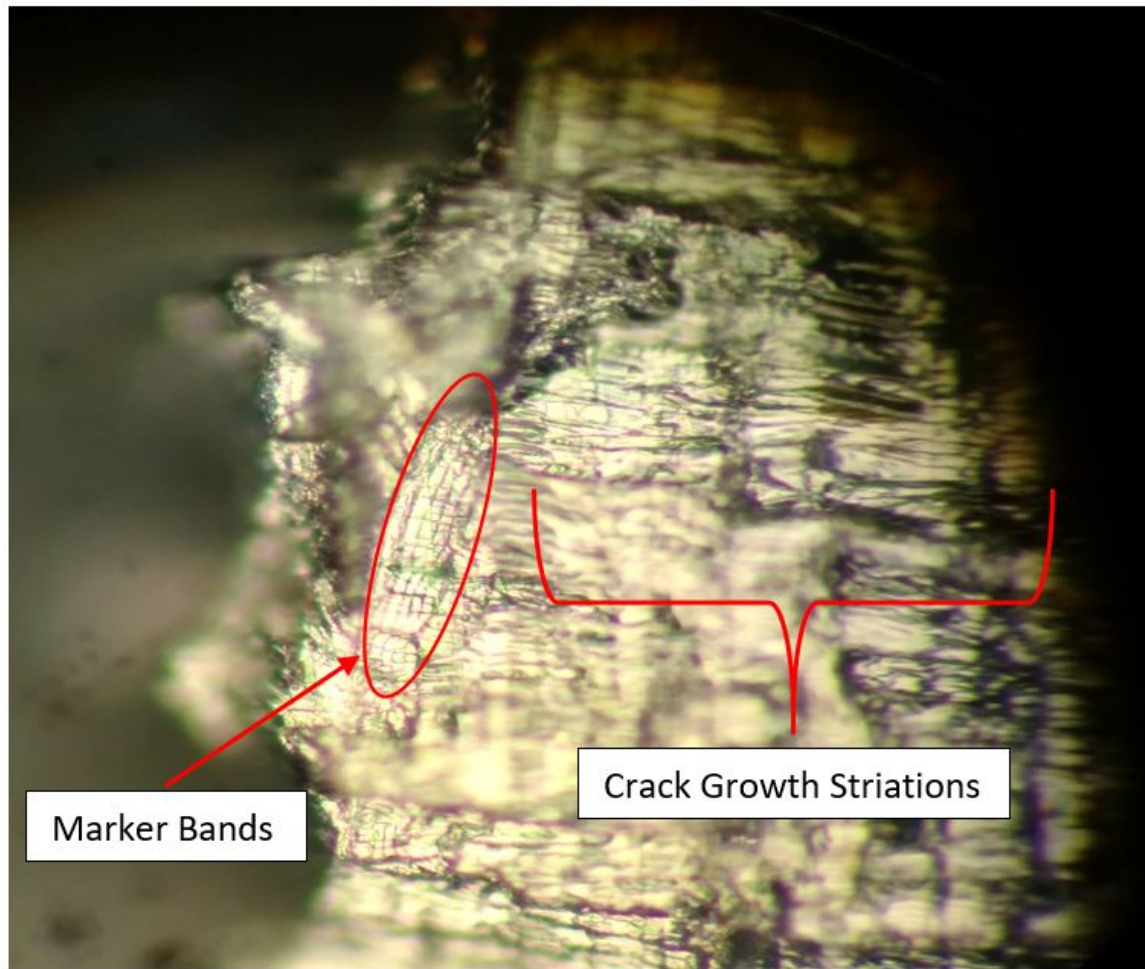


Figure 2.10. Fracture surface showing typical fatigue striations and an induced sequence of marker bands.

During fatigue crack growth, each cycle will cause an incremental amount of crack growth, called striations (Figure 2.10). The most accepted fractographic method is to study the fracture surface using a scanning electron microscope (SEM) [20]. SEM images can show higher fidelity than optical microscopes. The advantage of fractographic images generated by an SEM is when crack initiation or mode of fracture is in question, which can be a time-consuming effort. A relatively new microscopic, and in some cases macroscopic, method that has been developed is that of marker

banding [20]. The method causes visible striations on the fractured surface which appear significantly different than that of typical striations for the material under similar loading (See Figure 2.10). This process can be employed in both constant amplitude and spectrum loading, if properly designed/sequenced. Of concern in this experiment is constant amplitude loading, thus only this one will be discussed. Marker bands can be induced on a fatigue surface by one of the following methods:

- a.** “Instantaneous change in the plane of crack growth, followed by return to the dominant plane of crack growth. The associated change in contrast is registered on the fracture surface” (Figure 2.11a) [20].
- b.** “Instantaneous change in crack growth rate leading to associated change in fracture surface appearance and/or crack front shape, followed by possible return at some point to the original crack growth rate. Typically, lower growth rates would leave a smooth surface and a straight crack front. The difference in surface reflectivity can be seen as a contrast change under the optical microscope” (Figures 2.11b/c) [20].
- c.** “A combination of a and b” [20].

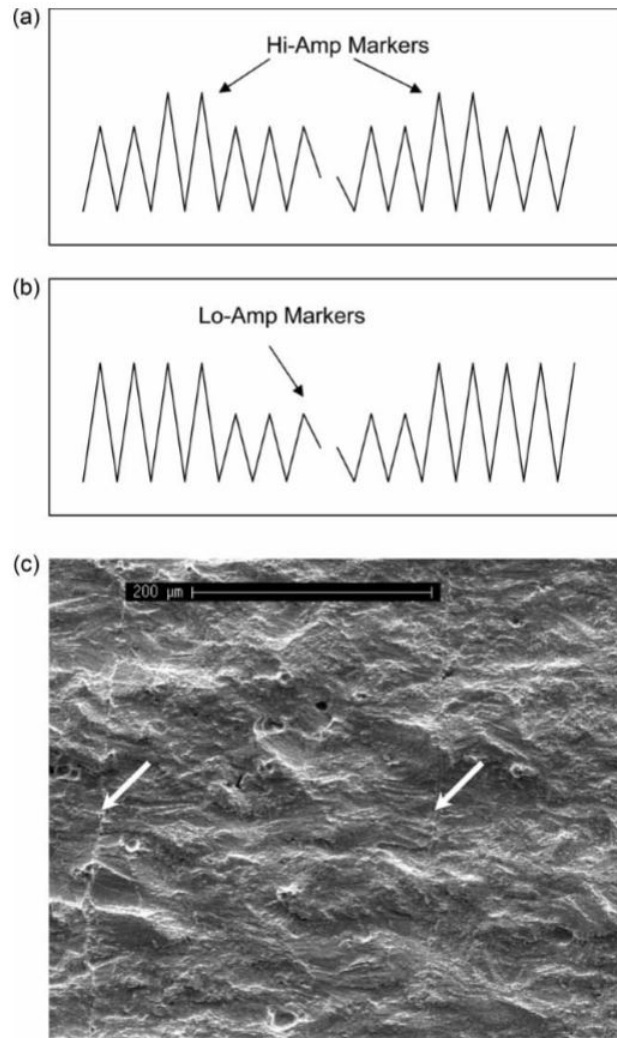


Figure 2.11. “(a) Marker loads exceed baseline loading in magnitude. Few cycles are adequate to leave a discernible mark on the fracture surface, and can cause load interaction effects. Such markers were used in the present study to control closure, (b) large number of reduced range cycles are applied as markers. Range is selected to ensure near-threshold growth rate during markers. Such markers will not introduce noticeable load interaction. However, their large number can extend test duration. Example appears as (c), and (c) typical fractograph obtained on a nickel-base super-alloy using small cycle markers (see arrows).The band on the left was caused by 75000cycles.The one on the right was caused by 15000 cycle” [20].

There are only a few parameters that can be varied when applying marker banding to a constant amplitude fatigue test; the load amplitude, the stress ratio, or the number of cycles. A change in amplitude will alter the rate of fracture resulting in either thicker or thinner striations. When the stress ratio is altered the rate of fracture and the fracture plane will change. This alteration in fracture plane is easily seen under optical magnification and will result in either a dark or light striation. The number of cycles can be altered in the marker band sequence to increase or decrease the spacing between striations.

2.7 Laser Shock Peening

Laser shock peening is a type of surface treatment process that mechanically cold works material through the use of laser generated shock waves. These shock waves plastically deform the surface and sub-surface material inducing a compressive residual stress layer. The plasma is formed when a high-energy laser beam vaporizes either the materials surface or an opaque ablative layer adhered to the surface of the material (paint or tape). This impact ablates forming a rapidly expanding plasma bubble. To confine this plasma and direct its expansion inward towards the material a transparent confinement overlay, typically water, is provided on top of the ablative layer. The expanding plasma causes shock waves to form in the material [21].

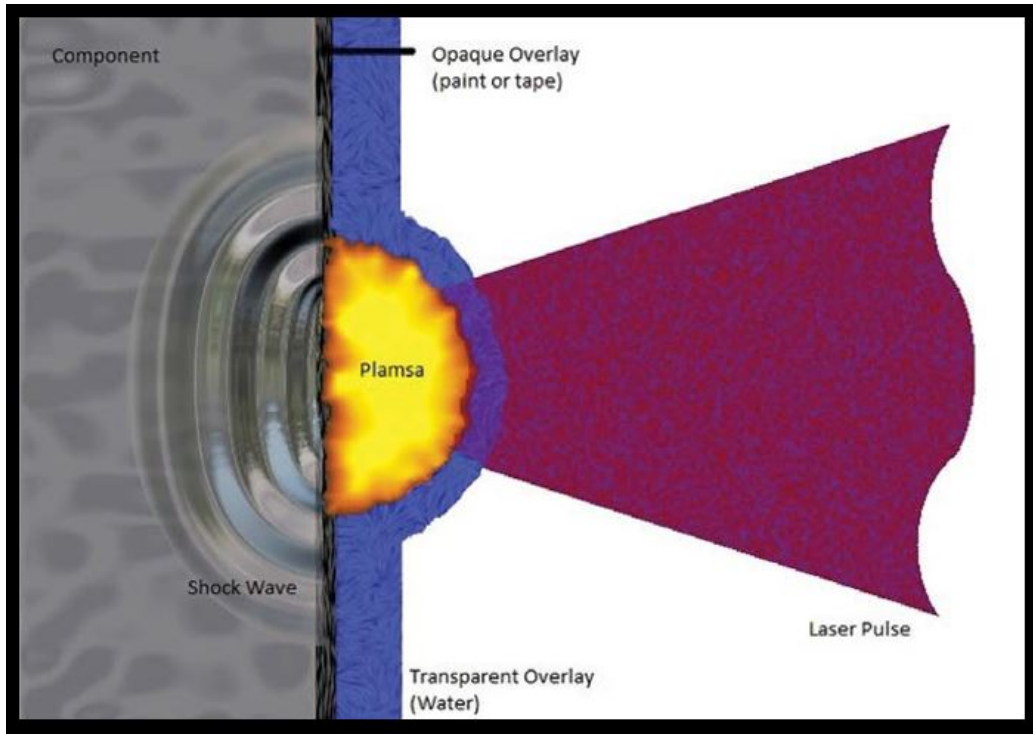


Figure 2.12. Characterization of LSP process [22].

At this point in the development of the LSP field, there are many differing paths as to which type of laser (YAG, Nd-glass, etc.), laser pulse parameters (energy, spot size, spot shape, pulse duration), need/type of ablative layer and plasma confinement medium, and many other properties that vary the RS field imparted by the LSP process. The key parameter that merge many parameters together and can be translated across laser types is the laser Power Density (Equation 3.1).

$$LaserPowerDensity = \frac{Energy}{PW * A} \quad (2.7)$$

Where the Energy term is the average energy output of the laser in Joules, PW is the pulse width per impact in nanoseconds, A is the area of the laser impact. All these could be independently varied to alter the power density applied to the material.

When the power density exceeds a materials threshold, the RS will increase with depth but decrease at the surface [21]. This threshold is known as the saturation

point. When the saturation point is surpassed, the surface RS can have significantly less compression and may actually transition to a state of tension. The variation in surface RS can cause microcracks or microvoids to form, potentially degrading the materials performance [21].

LSP causes a compressive RS field on the surface but to maintain equilibrium of stresses within the material, there must be tensile RS regions that have formed. Thus the LSP process induces both compressive and tensile residual stress fields [23]. They can be oriented in any/all of the 3-dimensions. A typical rolling or transverse RS (3.2) profile through the thickness of a laser peened specimen can be seen in Figure 2.13.

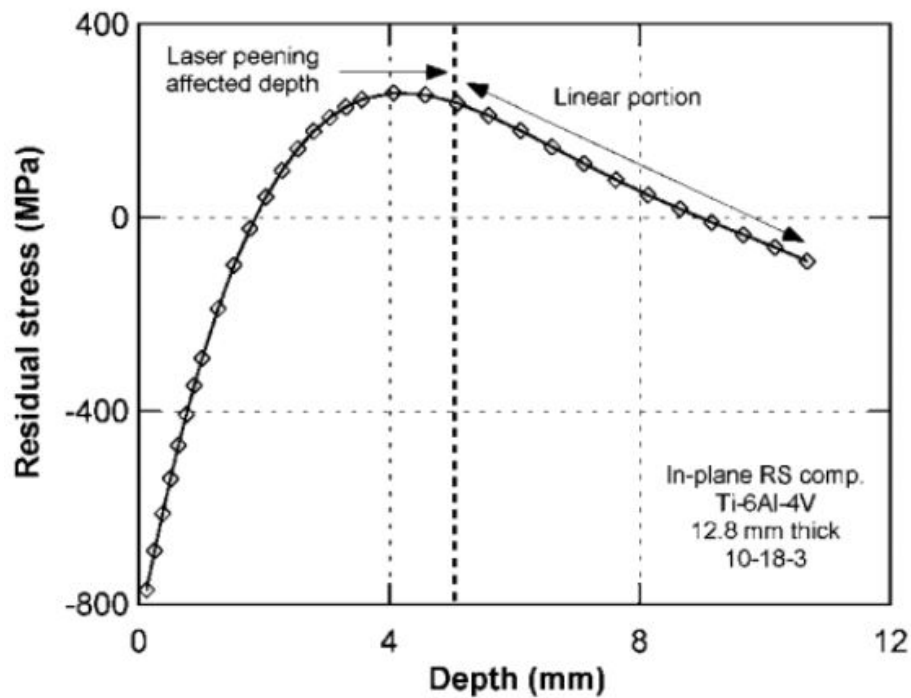


Figure 2.13. Typical residual stress profile of a laser peened specimen [23].

While the compressive RS region compared to other surface treatment methods may be beneficial, the tensile stress field is the greatest concern when a flaw is present in a material. To reiterate, aircraft sustainment engineers must assume a standard

flaw (crack) size to determine damage tolerance, which is the basis for this research. When a surface crack is present within a RS field similar to that of laser peening there is the concern that the summation of tensile RS and applied stress will increase the stress intensity at the crack tip. This increase can result in an increased crack growth rate and reduction in fatigue life. Which is another primary objective of this research. That is to see if LSP is an advantage or disadvantage to the fatigue failure.

2.8 Summary

LSP has shown great potential in the fatigue community, however for the industry to truly embrace the technology, further research is required. The research conducted here provides a small but critical step in the transition of this technology. The remaining chapters will discuss the methodology used and provide results of the research.

III. Research Methodology

3.1 Chapter Overview

To answer the three objectives (Section 1.2) of this research an empirical approach was taken. This testing requires multiple steps of experimentation to be completed in a specific order, to mimic the fundamental structural loading and crack formation. A brief outline of the steps taken are shown in Table 3.1, with subsequent giving further explanations of each step.

Table 3.1. Specimen Process Flow

Step	Name	Section
1	Specimen Machining	3.2
2	Starter Notch Formation	3.3
3	Initial Pre-Cracking	3.4
4	Final Thickness Machining	3.5
5	Pre-Crack Shape Formation	3.6
6	Marker Banding	3.7
7	Laser Shock Peening	3.8
8	Fatigue Testing	3.9
9	Residual Stress Measurements	3.10
10	Fractography	3.11

3.2 Specimen Machining

Specimen were fabricated from five different 18" x 18" x 0.625" (45.72 cm x 45.72 cm x 1.59 cm) (Figure 3.1) plates of aluminum alloy 7075-T651. All five plates were processed from the same batch, and documentation of its chemical composition and AMS certification testing was provided with the material (Appendix B). All specimens are manufactured by wire electrical discharge machining (WEDM) machine to a geometry of 16" x 4" x 0.625" (40.64 cm x 10.16 cm x 1.59 cm) (Figure 3.2). This

specimen geometry is ideal so that the crack and peening area contain a significant amount of material to reduce edge effects.



Figure 3.1. Material size as delivered, five specimens machined out of each plate. Hashed lines in figure show unused material.

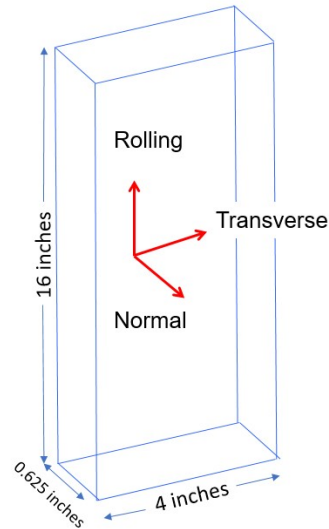


Figure 3.2. Stress Orientation Directions in each Sample

The numbering of the plates is a bi-product of the specimen machining order. As stated, all specimens are cut from five plates and from each plate five specimens are produced; thus the numbering of the plates represents the plate number and the specimen number from that plate (i.e. 5/3, would be the third specimen cut from the fifth plate) Unused specimens were retained as spares and for future work. See Appendix D for additional explanation.

3.3 Starter Notch Formation

Creation of the starter notch is critical to ensuring that the crack originates in the proper location for testing. If the starter notch had not been utilized, crack initiation location could not be controlled. Ensuring the crack is located in the center of each specimen is essential to fatigue results. A center location reduces edge effects from

surfaces not incorporated in the test results. The only incorporated surfaces are the front and back faces of the plate.

The size, shape, location and method of starter notch generation are equally important. The starter notch location is easily determined as the center of one of the plate's broad faces. The final notch size and shape was determined to be a semi-circular filleted groove. This shape is desirable because it only removed material in the direction of expected crack propagation, perpendicular to the load. Additionally, it was chosen for ease of notch generation. A mechanical cutter is used to mill the material. The notch is cut using a CNC milling machine with a 0.020" (.508 mm) diameter ball end mill (Figure 3.3) to cut a semi-circular filleted groove with a radius of 0.050" (1.27 mm). The mill uses liquid coolant to reduce heat buildup, thereby reducing residual stresses imparted into the material during the machining process. Additionally, the machining of the notch was not accomplished in a single pass of the cutting tool. Multiple passes were used to further reduce residual stress generation. A computer generation of the starter notch can be seen in Figure 3.4 and in the profilometer scan of the notch is shown in Figure 3.5.



Figure 3.3. 0.020" Diameter Ball End Mill with Full Radius Tip

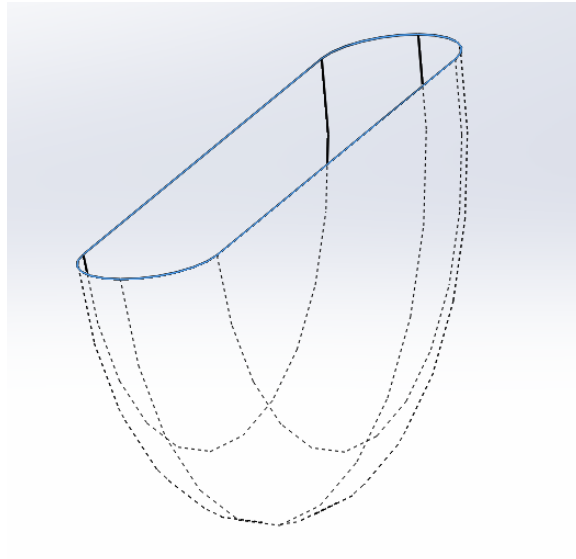


Figure 3.4. 3-D Representation of the Starter Notch.

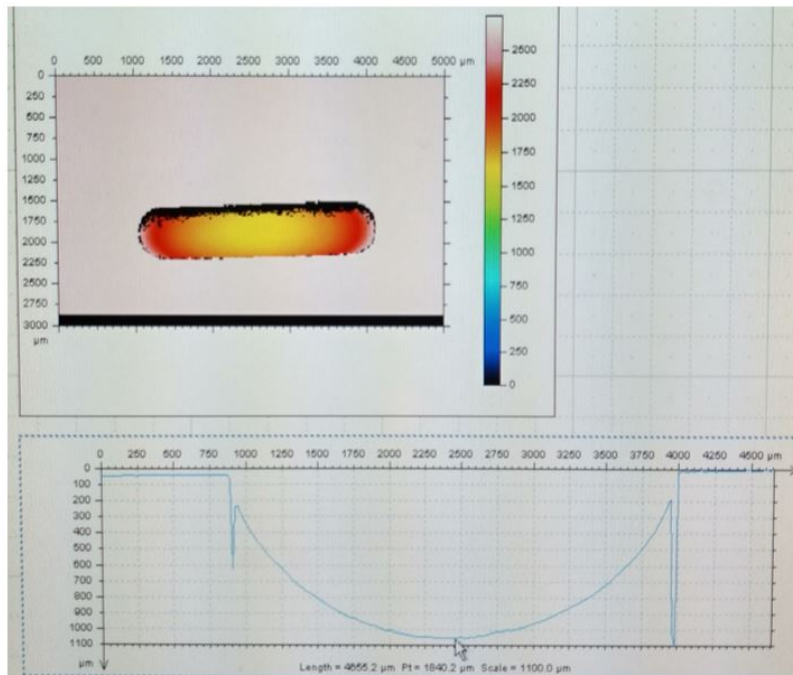


Figure 3.5. Laser profilometer scan data of starter notch. Note that spikes on either side of the lower image are due to extreme non-perpendicularity of the surface and laser.

3.4 Initial Pre-Cracking

Initial pre-cracking step is used to generate a substantial crack in the surface of the material, such that when the surface of the material is removed (Final Thickness Machining Step, Section 3.5) a portion of the crack remains on the surface of the material. Additionally, the remaining crack must have a surface crack length such that the crack can be grown to the minimal detection length of 0.250" (6.35 mm) (Section 3.6).

This step was accomplished by inserting each specimen in a MTS load frame and applying a tensile cyclic loading. (Figure 3.6) The fatiguing of the specimen was conducted under load control to ensure a consistent crack growth and crack front shape.

To promote crack initiation, a stress level of 25.6 ksi (176.5 MPa) was applied to initiate the crack in a shorter number of cycles, rather than the final stress level of 15 ksi (103.4 MPa) with a larger number of cycles. The 25.6 ksi level was determined experimentally, to cause crack initiation in an acceptable time frame. A load ratio of $R = 0.1$ was maintained and applied as a tapered sign wave. The load was then decreased by 10% when both the left and right crack length grew by 0.010" (0.254 mm), which is outlined in ASTM E647. This would allow for an even and standard load shedding, minimizing load sequence effects. The load was shed down (reference 2.5) to the final stress level of 15 ksi (103.42 MPa); then maintained at that stress level until the total length of the crack reached 0.030" (7.62 mm). Crack lengths were measured using a load frame mounted traveling microscope with 20X magnification and a 1.26" (32 mm) focal length (shown in Figure 3.6). Crack tip measurements are taken from crack tip to crack tip and are inclusive of the starter notch. Load shedding was conducted under incremental steps shown in Table 3.2.

Table 3.2. Incremental Load Shedding

Force		Cross-Sectional Area		Stress	
lbf	N	in ²	cm ²	ksi	MPa
64000	284.68	2.5	16.129	25.60	176.51
57600	256.22	2.5	16.129	23.04	158.86
51840	230.60	2.5	16.129	20.74	143.00
46656	207.54	2.5	16.129	18.66	128.66
41990	186.78	2.5	16.129	16.80	115.83
37500	166.81	2.5	16.129	15.00	103.42



Figure 3.6. MTS Load cell with traveling microscope attached

3.5 Final Thickness Machining

The material was required to be machined to a final thickness of 0.350" (8.89 mm) thickness for various reasons: the thickness more closely emulates the thickness of generic aircraft structural members; to remove the starter notch prior to LSP application; to remove grain size variation through the thickness of the material.

Aircraft structural member thickness varies greatly between components based on many different factors (too many to list here). The thickness chosen was both adequate to represent common thicknesses present in typical aircraft structure and so that these surface flaws would spend a majority of their life growing through the thickness before transitioning to through-thickness flaws. Additionally, the thickness needed to be reduced to remove the starter notch. The starter notch removal requirement was crucial to ensuring that the pressure wave generated from the LSP process did not reflect off of the surfaces of the notch potentially causing different residual stress profiles in the specimens near the starter notch.

The variation in grain sizes through the thickness was due to the initial material processing by the manufacturer. The material forming process caused an elongation and flattening of the top and bottom surface grains. It was determined that limiting the variation in grain sizes in the final specimens would be desired due to the possibility of crack growth variations between the various grain sizes and effects of LSP on the different grain sizes [24]. Figure 3.7 is a micrograph of the internal structure through the thickness dimension of the plate. The lines (red-hatching) on Figure 3.8 represent the material removed and the remaining material (bound by green lines) is the final specimen thickness.



Figure 3.7. Grain structure through the thickness of as received material. Note variations in grain sizes from top/bottom edges to the center.

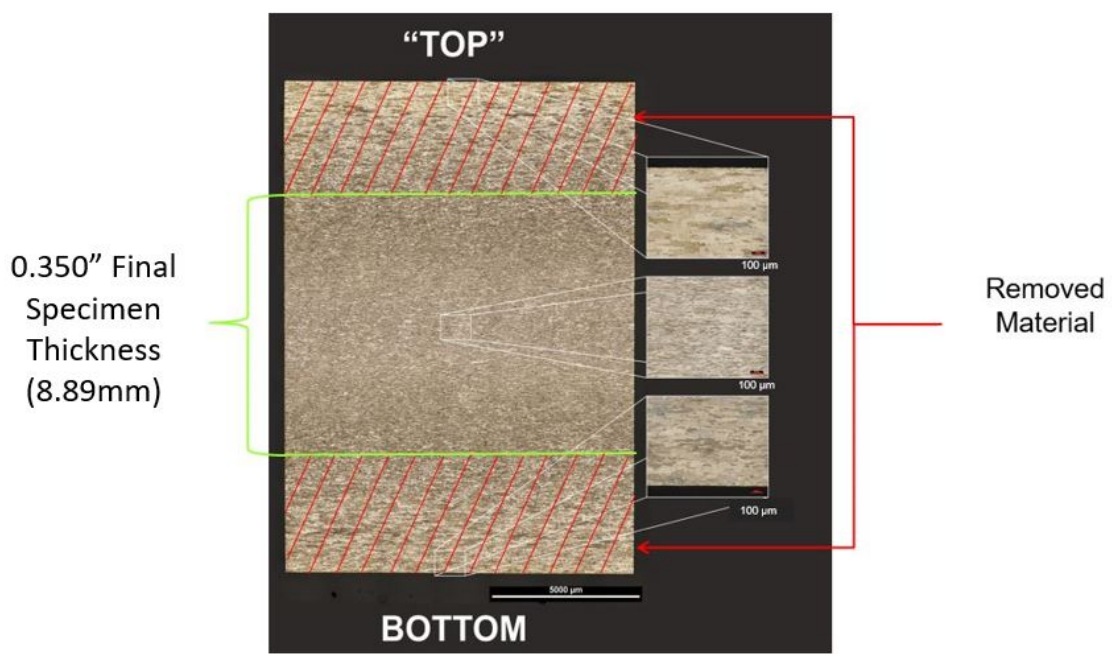


Figure 3.8. Final specimen thickness with areas of material removed.

When trying to maintain consistency between specimens, care was taken to define specific procedures. A variation in the removed material between sides/specimens will result in a variation of remaining surface crack length ($2c$), amount of warping, and in this case the grain structure variation through the thickness. The specimens had material removed in stages during the machining process. Anytime material is machined internal stresses will be released, especially when altering the materials thickness [19]. Unfortunately, these specimens for this work required 44% of the original material thickness be removed to reach the desired final thickness: this is a significant amount of material. The specimens were then flipped from back to front in the CNC mill during material removal to allow stress relief in stages in an attempt to limit variation in warping between specimens. Specific steps are outlined in Appendix A.

3.6 Pre-Crack Shape Formation

Once the pre-cracks have been grown and the machining process completed, the resulting internal shape of the crack is not representative of a naturally grown crack. These resulting cracks have shallower depth to surface ratios (a/c) and the surface crack length would be shorter than the desired final crack length of 0.250" (6.35 mm). The specimens were loaded back into the MTS load frame and fatigued at the same stress level of 15 ksi (103.42 MPa), with a load ratio of $R= 0.1$, identical to the initial pre-cracking step.

When the desired final crack length of 0.250" (6.35 mm) was reached in the final thickness specimen, as verified by the traveling microscope, a series of varied load ratio cycles called a marker band were applied. The marker band is used to mark the position of the crack face prior to LSP application. This step was crucial for post-mortem examination of the fracture surface. The marker band will be explained

in the following section.

3.7 Marker Band Development

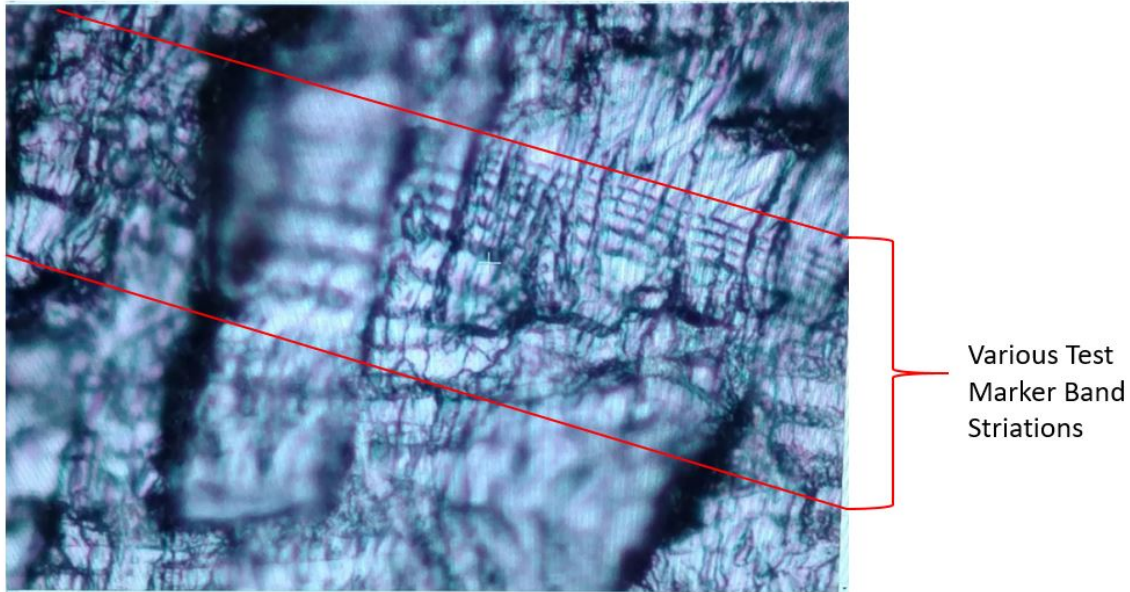


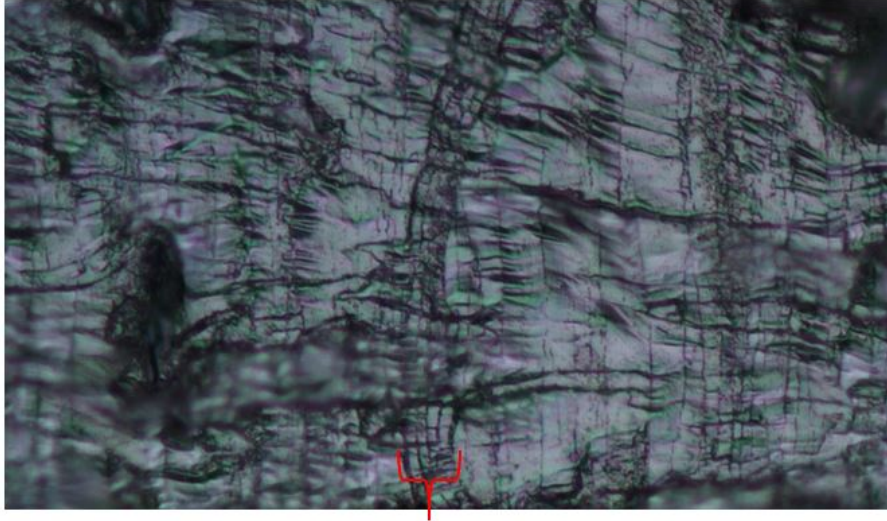
Figure 3.9. Fractured Surface Showing the Marker Band Experimentation.

The marker band sequence used was determined experimentally during the initial pre-cracking stage (Section 3.4). Testing was accomplished by varying the loading parameters (number of cycles and load ratios (R)) to generate various marker band sequences (Figure 3.9). The results of these sequences are not externally visible during the fatigue test. Once the specimen is fractured and the fracture surface is examined can any parametric effects be determined. These specimens were optically inspected using a Nikon MM-60 optical measuring microscope with a Metronics Quadra-Chek 2000 digital readout. Figure 3.9 shows the three types of marker bands tested: the load ratio remained the same across all sequences ($R=0.75$ for the dark striations and $R=0.1$ for the light striations) and the cycle count at each ratio was varied. From the top of Figure 3.9 down the number of cycles were doubled from 250/25 to 500/50 to 1000/100 to create the light and dark striations, respectively.

The sequence chosen was the 250/25, shown at the top of Figure 3.9. It was chosen for its visibility during slower crack growth (during a shorter surface crack length) and during faster crack growth (near critical crack length of specimen). Additionally, considerations were made to ensure marker band growth did not contribute substantially to the overall crack growth. The marker band sequence that was decided upon is shown in Table 3.3. In an attempt to further distinguish the marker band from the surrounding constant amplitude striations, an additional severe marker band was applied on either side to further demarcate the two(500 cycles at R=0.75) (Figure 3.10).

Table 3.3. Marker Band Sequence

Cycles	Load Ratio (R)	High Load		Low Load	
		lbf	kg	lbf	kg
500	0.75	21000	9525.4	15750	7144.1
25	0.1	21000	9525.4	2100	952.5
250	0.75	21000	9525.4	15750	7144.1
25	0.1	21000	9525.4	2100	952.5
250	0.75	21000	9525.4	15750	7144.1
25	0.1	21000	9525.4	2100	952.5
250	0.75	21000	9525.4	15750	7144.1
25	0.1	21000	9525.4	2100	952.5
500	0.75	21000	9525.4	15750	7144.1



Marker Band

Figure 3.10. Fractured surface showing the Marker Band.

3.8 Laser Shock Peening

LSP was applied over the cracked region for each designated LSP specimen replicate. While both LSP processes were similar, laser parameters do not translate exactly between laser systems. Variations in LSP parameters were necessary due to the fundamental differences between square and circular spot shape systems. Initial LSP parameter testing was accomplished with the circular spot shape laser to determine adequate laser parameters to increase fatigue performance. As mentioned previously in Section 3.8, the key parameter that can be translated between various laser systems is the power density. As a reminder, the equation for power density is

$$LaserPowerDensity = \frac{E}{PW * A} \quad (3.1)$$

Where the Energy term is the average energy output of the laser in Joules, PW is the pulse width per impact in nanoseconds, A is the area of the laser impact. The power density, laser energy, pulse width, and spot size of the initial testing were

provided for reference to the company accomplishing the square spot laser peening. Explanation of the initial testing and peening process is discussed next.

3.8.1 Laser Energy and Number of Application Determination

The crack position as related to the tensile RS field could potentially cause an increase in fatigue crack growth rate (Section 2.4). Attempting to place the transition point of the RS field (reference 2.13 near the tip of the crack was the driving factor in the determination of the number of LSP applications and the laser energy. The magnitude and depth of the compressive residual stress imparted into the material increases with repeated applications until saturation is reached. Thus, the decision was made to use two applications to have the highest probability of ensuring the depth and magnitude of compressive stress is adequate. This decision was not difficult, however the lasers energy level decision required testing.

The determination of the appropriate laser energy level is of great concern for the LSP process (reference Chapter 3.8). Experienced researchers using circular spot laser system and this spot size are in the process of conducting research on 7075-T6 aluminum and their experience led them to speculate that the saturation point may be near 3 Joules (reference Section 3.8). This portion of testing used a sample of unused material to verify this saturation energy. The material was machined using the same process as the primary specimens ending at a final thickness of 0.350" (8.89 mm). The test piece had two different 0.4" x 0.4" (1 cm x 1 cm) LSP patches applied, one with an energy level of 2.5 Joules and the other with an energy level of 3.5 Joules. (Figure 3.11). The surface residual stress was measured at the center of those patches using X-ray diffraction (Section 2.4.2.1). The measured results showed near 4.3 ksi (30 Mpa) increase in surface compressive residual stress from 2.5 to 3.5 Joules. Thus the decision was made to proceed with an energy level of 3.5 Joules for the primary

specimens.

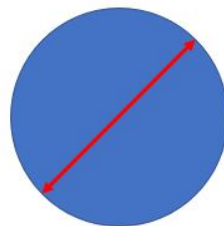


Figure 3.11. Energy Level Test Samples. (Left image shows the test with a laser energy of 2.5 J with two applications. Right show the test with a laser energy of 3.5 J with two applications.)

3.8.2 General LSP Parameters

The LSP application was only applied on a single side (over the crack) of the specimens with the crack positioned roughly in the center of the peened area in both directions. The decision to peen one side was made to mimic an LSP process that would likely occur on the aircraft (to only one side of the component accessible). The list below shows key parameters of the circular spot LSP process.

3.8.2.1 Circular Spot Laser Parameters



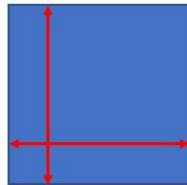
Ø 0.0807 inches
(2.05 mm)

Figure 3.12. Circular Spot Laser Peening Cross-Section

Table 3.4. Circular spot laser parameters

Spot Geometry	Circular, Diameter of 0.0807" (2.05 mm)
Laser Energy	3.5 J
Pulse Width	20-22 ns
Power Density	4.8 $\frac{GW}{cm^2}$
Number of applications	2 (4 offset sequences per application)
Peened Area	Approximately 2" x 2" (50 mm x 50 mm)
Ablative Material	Opaque tape, Single layer (3M471, Black)
Transparent Overlay	Deionized flowing water

3.8.2.2 Square Spot Laser Parameters



0.160 inches square
(4.70 mm)

Figure 3.13. Square Spot Laser Peening Cross-Section

Table 3.5. Square spot laser parameters

Spot Geometry	Square, 0.160" x 0.160" (4.07 mm)
Laser Energy	16 J
Pulse Width	18 ns
Power Density	4.02 $\frac{GW}{cm^2}$
Number of applications	2 (offset)
Peened Area	Approximately 2" x 2" (1st applications 52 mm x 52 mm, 2nd application 48 mm x 48 mm)
Ablative Material	Aluminum tape, 2 layers (3M427)
Transparent Overlay	Deionized flowing water

3.8.3 Sample Mounting Fixture

The use of a mounting fixture was employed to expedite the LSP process. This fixture also helped to ensure the repeatability of the LSP location. The specimen can easily be detached from the robotic arm to allow for easier replacement of the ablative material. The fixture shown in Figure 3.14 was used for the circular spot laser peening applications. The fixture used to accomplish the peening of the square spot laser applications is shown in (Figure 3.15). Based on the laser technician's previous experience the peening process is insensitive to the stiffness of the fixture.



Figure 3.14. Circle Spot Laser Peening Fixture

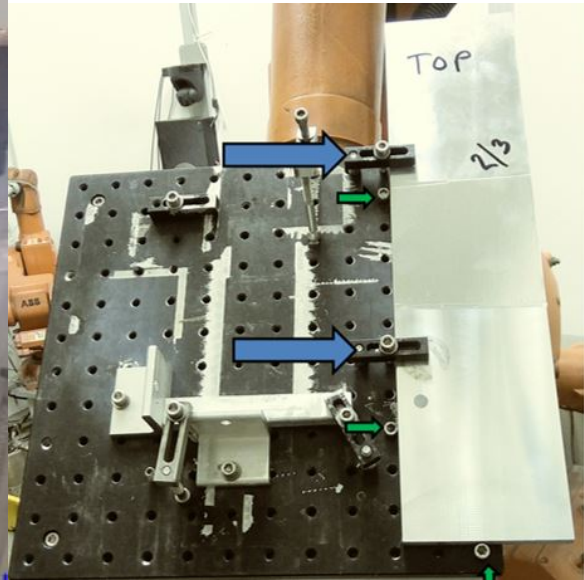


Figure 3.15. Square Spot Laser Peening Fixture

3.8.4 LSP Application Process

The process of LSP application is similar in both cases with some key differences that must be addressed. A detailed explanation of the process is discussed in paragraph 3.8.4.1. The differences and explanations as to why they arose are discussed in Sections 3.8.4.1 and 3.8.4.2.

3.8.4.1 Circular Spot Laser Peening Process

The circular spot LSP process consisted of two applications. Each application consisted of four sequences. Thus for specimens receiving the circular spot laser peening process, each specimen received a total of eight LSP treatments. This pattern

was provided by the experienced technicians with this particular laser system.

The specimens were peened one after another by being mounted into the support fixture, which was connected to a robotic arm. The robotic arm was programed to translate the specimens into the path of the laser and accomplish all repositioning for each laser impact thereafter. Each application sequence was applied in a unidirectional linear pattern running parallel to the width (4") of the plate (Figure 3.16). The plate was then relocated with the robotic arm so that each successive row was applied above the previous row with zero overlap. Each sequence was completed after the 2" x 2" (50 mm x 50 mm) peening area was completed. The specimen (remaining mounted in the fixture) was removed from the robotic arm (Figure 3.17) to replace the ablative layer (see Appendix C) for ablative layer images). Once the fixture and specimen were reattached to the robotic arm this process was repeated for the subsequent sequences.

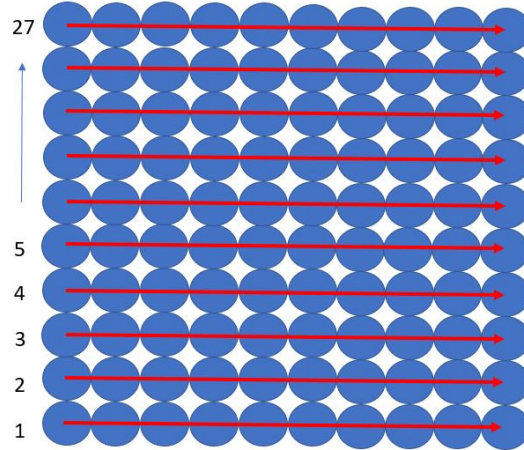


Figure 3.16. Circular Spot Laser Peening Path for Each Sequence



Figure 3.17. Robotic Arm Used to Relocate Sample in Beam's Path

All sequences were applied with rows of peening that have zero overlap between individual shots within the same layer. This zero overlap ensures that there is ablative material present over the entire area for the individual shots. To ensure full coverage of the desired surface, each sequence must be offset. The second sequence was offset by one radius to the right of the first sequence. The third sequence was offset one radius up from the first sequence. The fourth sequence was offset both to the right one radius and up one radius from the first sequence. Each of the four sequences are shown in Figure 3.18. Additionally, the second application, which again consisted of 4 separate offset sequences, was offset to the right and up one half of the radius of the first sequence of the first application (Figure 3.19). This additional offset further distributes the coverage of the peening process.

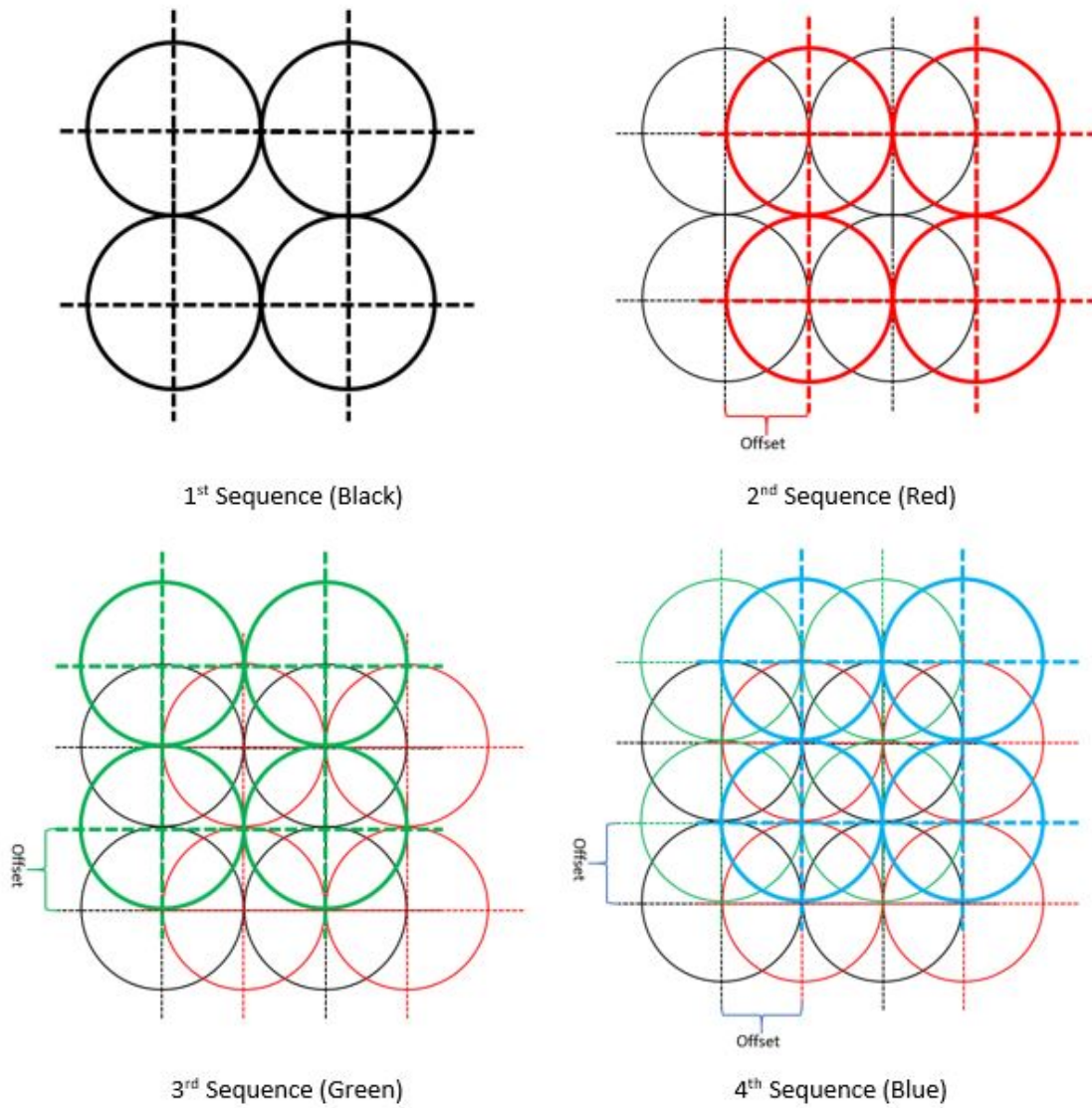


Figure 3.18. All Circular Spot Laser peening sequence patterns showing the offset for each.

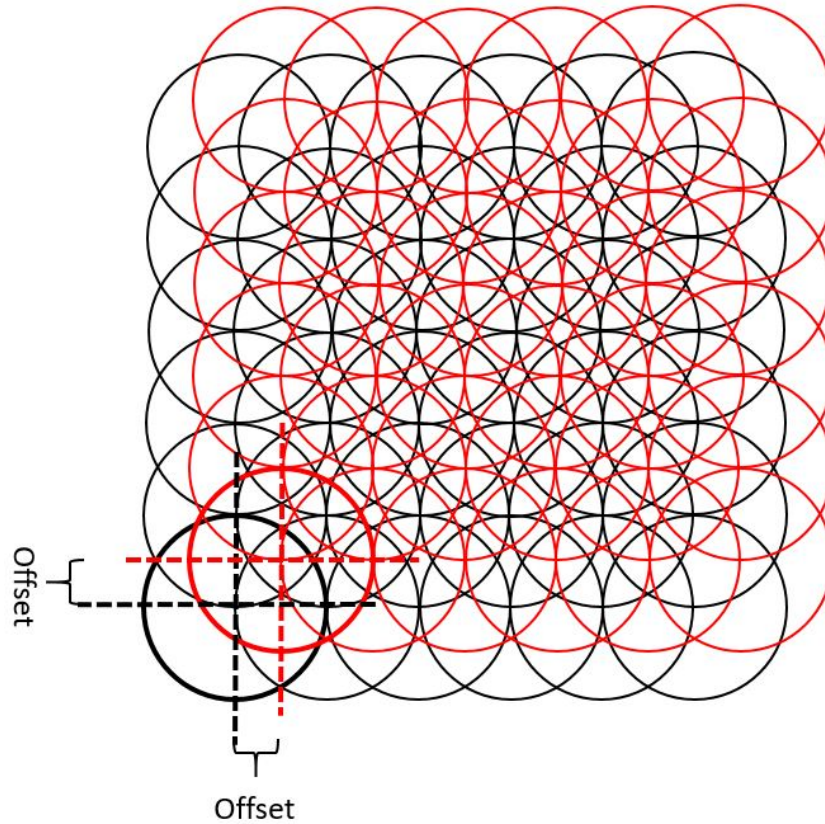


Figure 3.19. Circular Spot Laser Application Offset

3.8.4.2 Square Spot Laser Peening Process

The peening process used for the square spot laser was similar to the circular spot laser peening process. Each application is applied with rows of peening that have zero overlap between individual shots within the same layer. The pattern was applied in the same pattern starting from the bottom left corner (see Figure 3.20).

The primary difference between the peening processes is the result of the spot geometry being a square versus a circle. The square spot laser allows for fewer applications as each spot is directly adjacent to the previous shot, providing 100% coverage per layer (Figure 3.20) Based on the advice of the laser system scientist, a decision was made to only use two applications for this peening method. The second

application was offset both vertically and horizontally by half the spot size. (Figure 3.21) Additionally, the second layer size was smaller than the first by half of a spot size along all edges. Experienced personnel proposed this size change to dissipate the resulting stress field exterior to the peened region.

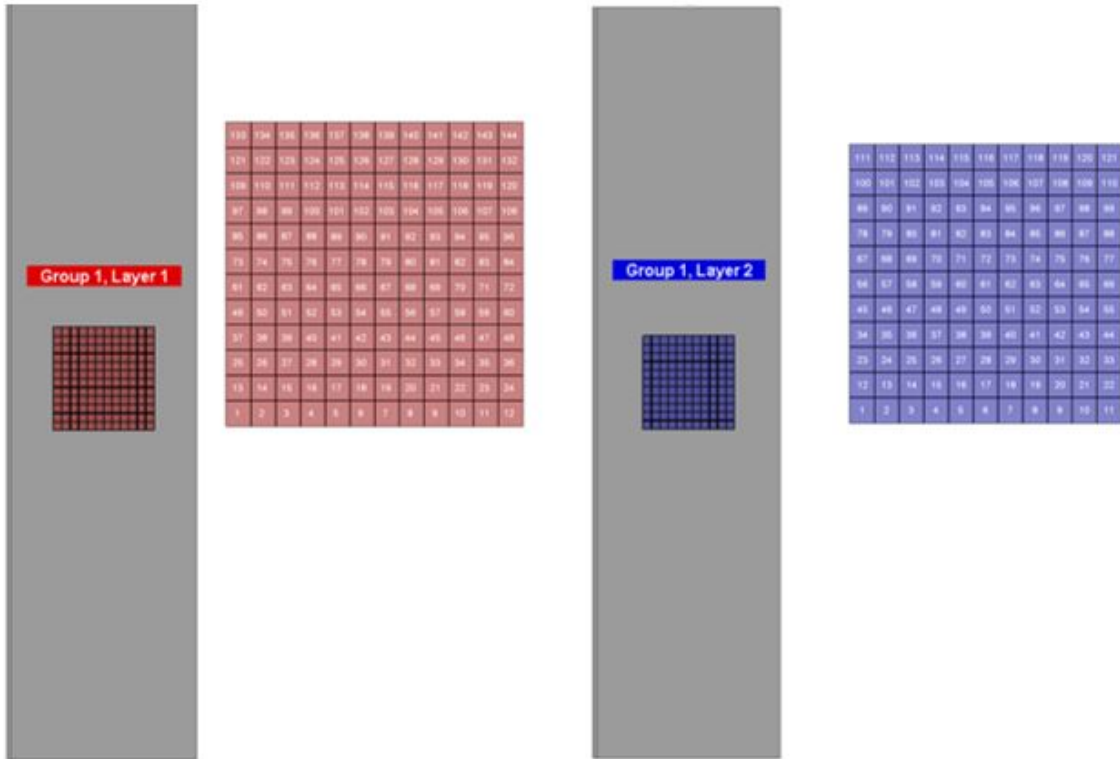


Figure 3.20. Square Spot Laser peening patterns for each application.

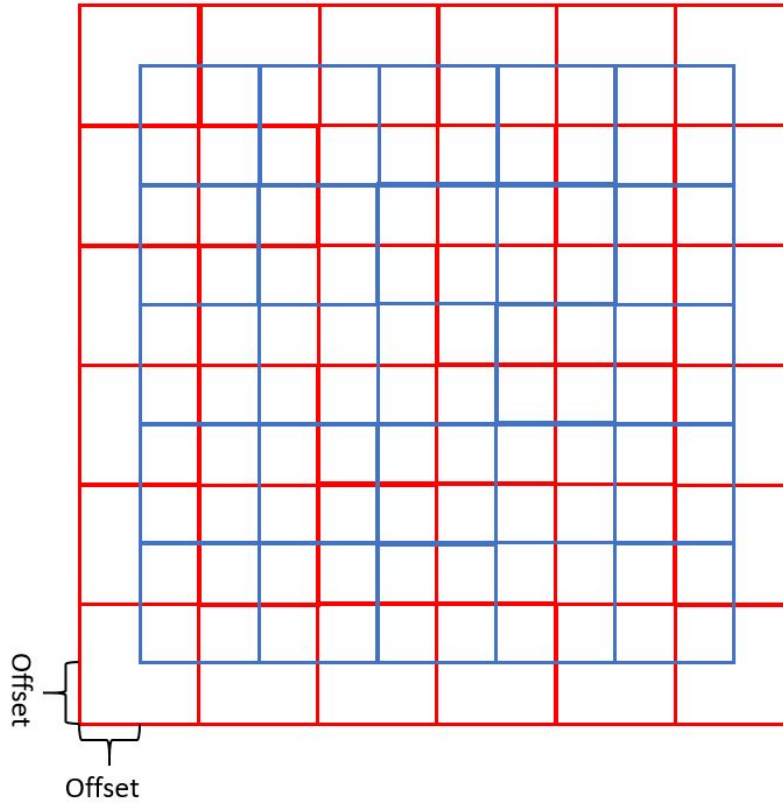


Figure 3.21. Square Spot Laser Application Offset

3.9 Fatigue Testing

Fatigue Testing was accomplished in a MTS load frame. Each specimen was mounted such that the specimens were loaded in pure tension. They were then cyclically fatigued at the same stress level and load ratio as when the cracks were generated, 15 ksi (103.4 MPa) and $R = 0.1$ respectively (Figure 3.22). Cyclic loading is applied as a sine wave verses the tapered sine wave used to generate the pre-crack. Ten thousand cycles of constant amplitude loading were applied to the specimens followed by a marker band load sequence.

If the crack is visible at the surface of the specimen (using the 20X magnification traveling microscope), the crack is measured after each 10,000 cycle blocks and after the subsequent marker band. The process of fatiguing the specimen, inspecting/mea-

suring the cracks length, applying a marker band, and inspecting/measuring the crack length was repeated until 60 thousand cycles was reached. This 60 thousand cycle threshold was set based on the number of cycles-to-failure of the unpeened specimens. If this cycle threshold was reached in the peened specimens, then they were allowed to cycle to either complete ligament failure or run-out is reached (one million cycles). Specimen run out was accomplished by repeating the application of 10 thousand cycles and a marker band sequence, without the requirement of inspecting/measuring the crack lengths. The one million cycle endurance limit was determined as being the point at which infinite life would typically be considered [25].

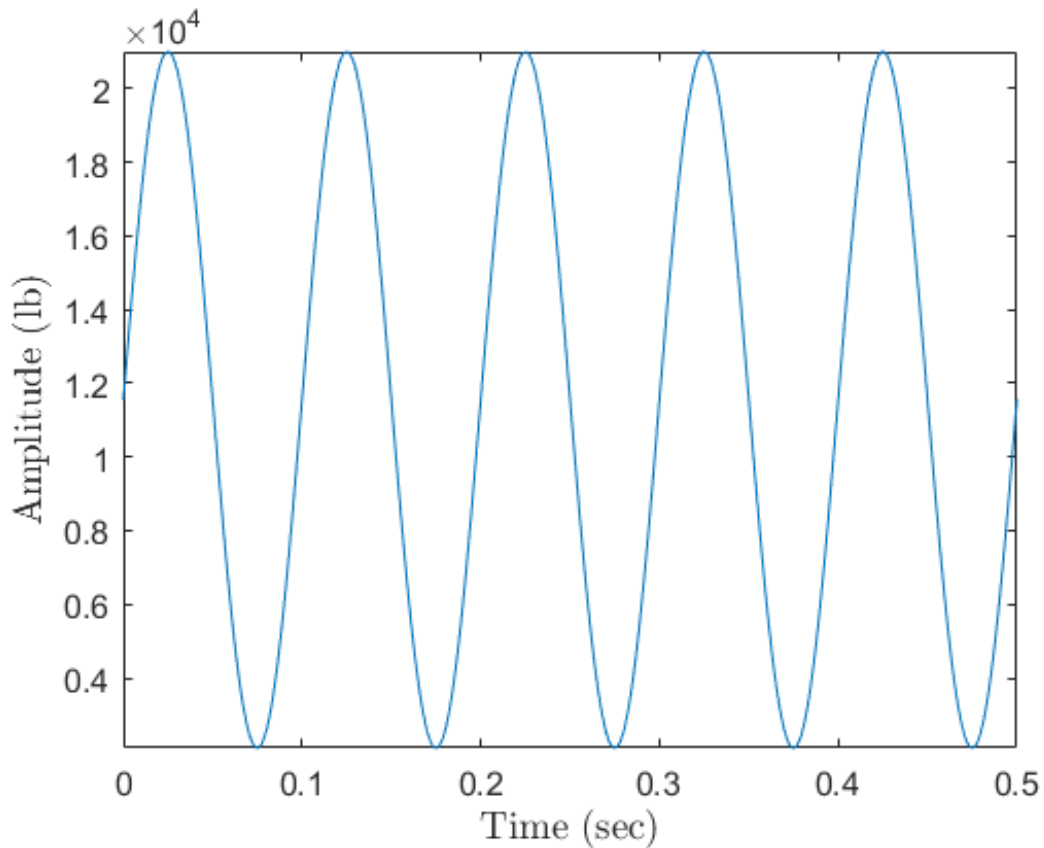


Figure 3.22. Cyclic Applied Load Depiction

3.10 Residual Stress Measuring

Residual stress measurements were taken by various methods to understand the imparted stresses from the laser peening processes. The use of destructive, partially destructive and nondestructive stress measuring techniques was employed; X-ray diffraction with layer removal, incremental hole drilling, and neutron diffraction, respectively. All measurements were accomplished by experienced and qualified personnel. All specimens were LSP processed and then evaluated for residual stress. Each of the two different types of peening processes were evaluated differently due to scheduling constraints, however incremental hole drilling was accomplished on both LSP processes. All residual stress measurements for each type of peening will now be discussed.

3.10.1 Circular Spot Laser Peening Residual Stress Measurement Techniques

The residual stresses of the circular spot laser peened specimens were measured using multiple techniques. One of the circular spot laser peened specimen was sent to an external agency, Hill Engineering LLC., to have the internal residual stresses measured by incremental center-hole drilling (accomplished per ASTM E837). The measurements were taken in an area of the peening (remote from crack location) and an area remote from the peening and gripping areas (Figure 3.23).

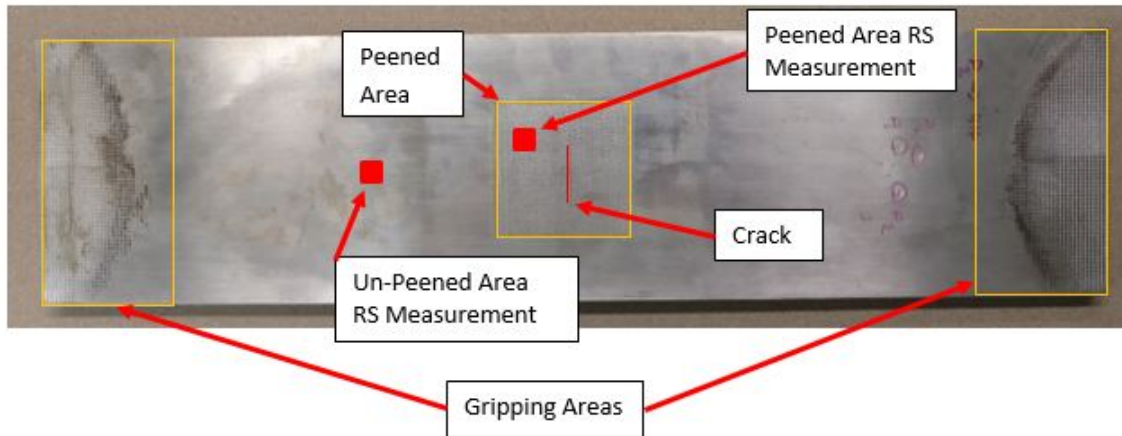


Figure 3.23. Residual Stress Measurement Areas for Hole Drilling

A specimen was also transported to the Canadian Neutron Beam Center, Chalk River Laboratories, Chalk River, Ontario Canada to accomplish Neutron diffraction RS measurements. The beam line used in the nuclear reactor (L3) was prepared prior to specimen arrival by installing a germanium crystal in the primary neutron path. The germanium crystal refracts a specific neutron wave length of 1.727 angstroms into the specimen. This wave length of neutrons was recommended by the neutron beam line scientist for use with aluminum alloys, which have a face-centered cubic (FCC) crystalline structure. The $\{311\}$ and the $\{220\}$ crystalline planes that were measured. The variation in crystalline plane measurements is likely due to the grain structure of the material in one direction being elongated, likely due to initial material processing.

The neutron diffraction measurements were accomplished such that RS measurements could be obtained through the thickness of two separate points of interest; within the peened area presumably at the crack plane and remote from the peened area. The location of the crack was not optically visible post-LSP application with either high magnification (100x) or with florescent dye penetrant and black light. These locations can be seen in Figure 3.24.

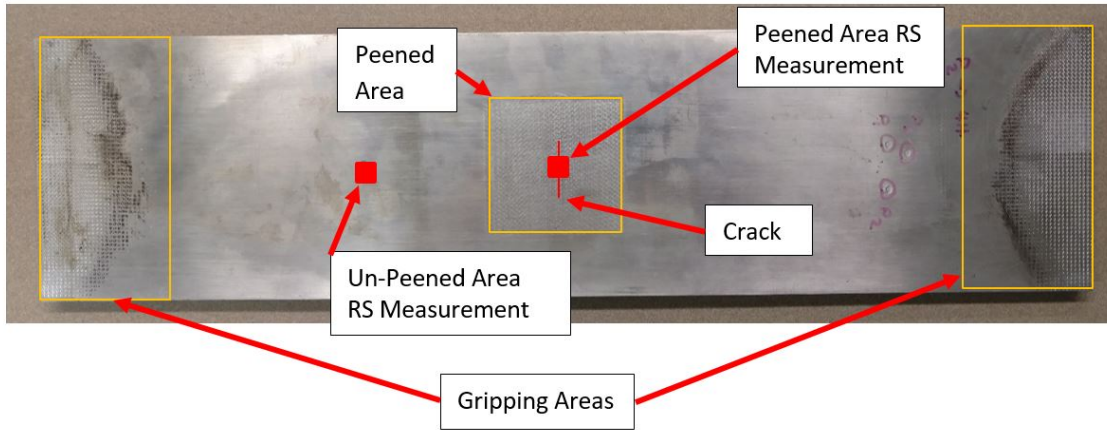


Figure 3.24. Residual Stress Measurement Areas for Neutron Diffraction

Each neutron diffraction measurement is measured through the thickness of the specimen. The gauge volume used for all neutron measurements is 0.0118" x 0.0118" x .2362" (0.3 mm x 0.3 mm x 6 mm). For completeness, Figure 3.25 shows a representation of the orientation of the gauge volumes used at each location to generate data.

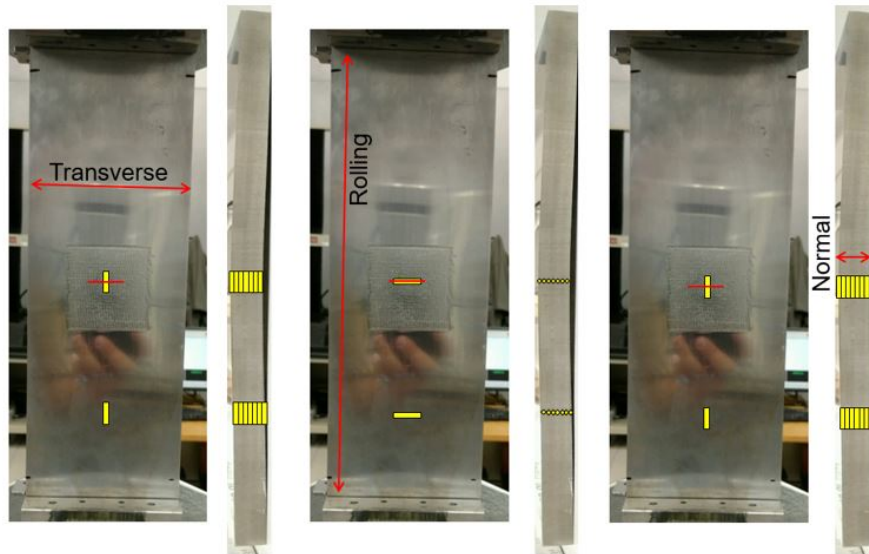


Figure 3.25. Neutron Diffraction Gauge Volume Representations Used for Each of the Three Strain Directions. (Not to Scale)

3.10.2 Square Spot Laser Peening Residual Stress Measurement Techniques

The square spot laser peened specimens had RS measurements accomplished by incremental center-hole drilling and X-ray diffraction with layer removal. The specimens were not completed with the peening process in time for the neutron diffraction experiment, thus this technique was not accomplished on this type of peening. The incremental hole drilling was accomplished in the same manner and at the same locations as previously described (Figure 3.23).

Another specimen was sent out for X-ray diffraction with layer removal. The specimen had measurements accomplished within the peening area and outside the peening area (Figures 3.26 3.27). These measurements were conducted using a cobalt-potassium (Co-K alpha) target with an aperture of 2 mm, employing a 3-degree oscillation during the measurements.

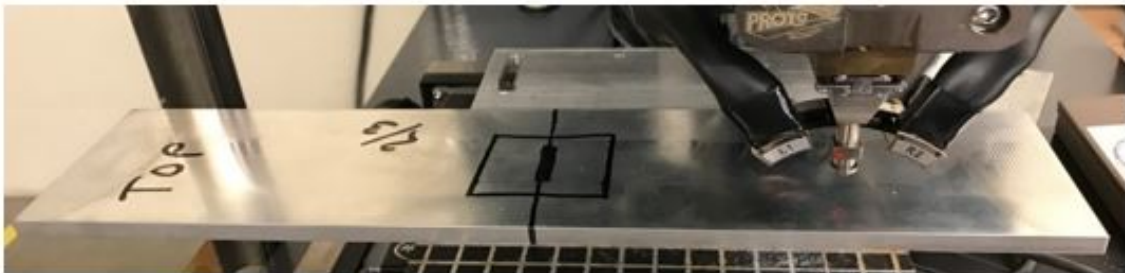


Figure 3.26. Unpeened Residual Stress Measurement Area for X-Ray Diffraction

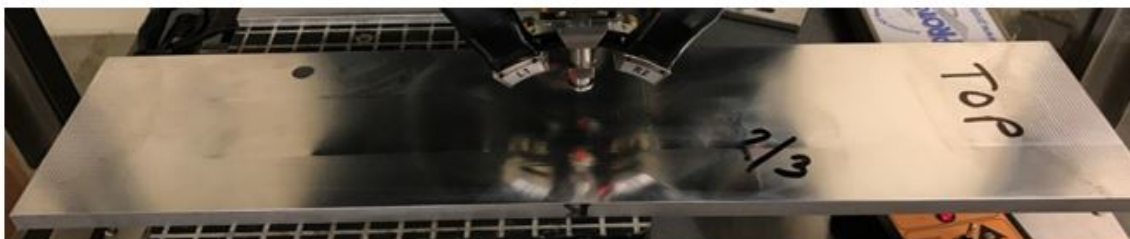


Figure 3.27. Peened Residual Stress Measurement Area for X-Ray Diffraction

3.11 Fractography

“Fractography is the interpretation of features observed on fracture surfaces” [26] to determine the cause of component failure. The purpose of this fractographic analysis was to map the crack face propagation through the specimens and understand the effects of the LSP process on the present partially-through the thickness surface crack. Thus the fidelity requirement of an SEM was not required. The approach used only required the use of an optical microscope with a calibrated measuring device to map the crack growth in the specimens (Figure 3.28) The use of marker bands was the critical component to ensuring an optical microscope would be sufficient to see and map the crack growth. This approach reduced research time dramatically.



Figure 3.28. Optical microscope with integrated XY measuring table.

3.12 Summary

This chapter presented the procedures followed to test, measure, and evaluate the effects of two different Laser Shock Peening processes over the top of a minimally detectable partially-through the thickness surface crack. The procedures used to understand the crack shape and marker banding sequence in the material is a critical component to the overall research and any future research involving other materials. The use of marker bands was a unconventional approach to fractographic analysis which avert the use of scanning electron microscopy. Analyses and results of the various phases described in this chapter will be presented in Chapter IV.

IV. Results and Discussion

4.1 Chapter Overview

This chapter will discuss the results of this research and how they address the objects. To remind the reader, there are 3 objectives:

- Does the presence of a minimal detection level surface crack affect the Laser Shock Peening Process?
- Does the presence of a minimal detection level surface crack prior to LSP application cause detrimental effects to the fatigue life?
- Investigate above objectives of two cross-sectional laser shapes, circular and square.

4.2 Initial Crack Shape Investigation

Understanding how the crack propagates through the material is crucial for determining the crack length to use for the initial pre-cracking step. Two test pieces, manufactured from the same material, were fabricated and fatigued in the same manner as the primary research specimens through the initial pre-cracking step but with the following dimensions: 8" x 4" x 0.625" (203.2 mm x 101.6 mm x 15.875 mm). These test pieces were fatigued until a one inch crack was grown on the surface, utilizing the procedures in Section 3.9. The first test piece then had an increasing load applied, causing unsteady crack growth inducing failure of the ligament. The fracture surface was inspected and marker bands mapped. The a/c ratio was calculated for each marker band (Table 4.2) and used to determine a crack length to test on the next test piece. The second test piece crack was grown to 0.425" during the initial pre-cracking step, then machined to the final thickness of 0.350" (8.89 mm) per Section 3.2 and then fatigued to failure. The fractured surface was inspected and mapping of

the marker bands was accomplished (Table 4.2). Figure 4.1 shows the fracture surface of the two test pieces.

An initial prediction of crack shape was obtained by through the use of AFGROW, a common crack prediction tool used in the field. AFGROW predicts an a/c ratio that varies between .84 and 0.97, depending on the criterion for fracture. When comparing the predicted a/c ratio to actual test results it showed an under estimation in test piece one (no machining) and an under estimation in test piece two (machined to final thickness). This is graphically shown in Figure 4.2.

Table 4.1. Specimen Fatigue Results

Sample number / Marker Band	2c (inches (mm))	a/c
1 / 1	.249 (6.32)	1.267
1 / 2	0.519 (13.18)	1.235
1 / 3	0.816 (20.73)	1.071
1 / 4	0.839 (21.31)	1.143
2 / 1	0.348 (8.84)	0.710
2 / 2	0.373 (9.46)	0.730

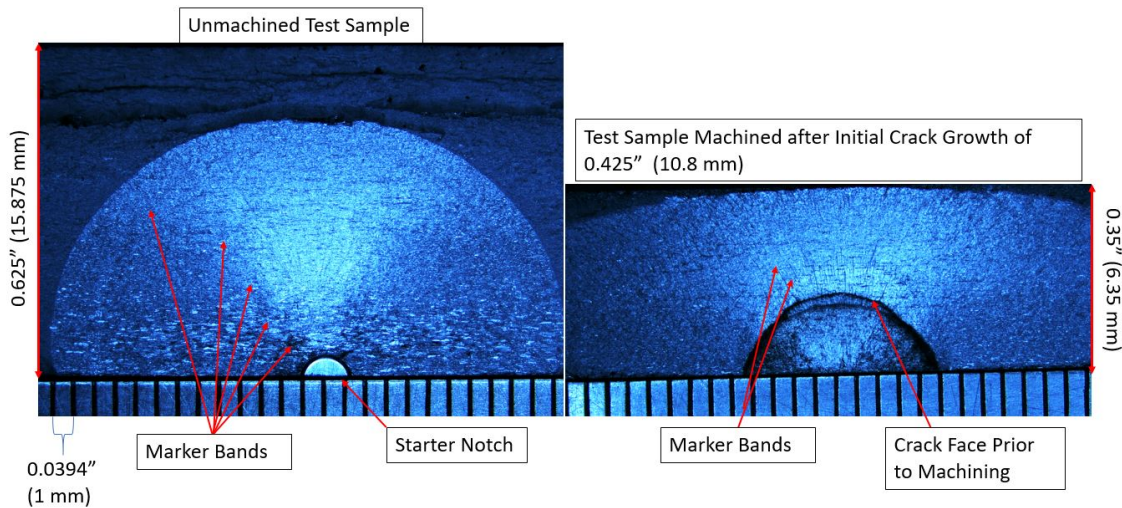


Figure 4.1. Test samples for crack shape investigation

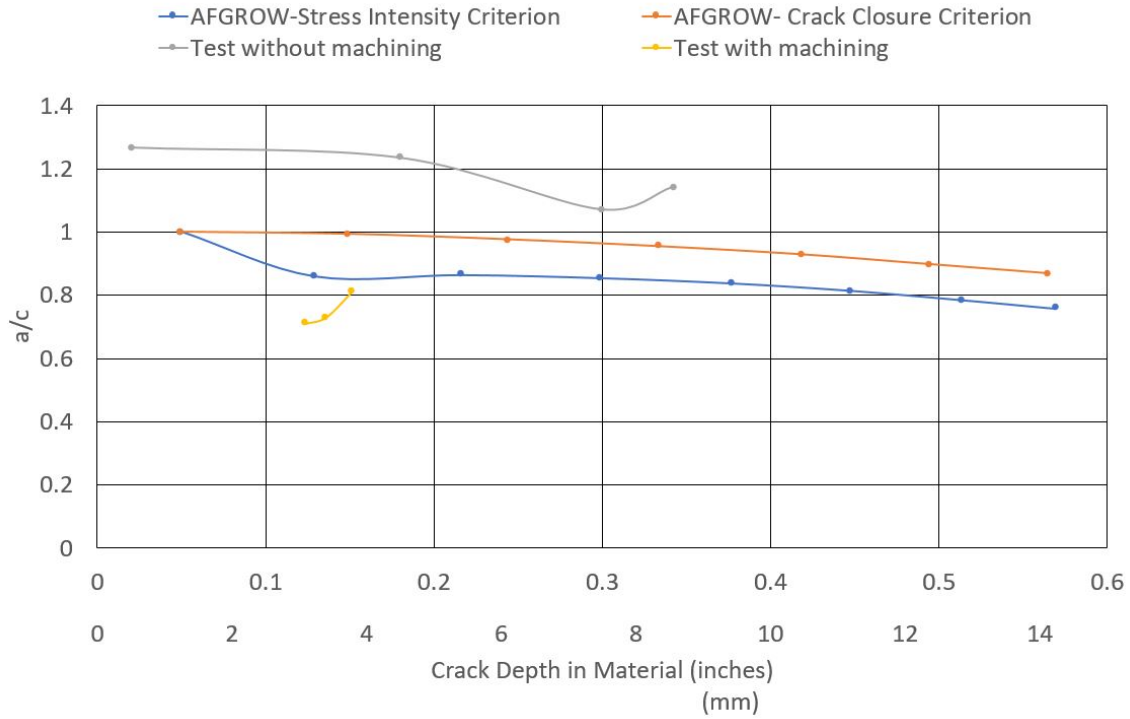


Figure 4.2. Crack Ratio vs. Crack Depth

It is hypothesized that the over estimation is due to RS in the material not accounted for in the model. Further investigation is not required because the reason for this portion of the test was to generate and predict a crack growth in this 7075-T651 aluminum for the Initial Pre-Cracking step (Section 3.4). The crack is required to meet the following criteria; large enough to allow for surface machining while leaving a portion of the crack in the material and to ensure that the surface length of the crack (2c) remaining is not above the 0.250" (6.35 mm) final crack length requirement of Pre-Crack Shape Formation Phase (Section 3.6). It is determined that a surface crack of (2c) 0.300" (7.62 mm) would accommodate both criteria.

4.3 Specimen Crack Shape Results

Once the research specimens fractured the surfaces were inspected and marker bands mapped using an optical microscope. The first applied marker bands were of

primary concern to identify the shape of the crack and depth of the crack prior to LSP application and fatiguing. During inspection it was noticed that the crack expanded under the material surface creating a cupping effect. Thus, reported crack length in Table 4.2 has both values, the measured surface crack length (2c) and the maximum crack length (2c max). The variation is minimal but for completeness was reported here.

Table 4.2. Specimen Crack Shape Measurements (Only reported in British units)

Spec.	2c Pre- Milling (in)	2c Post- Milling (in)	2c Post Pre-Crack Shape Form. (in)	2c max Surface (in)	a (in)	a/c Surface	a/c Max
3/3	0.3030	0.2225	0.2510	0.25404	0.11582	0.916	0.912
4/5	0.3000	0.2565	0.2620	0.26458	0.1134	0.859	0.857
2/4	0.3000	0.1660	0.2500	0.25266	0.12252	0.978	0.970
5/1	0.3010	0.2530	0.2530	0.25300	0.08618	0.694	0.694
4/2	0.2995	0.2230	0.2530	0.25866	0.12790	0.996	0.989
1/2	0.3015	0.2000	0.2505	0.25500	0.11798	0.933	0.925
2/1	0.3015	0.2490	0.2505	0.2505	0.08108	0.662	0.662
3/4	0.3000	0.1805	0.2535	0.25828	0.12590	0.988	0.975
1/3	0.3010	0.1415	0.3220	0.33010	0.15928	0.982	0.965

Again using AFGROW to model the expected crack shape in the research specimens, it is predicted that a surface crack length (2c) of 0.250" (6.35 mm) will have an a/c ratio of 0.84 and 0.97 for the crack growth criterion of stress intensity and crack closure, respectively. As it can be seen in Table 4.2 that not all of the specimen crack shapes developed that way. The root cause for this variations is most likely due to variability in machining the thickness. It was discovered that the machinist attempted to maintain the flatness of the plate verses following the given directions, resulting in a varied amount of material removed from each stage of machining. Specimens that present cracks lengths near the required crack length of 0.250" (6.35 mm) after the Final Thickness Machining step (Section 3.2) resulting in an inadequate number of cycles required to grown the crack deeper before a surface crack length (2c) of 0.250"

(6.35 mm); which is a research objective requirement of the surface crack to be at the minimal detection level of 0.250" (6.35 mm).

4.4 Does the presence of a minimal detection level surface crack affect the Laser Shock Peening Process?

This question addresses whether or not LSP will still be effective in imparting a substantial amount of RS into the material if a crack is present. Remember that the minimally detectable crack surface length ($2c$) is 0.250" (6.35 mm), for the NDI method chosen (surface scan eddy current). A larger length crack is expected to be identified, through NDI methods, prior to the peening process being accomplished. There are two different peening methods thus the results will be divided the same.

4.4.1 Circular Spot Laser Residual Stress Profile

The RS of the circular spot laser peened specimens were measured by both neutron diffraction and incremental hole drilling techniques. The neutron diffraction method indicated that a compressive residual stress field was induced to a depth between 0.104" (2.65 mm) and 0.122" (3.10 mm) in the rolling and transverse directions, respectively. The maximum RS is between -39.9 ksi (-275 MPa) to -44.8 ksi (-309 MPa), again in the rolling and transverse stress directions, respectively. The complete stress profile is shown in Figure 4.3.

The RS measurements were taken at an area presumed to be directly through the crack (Figure 4.3) and at an area remote from the peened and gripped areas (Figure 4.4). See Figure 3.24 for clarity of locations. Issues with the nuclear reactor during the experimentation time period hampered full data collection. The data in Figures 4.3 and 4.4 was all the stress data able to be calculated. The RS profile for the area remote from the LSP and gripping areas, is not complete due to inconsistent

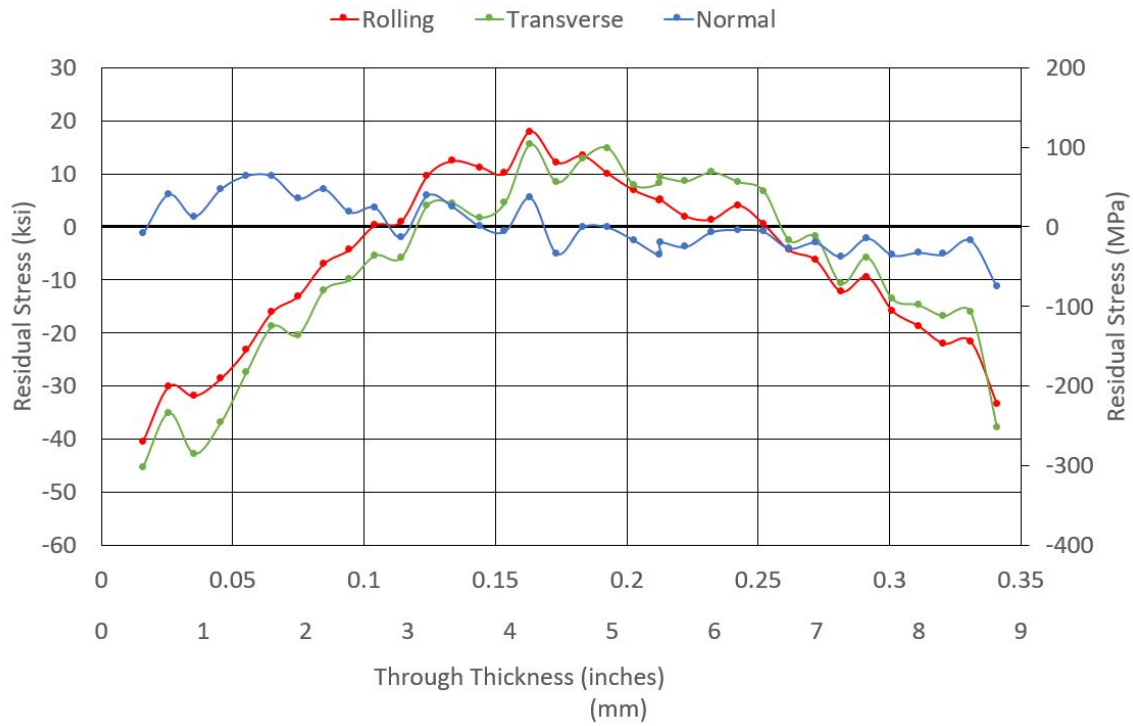


Figure 4.3. Neutron diffraction residual stress through the thickness of specimen at a location through the crack and LSPed area (reference 3.25). Left axis represents the laser peened face.

gauge volume positioning between the three different strain directions. Consistent data was only collected from a depth of 0.115” (2.92 mm) through 0.321” (8.16 mm). However, the RS through the measured thickness varied little and remained close to zero. It can be reasonable assumed that the same trend would continue through the entire thickness. This assumption allows for a comparison of the two different areas, showing that the vast majority of the RS imparted into the material was from the LSP treatment.

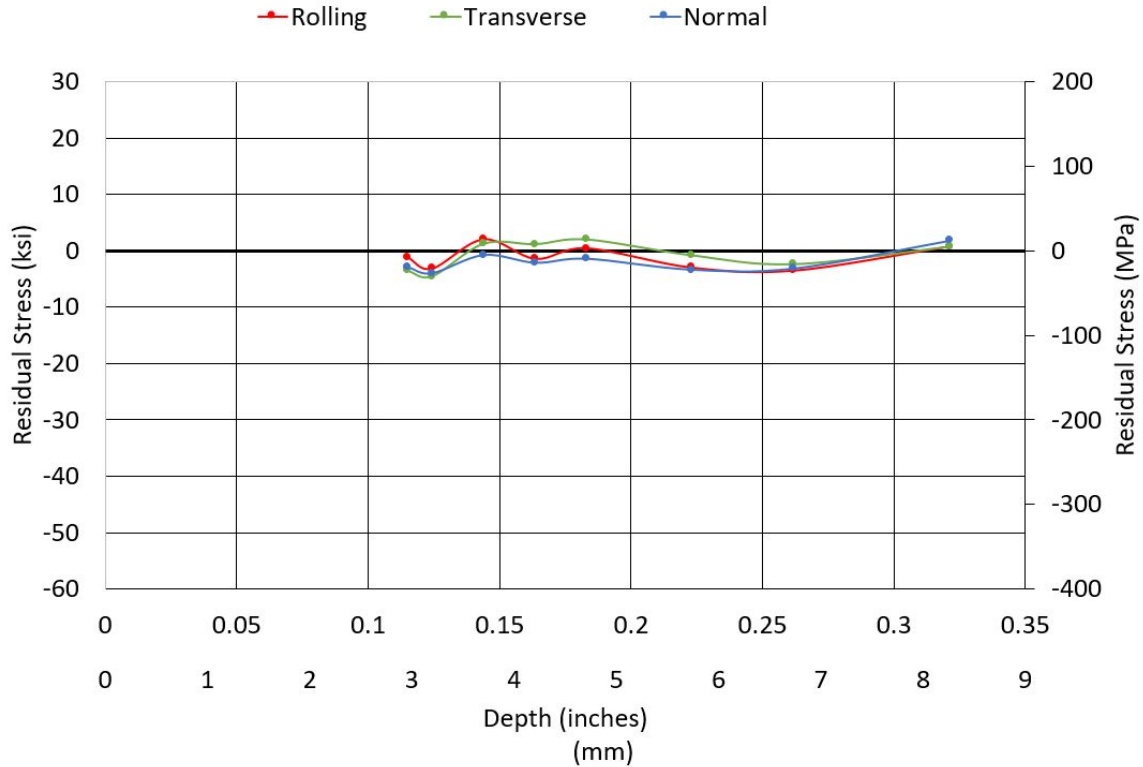


Figure 4.4. Neutron diffraction residual stress through the thickness of specimen at a location remote from the LSPed region and gripping areas (reference Figure 3.25). Left axis represents the laser peened face.

Incremental hole drilling was also used to measurement RS. Measurements were taken in two different areas, one inside the LSPed area remote from the crack and one remote from the LSP and clamping areas (see Figure 3.23). The results, shown in Figures 4.5 and 4.6, depict a RS on the surface of -48.0 ksi and -49.1 ksi (330.9 Mpa and 338.5 Mpa) in the rolling and transverse directions, respectively. Also shown is the shear stress, which is near zero in both the laser peened and non-laser peened area. As a reminder, incremental hole drilling cannot measure the normal stress due to the point of measurement being a free surface, therefore no normal stress is present.

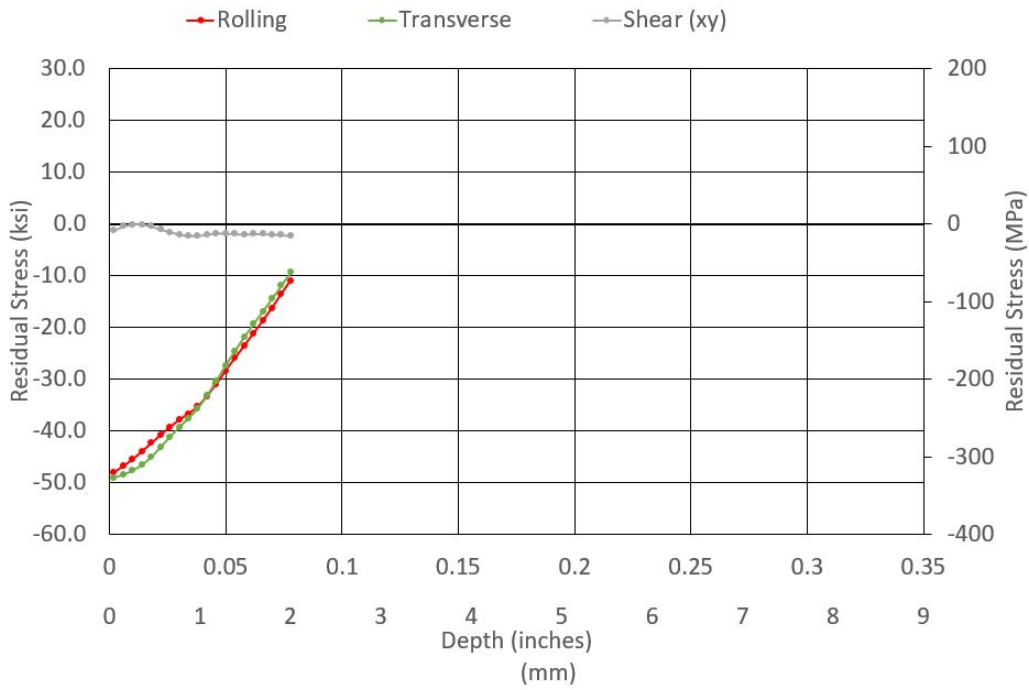


Figure 4.5. Hole Drilling Results for Circular spot Laser Peened Region

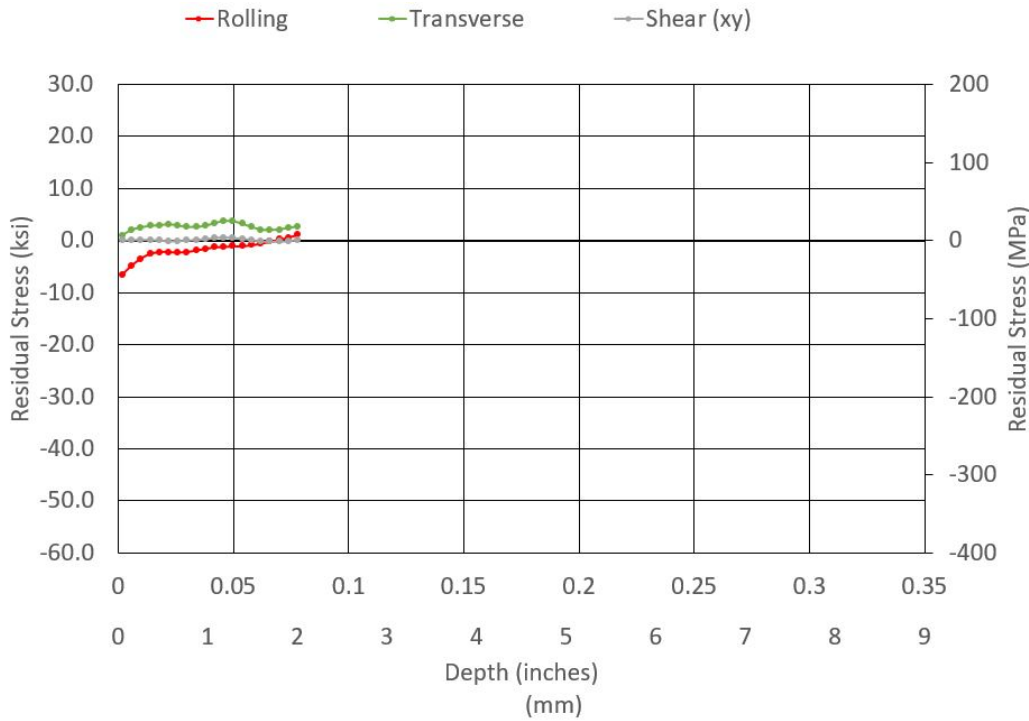


Figure 4.6. Hole Drilling Results for unPeened Region

Comparing the two measurement techniques shows a close comparison within the region of overlap (Figure 4.7). In the region near a depth of 0.025" (0.635 mm) of the neutron diffraction results shows a large oscillation. This could be due to material inconsistencies such as a large grain present in the location during measuring. It is not likely that the stress field would vary in that way, thus the RS measurements of the hole drilling would be more valid in that region. The RS was also compared in the region remote from the LSPed and clamped areas (Figure 4.8). There was no overlap of the two measurements however there is a trend showing that the RS remains near zero through the entire thickness.

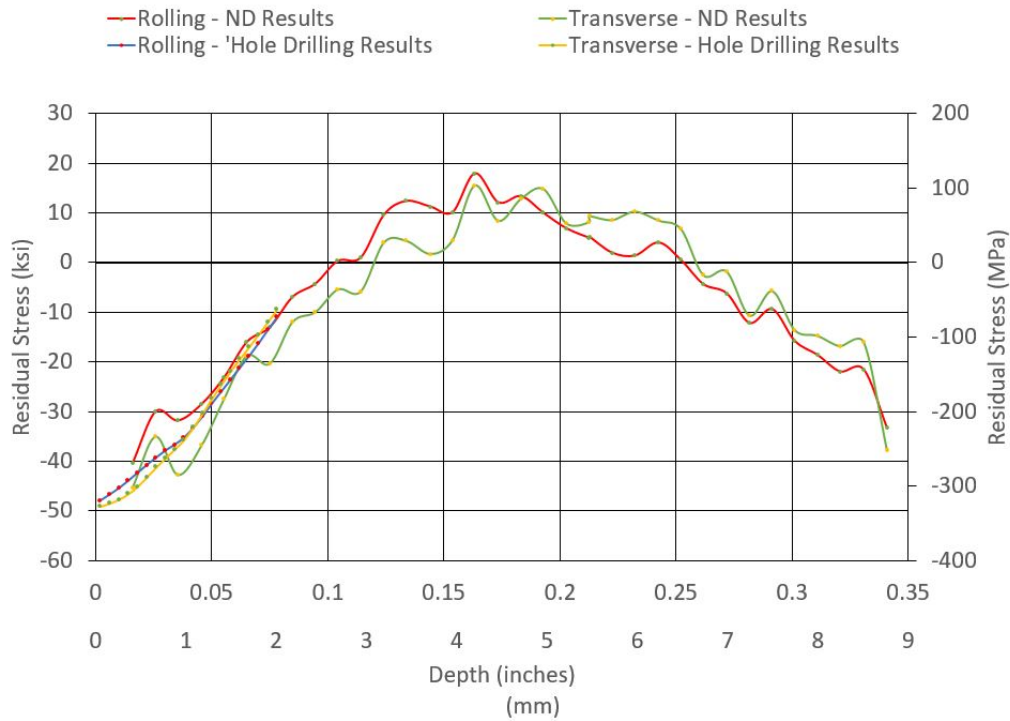


Figure 4.7. Circular spot Laser Peened RS Comparison in LSPed Area. (Shear stress shown for completeness.)

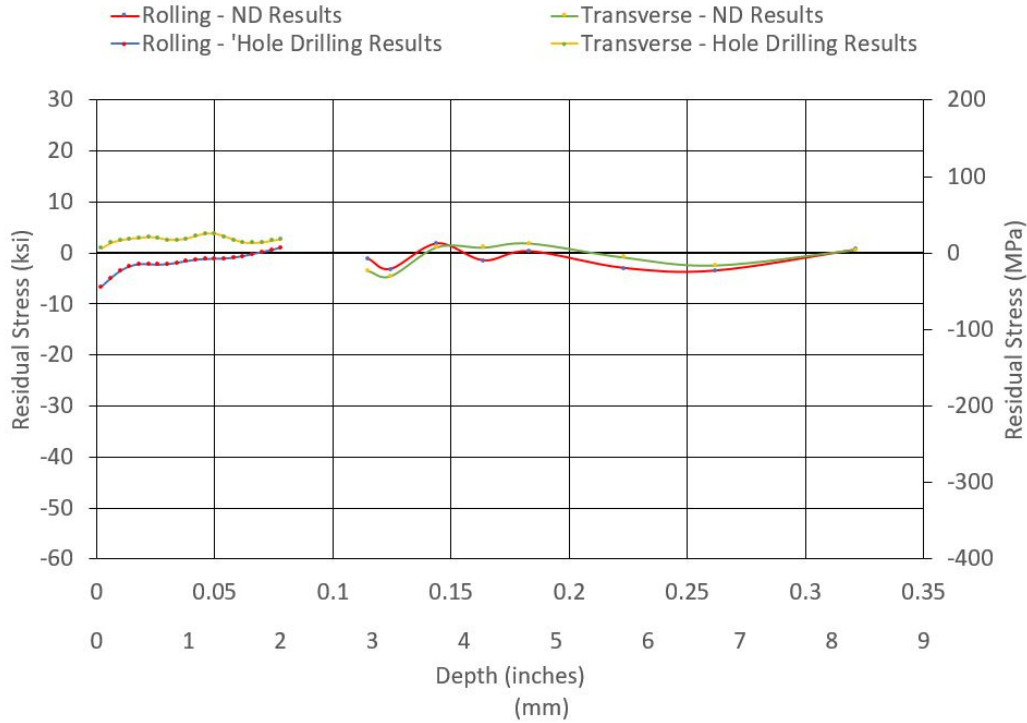


Figure 4.8. Circular spot Laser Peened RS Comparison in Unpeened Area. (Shear stress shown for completeness.)

The RS data that was measured by two different measurement techniques show that a significant amount of RS was present in the material as a result of the circular spot LSP process. As a reminder, the RS measurements were taken in different locations within the LSP area. The neutron diffraction data was measured in the area of the crack, while the incremental hole drilling was accomplished in an area remote from the crack. The close comparison of the data indicates that the crack had minimal, if any, effect on the RS being imparted into the material using the circular spot laser peening process.

4.4.2 Square Spot Laser Residual Stress Profile

The RS profiles of the square spot laser peened specimens were measured by X-ray diffraction (XRD) with layer removal and incremental hole drilling techniques. The XRD results showed a maximum value of imparted residual stress to be -43.0 ksi (-296

MPa) in the rolling direction. The transverse stress was not measured. As shown in Figure 4.9, the depth of measurements did not extend to the compression-tension transition point and due to the high variability of RS profiles due to laser peening, an extrapolation of data is not advised. The data shown depicts both the measured and corrected stress values provided by the vendor. The software in the XRD machine, uses the Moore-Evan’s correction, which assumes that the entire surface of the specimen is at the same depth during calculations of corrected values [27]. However, the process used only removed a 3 cm diameter of material. Thus, the true stress of the component will lie between the measured and corrected values.

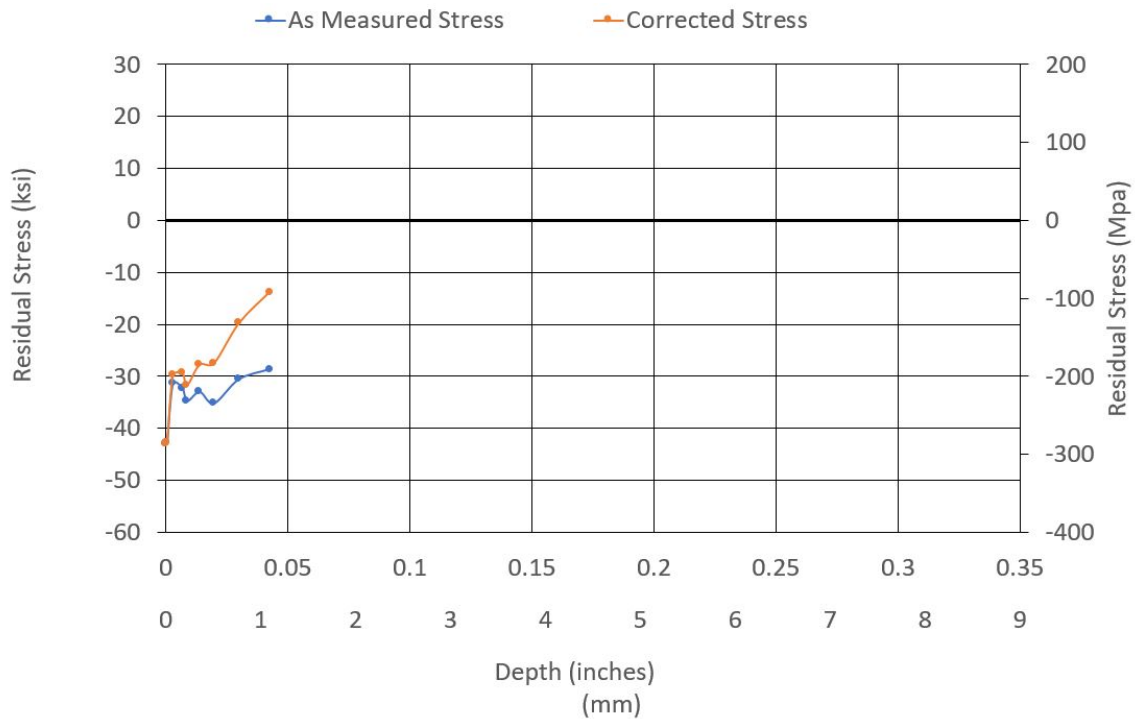


Figure 4.9. Residual stress data measured by X-ray diffraction.

The incremental hole drilling provided a RS profile with a surface RS of -43.8 ksi (-301.99 MPa) and -51.3 ksi (-353.70 MPa) in the rolling and transverse directions, respectively. The compression-tension transition point of the specimen is 0.085” (2.159 mm) and 0.077” (1.926 mm) in the rolling and transverse directions, respectively.

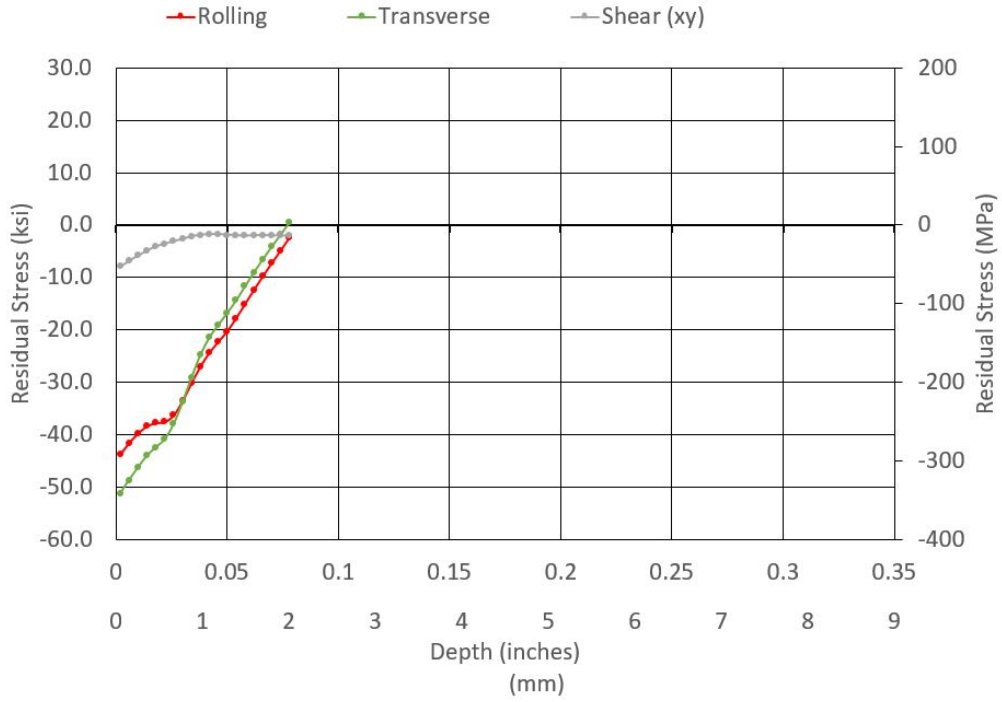


Figure 4.10. Hole Drilling Results for Square spot Laser Peened Region. Shear stress shown for completeness.)

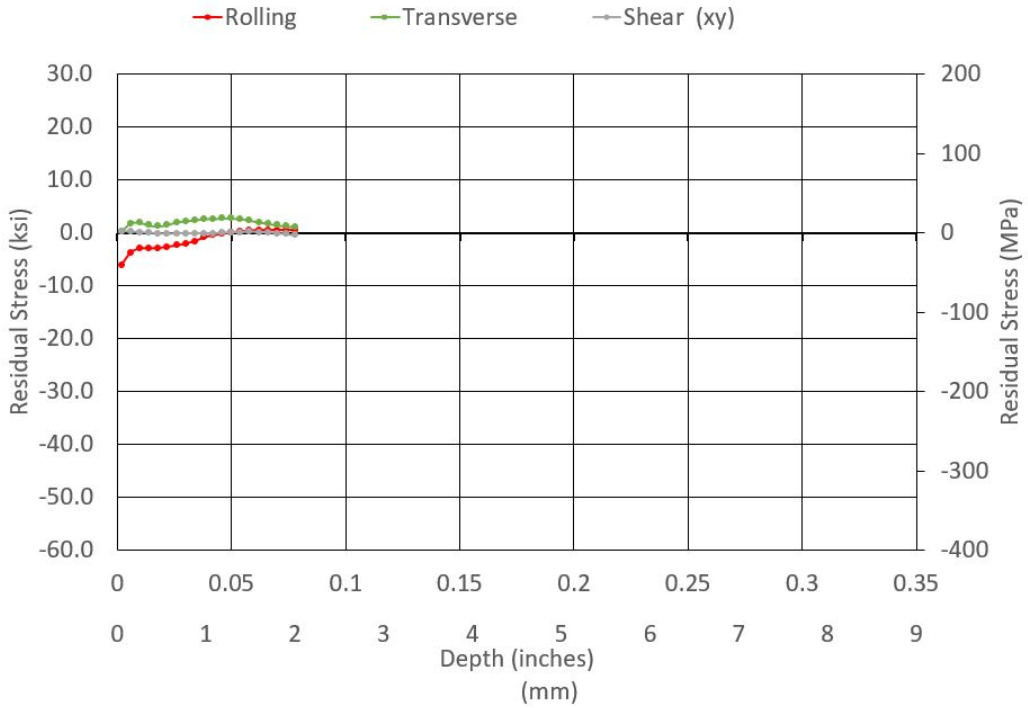


Figure 4.11. Hole Drilling Results for UnPeened Region. (Shear stress shown for completeness.)

When comparing the measurements of XRD and incremental hole drilling methods (Figure 4.10) it can be seen that the surface measurements are nearly identical at -43 ksi (-296.48 MPa) but diverge until 0.03” (0.762 mm) into the material, where the data again converges. Additionally, Figure 4.11 shows that the RS in an area remote to the LSPed and clamping areas had low amounts of RS measured by both XRD and incremental hole drilling techniques. This research was not an effort in comparison of various RS measurement techniques thus the variations are not explored. The results garnered from this comparison show that there is still a significant amount of RS present in the material after the square spot laser peening process. It must be noted that the measurements taken, unlike the circular spot LSP specimens, can not be used to infer whether or not the crack had any effect on the process, because no measurements were taken in the area of the crack. It can only be said that the square spot laser peening process did impart a significant amount of RS to a substantial depth.

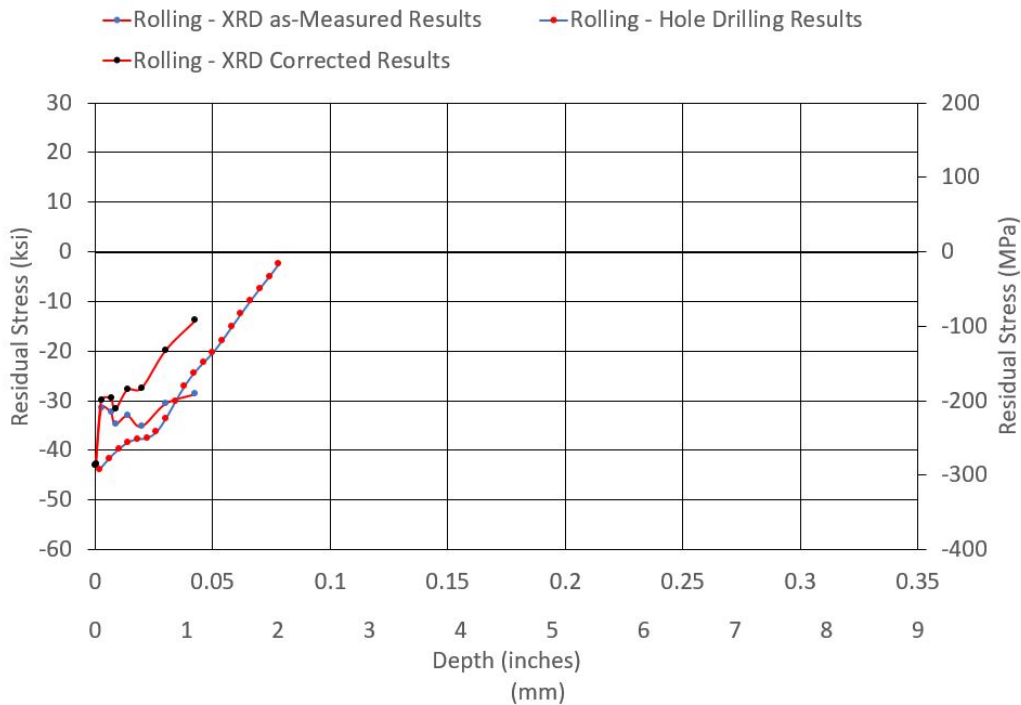


Figure 4.12. Square Spot Laser Peened RS Comparison in LSPed Area

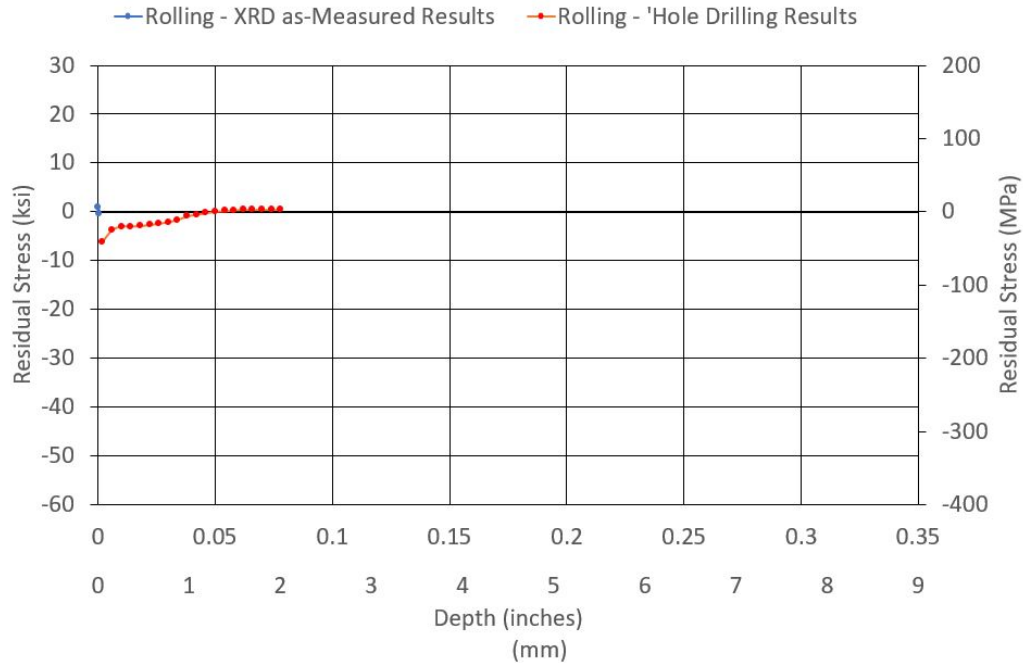


Figure 4.13. Square Spot Laser Peened RS Comparison in Unpeened Area

4.5 Does the presence of a minimal detection level surface crack prior to LSP application cause detrimental effects to the fatigue life?

The question of whether or not LSP over a minimally detectable crack would cause detrimental effects to fatigue life could be complicated. The primary concern addressed here, is whether or not the summation of the applied stress and residual stress field will generate negative fatigue results. To reiterate, the fatigue tests were conducted with a constant amplitude cyclic stress, operated under load control parameters. The maximum stress applied was 15 ksi (103.42 MPa) with a load ratio of $R = 0.1$. Each specimen received 10,000 primary load cycles, then a marker band sequence (Section 2.6). This process was repeated until failure or run-out was reached (one million primary load cycles).

Four specimens did not receive LSP treatment and were fatigued as described. These baseline results were used to evaluate both types of LSP specimens. The

results of the fatigue data is shown in Table 4.3. All baseline specimens fatigued to failure with an average number of cycles of 49,048.

Three circular spot laser peened and four square spot laser peened specimens were also fatigued in the same manner. All of the laser peened specimens survived to run-out (one million cycles). These specimens were then subjected to a 5 kip/s (22.24 kN/s) constantly increasing load until failure occurred. For completeness the failure loads are notes in Table 4.3.

Table 4.3. Specimen Fatigue Results (Note: Specimens 5/4 and 4/3 were not cleaved)

Classification	Specimen Number	Failure (Y/N)	Cycles	Cleaving Load kips (kN)
Baseline	3/3	Y	42682	N/A
Baseline	4/5	Y	53004	N/A
Baseline	2/4	Y	43869	N/A
Circular-Laser	4/2	N	1000000	108.3 (481.7)
Circular-Laser	5/4	N	1000000	— (—)
Circular-Laser	1/2	N	1000000	108.3 (481.7)
Square-Laser	2/1	N	1000000	113.5 (504.9)
Square-Laser	4/3	N	1000000	— (—)
Square-Laser	3/4	N	1000000	107.4 (477.7)
Square-Laser	1/3	N	1000000	105.1 (467.3)

The fracture surfaces of every specimen, both peened and unpeened, were inspected with an optical microscope (see Section 3.11). Visible marker bands were mapped, to track crack growth. As expected, baseline specimens showed continuous crack growth from the initial pre-crack length until the critical crack length was reached, causing failure of the specimen ligaments. Figure 4.14) shows the fractured surface of a representative baseline specimen. It is possible to identify the marker bands with little to no magnification, however Figure 4.15 shows where the marker bands are located more clearly. Under 50x magnification the marker bands appear on the surface as shown in Figure 4.16.

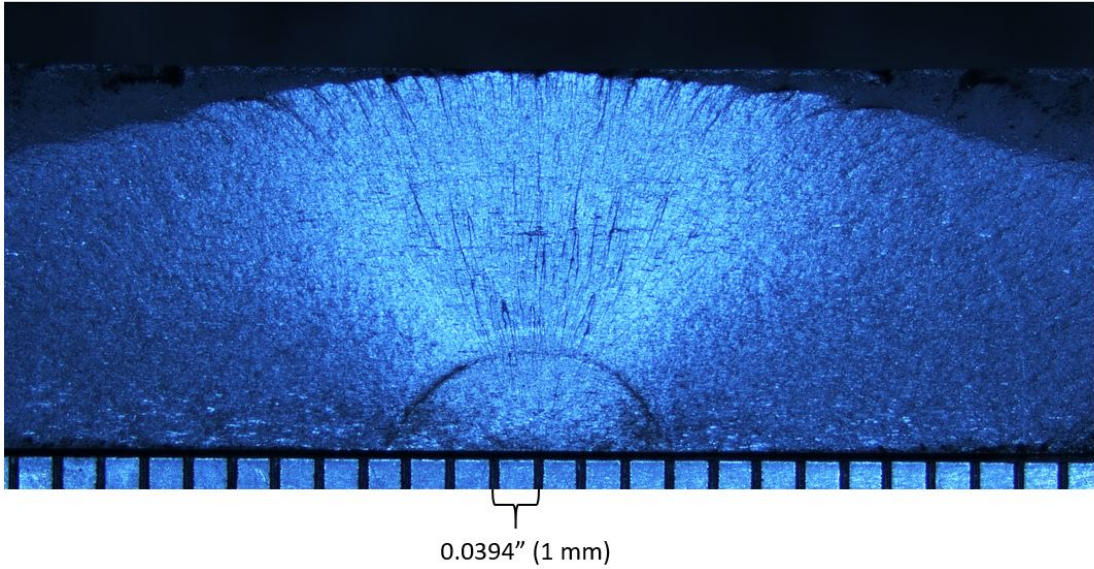


Figure 4.14. Fractured surface showing marker bands. Note that the dark arced line near the bottom is not a marker band. It was the crack face prior to machining the top and bottom surfaces.

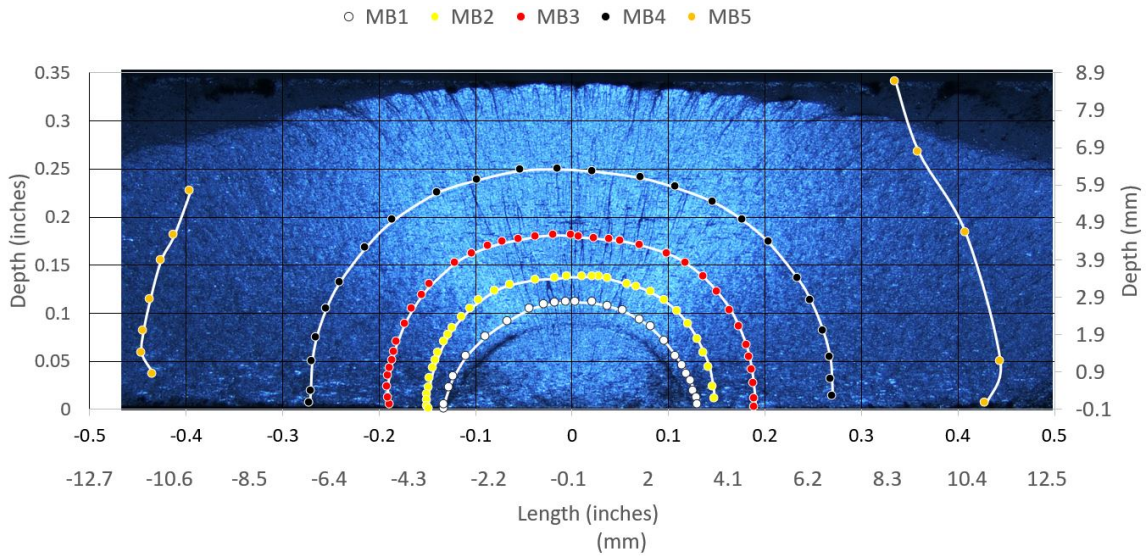


Figure 4.15. Unpeened specimen with marker band illustration overlay.

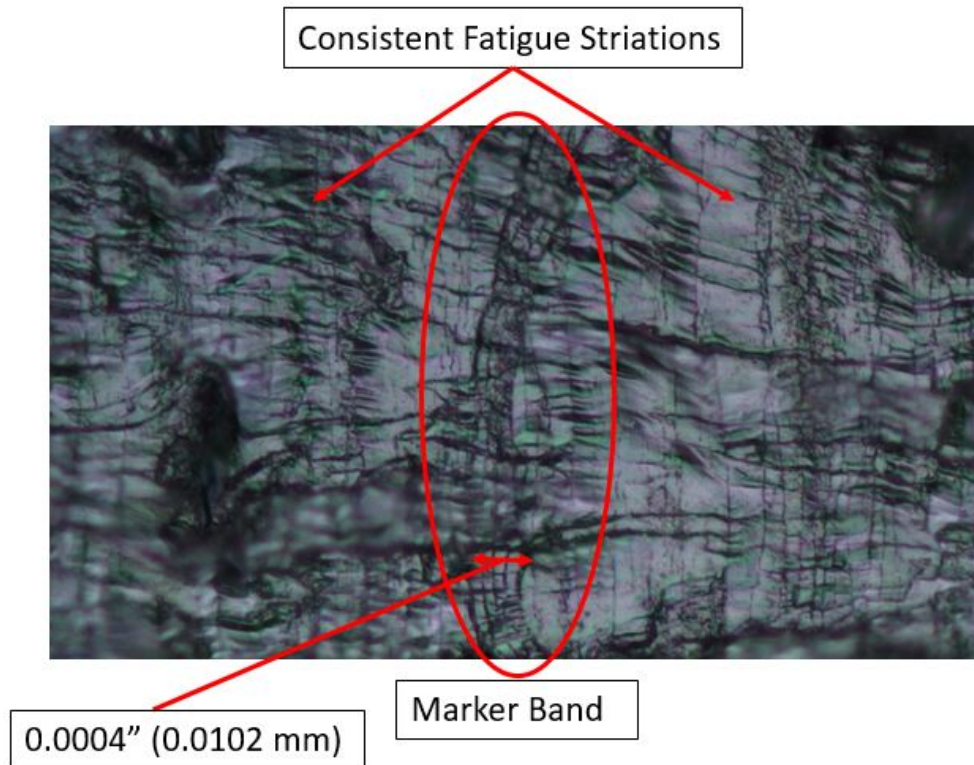


Figure 4.16. Unpeened specimen showing marker band.

The fracture surface of the laser peened specimens were significantly different than that of the baseline (unpeened) specimens (Figures 4.17 and 4.18). When magnified, the transition from the cracked plane to the fast fractured surface showed the presence of a single marker band (Figures 4.19 ??). The widths of this marker band was measured and compared to the width of the first marker band present on the baseline specimen. Both peened and the unpeened specimens presented a thickness between four and six ten-thousandths of an inch. This verified that there was no growth in any of the laser peened specimens, during the one million cycles of fatigue, which followed the laser peening applications. This clearly shows that these two types of laser peening (in this material) had a positive effect on fatigue life when specimens are subjected to this type of loading.

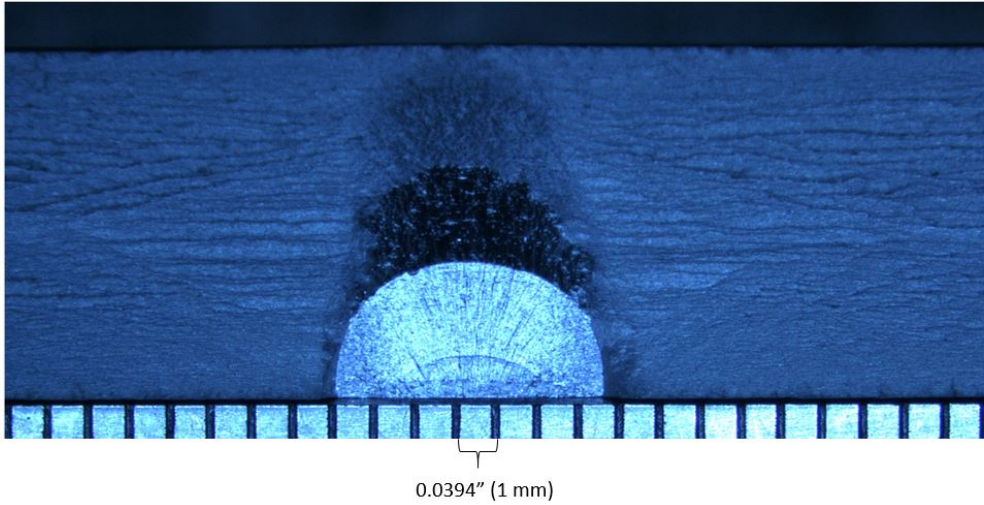


Figure 4.17. Square Spot Laser Peened Specimen showing no signs of fatigue growth after peening.

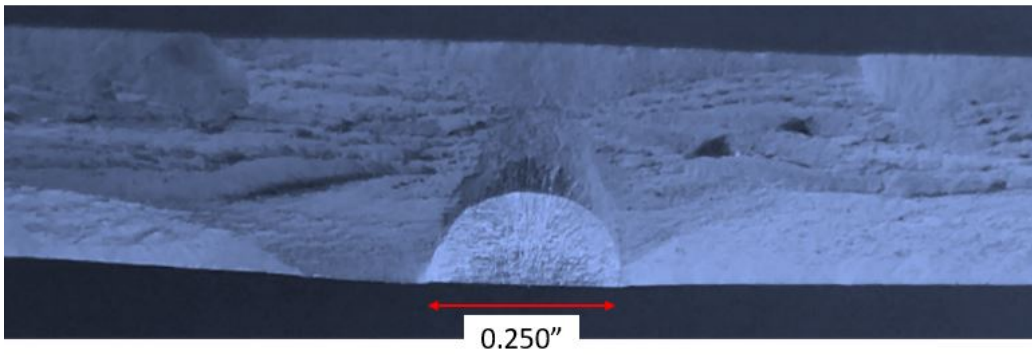


Figure 4.18. Circular Spot Laser Peened specimen showing no signs of fatigue growth after peening

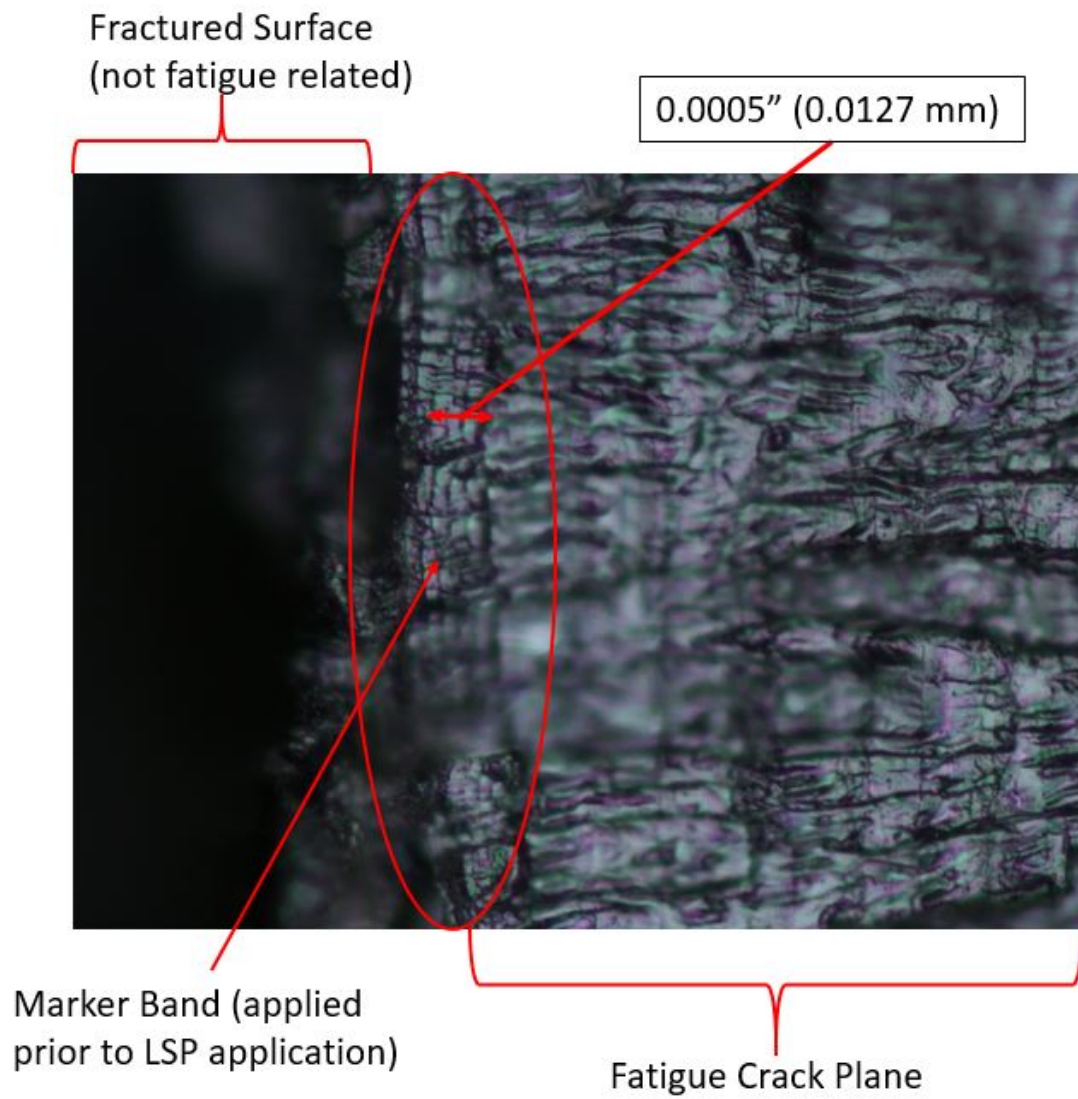


Figure 4.19. Fracture surface of a laser peened specimen. Marker band shown next to the fast fractured surface indicates no growth from fatigue testing post-LSP

4.5.1 Stress Intensity Factor Inspection

In an attempt to explain why there was no crack growth in the laser peened specimens, an evaluation of the stress intensity factors are accomplished. As defined in Section 2.2, the stress intensity is the effect of component geometry, cracked surface geometry, and forces acting on them. The cumulated stresses on the fractured surface are from the applied loads and RS present in the material. It must be mentioned here, that during the LSP process all specimens deformed/bent in the LSP application area. The primary deformation direction was along the length of the specimen. All specimens deformed in the same direction (center raised from ends toward the peened face) as seen in Figure 4.20. Each specimen was measured prior to fatigue testing with results are shown in Table 4.4.

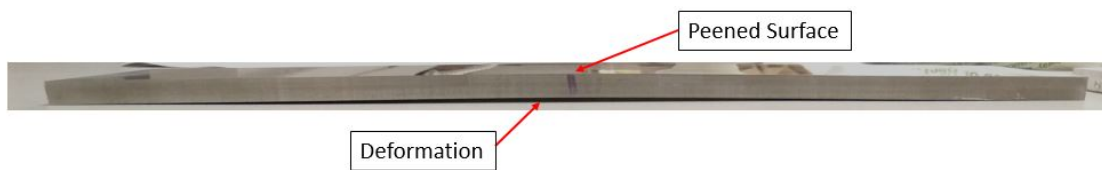


Figure 4.20. Profile of specimen showing bending due to LSP application

Table 4.4. Specimen Deformation Post-LSP

Classification	Specimen	Measure Deformation (inches (mm))
Circular Spot Laser	4/2	0.085 (2.16)
Circular Spot Laser	5/4	0.089 (2.26)
Circular Spot Laser	1/2	0.095 (2.41)
Square Spot Laser	2/1	0.050 (1.27)
Square Spot Laser	4/3	0.064 (1.63)
Square Spot Laser	3/4	0.062 (1.57)
Square Spot Laser	1/3	0.050 (1.27)

When the specimens are loaded in the MTS load frame and placed in pure tension a bending stress occurs due to the curvature of the beam. The maximum bending stress (σ_b) generated on the specimen surface with the crack is calculated to be -5.715 ksi (-

39.404 MPa) using the specimen with greatest deformation. The tensile stress applied to the specimens is +15 ksi (103.421 MPa). The RS field used was that measured by neutron diffraction since it was the only method capable of directly measuring the full depth of the crack. Inserting this information, along with others, into Equation 2.2a yields the average stress intensity of the crack tip on the material's surface ($\phi = 0^\circ$) as $K = -14.456 \text{ ksi}\sqrt{\text{in}}$ ($-15.89 \text{ Mpa}\sqrt{\text{m}}$). A negative K is not physical thus it is reported as zero. The average stress intensity calculated at the deepest measured crack depth ($\phi = 90^\circ$) of 0.128" (3.25 mm), was $K = +9.493 \text{ ksi}\sqrt{\text{in}}$ ($+10.43 \text{ Mpa}\sqrt{\text{m}}$).

Table 4.5. Parameters used to generate K vs. Crack Face Position plot
See Figure 4.21 for explanation of angle ϕ (* Estimated Values)

Angle Phi (Deg)	Depth inches (mm)	RS ksi (MPa)	Stress Intensity $\text{ksi}\sqrt{\text{in}}$ ($\text{Mpa}\sqrt{\text{m}}$)
0	Surface	-39.941 (-275.384)	0 (0)
10	0.022 (0.565)	-29.720 (-204.912)	0 (0)
20	0.044 (1.112)	-28.225 (-194.605)	0 (0)
30	0.064 (1.626)	-15.872 (-109.434)	0 (0)
40	0.082 (2.090)	-6.920 (-47.712)	1.85 (2.04)
45	0.091 (2.299)	-4.281 (-29.517)	3.05 (3.35)
50	0.098 (2.491)	0.227 (1.565)	5.04 (5.54)
60	0.111 (2.816)	0.895 (6.171)	5.42 (5.95)
70	0.120 (3.055)	9.000* (62.053)	8.99 (9.87)
80	0.126 (3.202)	9.433 (65.038)	9.23 (10.14)
90	0.128 (3.251)	10.000* (68.948)	9.49 (10.43)

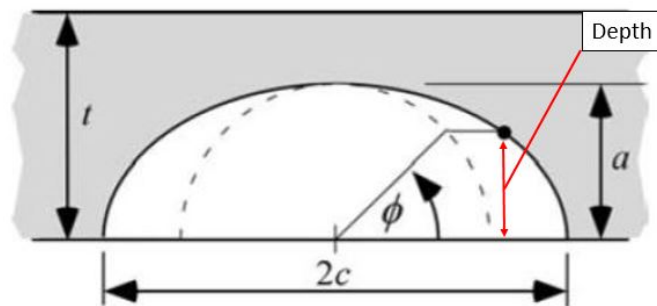


Figure 4.21. Depiction of angle Phi, showing how it relates to the point on the crack face.

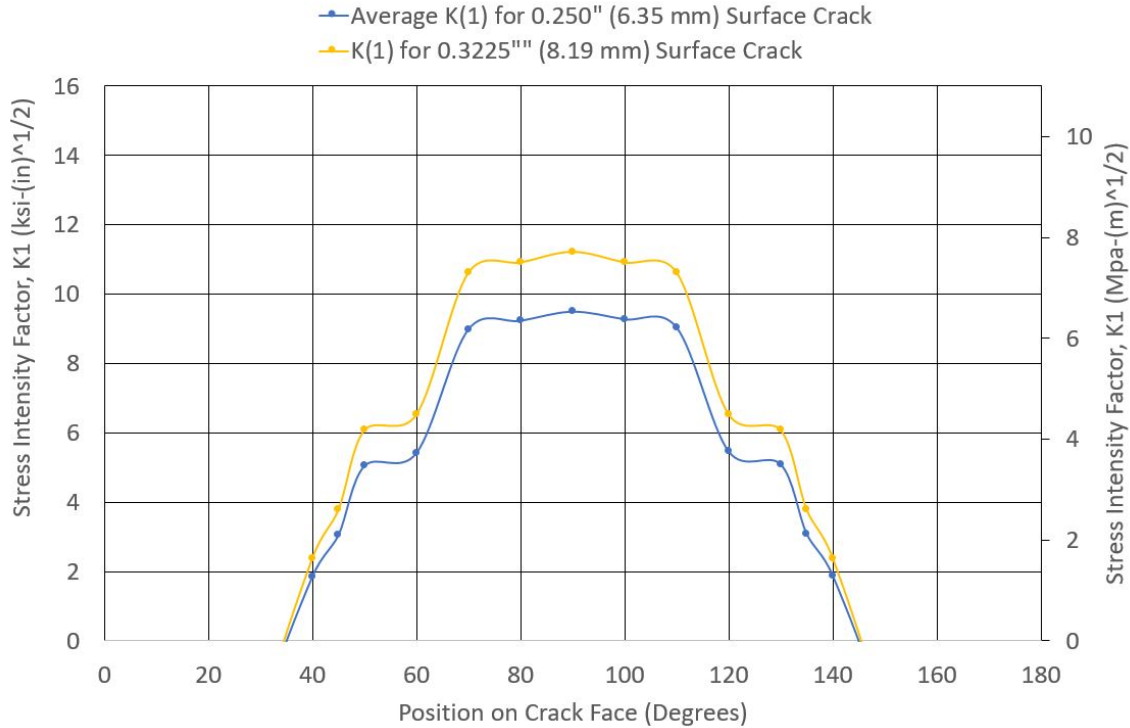


Figure 4.22. Plot of Stress Intensity (K) spanning full crack tip. Note stress intensity can not be negative thus the plot has been truncated.

Figure 4.22 depicts the stress intensity factors as a function of angle ϕ around the crack, remembering that the angle does not directly relate to the exact position on the crack (reference Figure 4.21) [8]. Table 4.5 shows the RS inputs required to calculate the stress intensity factor for each position. The greatest stress intensity is at the deepest portion of the crack. The step and flatness near the deepest portion of the crack is due to two factors: the semi-elliptical nature of the crack front (reference Figure 4.21) where there is less change in crack depth with increasing angle, ϕ ; and those points had small RS variation (reference 4.3).

After identification that the greatest stress intensity is at the deepest point of the crack face, $\phi=90$, ΔK was calculated using the measured parameters, that would induce the greatest ΔK , and compare it to the threshold ΔK required for crack growth (see Section 2.2). During steady state fatigue the ΔK is calculated to be 5.01. An

inspection of the crack growth curve shown in Figure 4.23 it can be seen that ΔK is above the threshold and indicates a crack growth rate near 4×10^{-6} in/cycle ($\sim 10^{-8}$ m/cycle). One million cycles were applied to each specimen with LSP, thus a crack growth of 4 inches should have occurred. Zero crack growth occurred thus there are components missing from the stress intensity calculation, one of which is crack opening load which was not calculated.

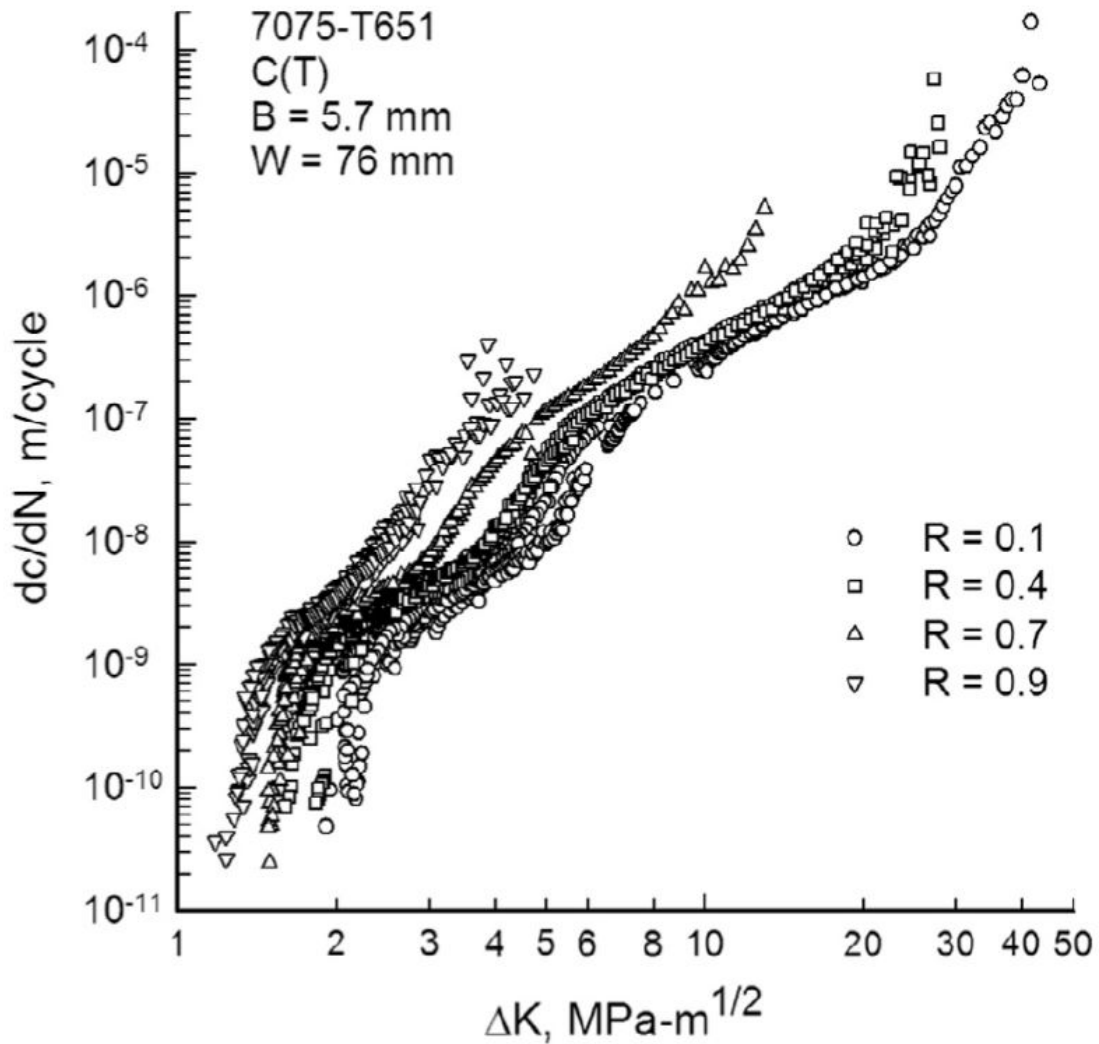


Figure 4.23. Crack growth rate curve for 7075-T651 Plate with a through crack under constant amplitude loading [28]

Also plotted on Figure 4.22 is the stress intensity of a larger crack than the minimal

detectable surface crack of 0.25" (6.35 mm). This specimen was accidentally grown to a surface length of 0.3225" (8.1915 mm) during the Pre-Crack Shape Formation Phase 3.6. It was processed in the same manner as all other square spot laser peened specimens. The fractured surface also showed no growth after reaching the endurance limit. The stress intensity factors show a slight increase of only 1% over the 0.25" (6.35 mm) cracked specimens. The ΔK value was calculated to be 11.225. MMPDS data shows that there should have been crack growth at a rate near 1×10^{-5} in/cycle. However, the surface did not show signs of growth, thus It could be inferred that with this material and under these peening conditions a significantly larger surface crack could be present before detrimental effects of the laser peening process.

4.6 Variations Between Circular and Square spot Laser Peening Results

Both peening processes performed exceptionally well during fatigue testing, showing absolutely no sign of crack growth. The stress intensity calculations (Section 4.5.1) were only calculated using the RS imparted by the circular spot laser peened specimens. The magnitude and depth of RS in the square spot laser peened specimens is smaller and shallower. Deeper measurements are required for use in stress intensity and ΔK calculations because the crack depth used in the calculations was 0.128" (3.25 mm) and RS measurements are only to a depth of 0.78" (1.98 mm). However, based on inspection of the RS data the stress intensity would differ between the two peening patterns. Further RS testing is required to verify that assumption.

There must be a note mentioned about the results of the peening and its process. The circular spot laser peened specimens received eight sequences, while the square spot laser peened specimens only received two. Additionally, the surface of both specimens were visually inspected after the peening process. The surface cracks are visible following the square spot laser peened specimens, but are not visible on the circular

spot laser peened ones. When the specimens were under an initial static loading of 16.8 kip (47.7kN) (80% of Maximum fatigue load) the crack was again inspected for. Only one of the three circular spot peened specimens had visual presence of the crack.

4.7 Summary

This section discussed results obtained by direct experimentation, utilizing in-house and commercial organizations. The results directly addressed the three key objectives of this thesis as well as providing additional information that is beneficial for the reader to understanding the complexities of this process/topic. The results have shown that the presence of a minimally detectable crack prior to the LSP has little effect on the introduction of RS into the material. Additionally, the concern of the tensile RS created during the peening process reducing fatigue life is found to be not valid for a crack of this size, in 7075-T651 aluminum, under these loading conditions. The following section will reiterate and provide further discussion on the results presented. Additional recommendations and areas of improvements of this research will also be discussed.

V. Conclusions and Recommendations

5.1 Chapter Overview

This chapter will summarize and further emphasize the conclusions of the research conducted. Also discussed here will be how the conclusions may be utilized for current use. This work raised other questions in which future research should address. Finally, recommendations are discussed for what future experiments conducted in a similar manner should consider to improve **accuracy** of test results.

5.2 Conclusions

To reiterate, the question that drove this research, “Does LSP cause unintended detrimental consequences if inadvertently applied over a flaw?” Inferred from this question was three targeted questions, the objectives of this research.

1. Does the presence of a minimal detection level surface crack affect the Laser Shock Peening Process?
2. Does the presence of a minimal detection level surface crack prior to LSP application cause detrimental effects to the fatigue life?
3. Will the two above questions be effected if two different cross-sectional laser systems are used, circular and square?

5.2.1 Does the presence of a minimal detection level surface crack affect the Laser Shock Peening Process?

This research presented here utilizing these two LSP processes, applied with the parameters and in the method defined within, are able to impart a substantial amount of RS into the surface of the material with the presence of a minimal detection level

partially-through surface crack of 0.250" (6.35 mm). The RS data presented shows that in the circular spot shape laser peened specimens a compressive RS near the surface near -50 ksi (-345 Mpa) and the compression-tension transition point is at a depth of about 0.110" (2.79 mm) (Section 4.4.1). The square spot shape laser peened specimens presented a compressive RS near -43 ksi (-296 MPa) with a transition point estimated to be near 0.090" (2.286 mm) (Section 4.4.2).

5.2.2 Does the presence of a minimal detection level surface crack prior to LSP application cause detrimental effects to the fatigue life?

Fatigue testing was accomplished on the following specimen types: baseline, circular spot shaped laser peened, and square spot shaped laser peened. Each specimen was subjected to a sine wave applied cyclic load with a maximum stress of 15 ksi (103.42 MPa) and a load ratio (R) of 0.1, until failure occurred or run-out (one million cycles) was reached. Baseline specimens show an average number of cycles to failure of 49,048. While both LPS specimen types achieved run-out (see Section 3.9). These results show a greater than 2000% increase in fatigue life.

Fractographic analysis of each specimen receiving LSP showed zero crack growth. This examination was accomplished through the use of marker band sequences during the fatigue process (Section 2.6), which allowed for a faster analysis through the use of an optical microscope verses an SEM. Additionally, a larger initial crack size of 0.322" (8.18 mm) was grown in one specimen and received square spot laser peening treatment, then fatigued. It too showed zero crack growth indicating that the LSP process could increase fatigue life in this material, under this loading, with a crack larger than the minimal detection level for the surface scanning eddy current NDI technique.

5.2.3 Will the two previous objectives be effected if two different cross-section laser systems are used, circular and square?

This research has shown that the difference in the cross sectional shape of the laser has little to no effects when LSP is applied over a partially-through the thickness surface crack. Both systems are able to induce significant amounts of RS into the material. Fatigue results were also non-differential in terms of the cross sectional laser shape, as both the circular and square spot shape laser peened specimens achieved fatigue run-out of one million cycles. With these results, there is little that can be inferred as differences of these two types of peening methods.

5.3 Recommendations and Discussions

Recommendations for other research that may follow this work on laser shock peening over partially-through the thickness crack will be presented here. As seen in Section 4.3) and Table 4.2, the crack shapes were not all uniform. To increase the likelihood of consistent crack growth, closer attention must be given to the machining process. The process presented here only called for the specimen to be “flipped” during machining five times. As discussed earlier, the machinist was of the understanding that the reason for defining the number of times to “flip” the specimen was to try and maintain a desired flatness and took it upon himself to flip each specimen a varied number of times to account for each specimen’s unique deformations. While the machinist had good intentions the result was a varied amount of material was removed from each side in each specimen, resulting in varied crack length post machining. Experimentalists attempting to repeat the procedures outlined here must discuss the best approach with their machinist and make a determination for themselves as to what is best for their experiment. Additionally, if possible the stock material used should be of a thickness closer to the final machined thickness to alle-

viate a substantial release of internal RS present in the material, which will further alleviate variations.

As discussed in Chapter I, if LSP is applied to a structural component having a crack below the minimum detection level of the NDI technique, that component could remain installed in the aircraft. This could prove problematic due to component deformation resulting from the LSP process. This deformation will induce additional stresses into the component and connecting structure, which must be identified and managed from a system level perspective.

As a reminder the research conducted here utilized only two specific laser shock peening techniques (see Section 3.8) which were applied to only one material (7075-T651). While the results could potentially be expanded to other materials and other LSP processes, further research is required. Which is why this research should not be used as standalone evidence that applying LSP over a minimally detectable partially-through thickness surface crack is successful in imparting RS into a material and increasing fatigue life. Instead this research should be used as a platform for experiments pertaining to a more specific condition.

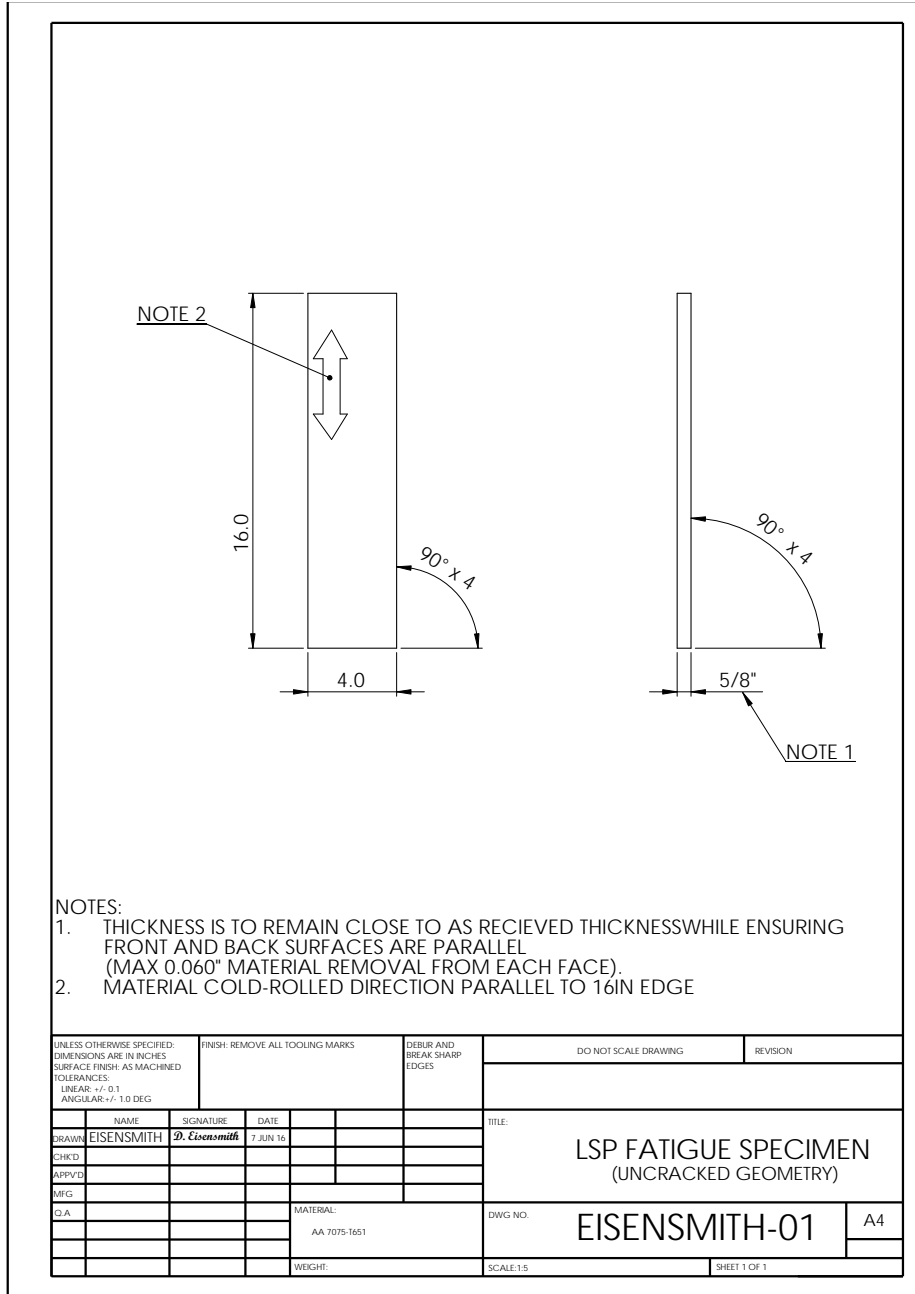
5.4 Future Research

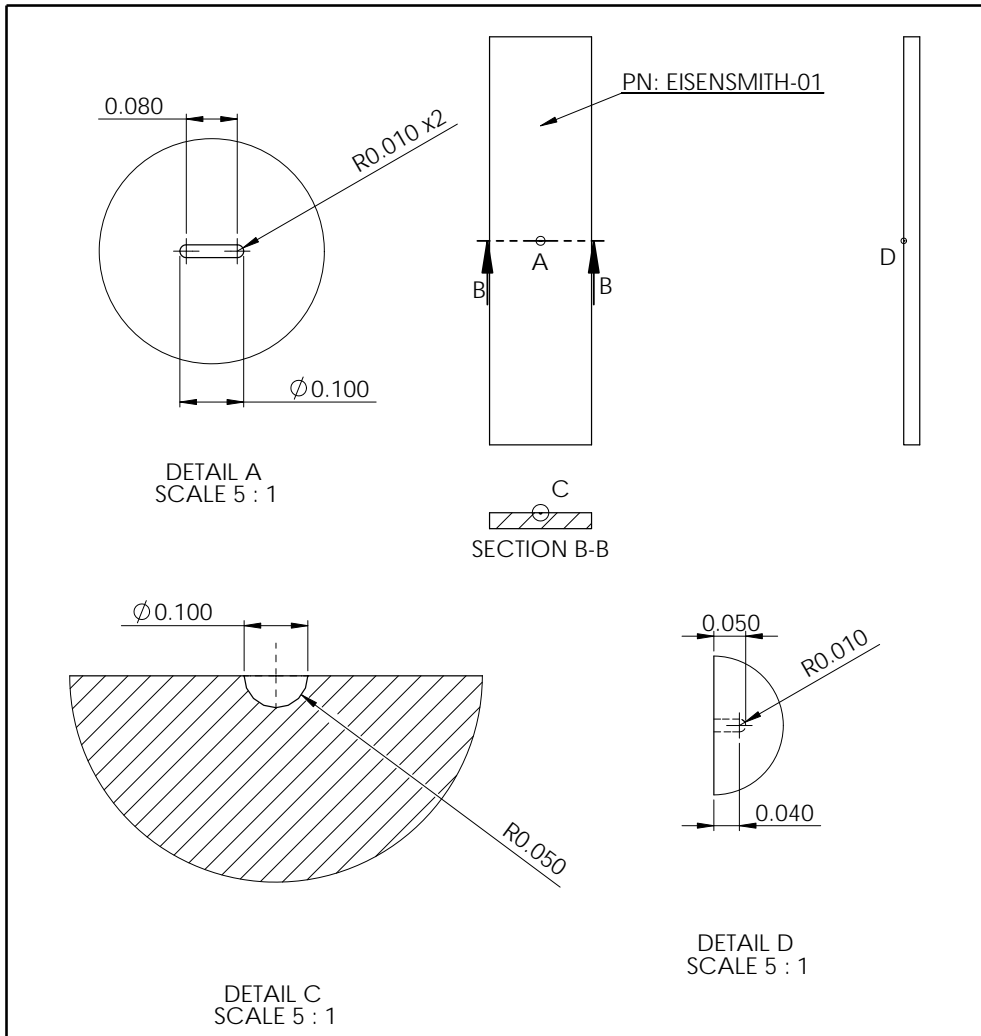
Much research is required before an over arching statement of the effects of LSP over partially-through the thickness surface cracks can be formulated. Presented here are a few topics that should be addressed to properly characterize these effects. This list cannot and will not be comprehensive as this specific research is in its initial stages.

- Analysis of larger partially-through the thickness cracks should be explored to identify a limit of crack surface length.

- Analysis of decreased power density should be investigated to determine the depth and magnitude of RS required to meet fatigue requirements.
- Research on various materials is required.
- Experiments conducting various fracture modes (See Section 2.2).
- Inspection of different types of geometry that are commonly found in aircraft structure, such as holes, radii, etc.
- If LSP is applied to installed structure, the delivery method of the laser is of concern. Access to areas may be of concern if laser delivery method is large. Some aircraft areas are quite dense with components and structure (i.e. fighter aircraft).
- The use of water as a transparent overlay is very common. However the use of continuously flowing water may be an issue when applying LSP on installed aircraft components, especially when access is limited. Research should be conducted to see if the removal/replacement of the water will still induce significant RS required.
- An exploration of the use of aircraft coatings (platings, paints, primers, etc.) as the ablative material versus a requirement to remove all coatings, apply ablative tape/paint, complete LSP process, reapplication of aircraft coatings.
- Inspection of support fixture stiffness required.
- Integrating accurate modeling of RS and component/surface deformation is required because of difficulty and expense of measuring these after application.
- Research should be conducted to understand if current NDI methods are adequate or if new methods for inspecting laser peened areas need to be developed.

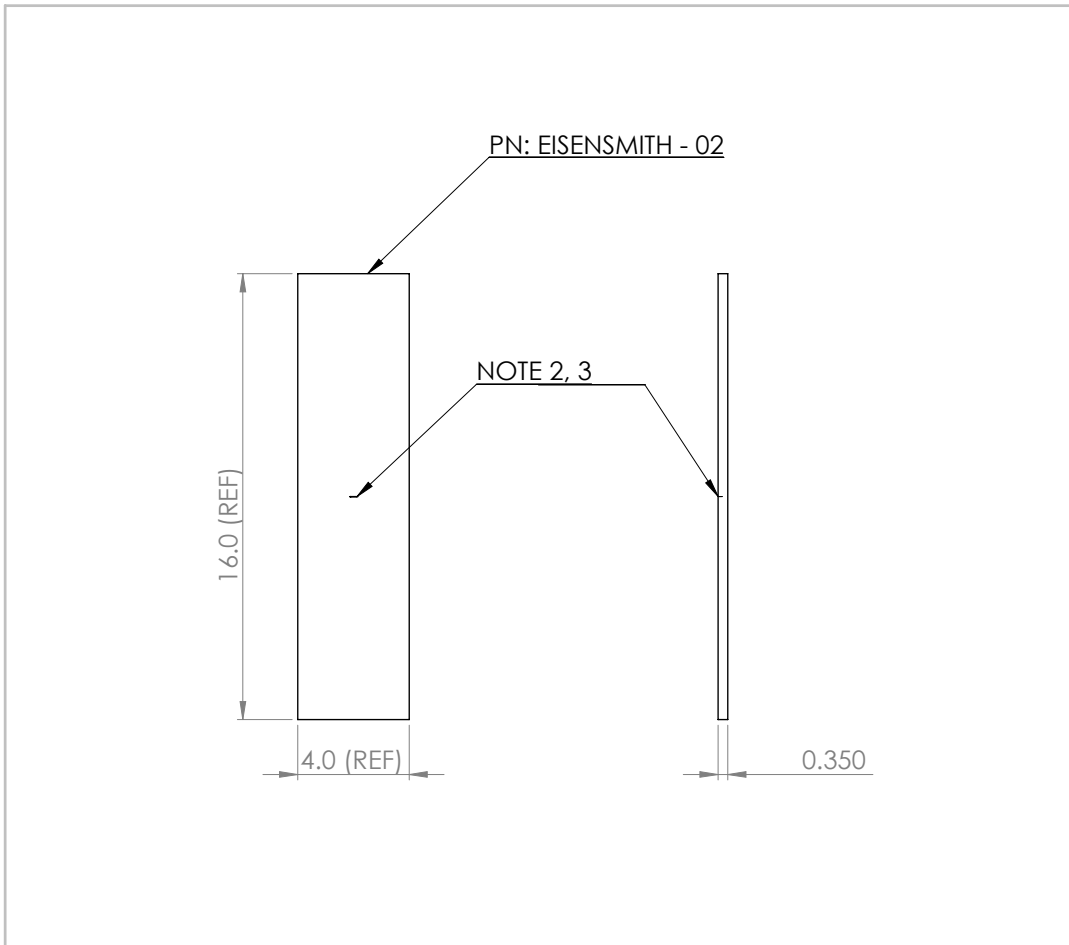
Appendix A. Test Specimen Drawings





- NOTE:
1. RATIO OF "SLOT DIAMETER TO SLOT DEPTH" IS CRITICAL PARAMETER
DEPTH MUST BE WITHIN +/- 0.001" OF RADIUS (0.005".)
 2. MAKE FROM PART NUMBER: EISENSMITH-01

UNLESS OTHERWISE SPECIFIED: DIMENSIONS ARE IN INCHES SURFACE FINISH: AS MACHINED TOLERANCES: LINEAR: AS NOTED ANGULAR:			DEBUR AND BREAK SHARP EDGES		DO NOT SCALE DRAWING		REVISION	
NAME			SIGNATURE		DATE		TITLE:	
DRAWN: EISENSMITH			D. EISENSMITH		18 JUL 16		LSP FATIGUE SPECIMEN (WITH CRACK INITIATION FEATURE)	
CHK'D:			APP'VD:		MFG:		DWC NO. EISENSMITH - 02	
Q.A.			MATERIAL:		A4		SCALE: 1:5	
WEIGHT:			SCALE: 1:5		SHEET 1 OF 1			



NOTES:

1. MACHINE PN: EISENSMITH - 02 TO DESIRED THICKNESS.
2. REDUCE MILL TRAVEL RATE TO A MINIMUM WHEN IN REGION OF DIMPLE/CRACK.
3. MACHINING INSTRUCTIONS:
 - a. MACHINE CRACKED FACE 0.050 INCH
 - b. FLIP SPECIMEN AND MACHINE BACK FACE 0.050 INCH
 - c. FLIP SPECIMEN AND MACHINE CRACKED FACE 0.050 INCH
 - d. FLIP SPECIMEN AND MACHINE BACK FACE 0.050 INCH
 - e. FLIP SPECIMEN AND MACHINE CRACKED FACE 0.01875 INCH
 - f. FLIP SPECIMEN AND MACHINE BACK FACE TO ENSURE FINAL PLATE THICKNESS IS 0.350 INCH.

UNLESS OTHERWISE SPECIFIED: DIMENSIONS ARE IN INCHES SURFACE FINISH: AS MACHINED TOLERANCES: LINEAR: +/- 0.005 ANGULAR:		FINISH:	DEBUR AND BREAK SHARP EDGES	DO NOT SCALE DRAWING	REVISION
DRAWN	NAME EISENSMITH	SIGNATURE <i>D. Eisensmith</i>	DATE 18 JUL 16	TITLE: LSP FATIGUE SPECIMEN (FINAL THICKNESS WITH CRACK)	
CHKD					
APPVD					
MFG					
Q.A.			MATERIAL: AA 7075-T651	DWG NO. EISENSMITH - 03	A4
			WEIGHT:	SCALE:1:5	SHEET 1 OF 1

Appendix B. Material Certification of Manufacturing Process, (AA 7075-T651)



Abnahmeprüfzeugnis 3.1 (EN 10204)
Inspection certificate - mill certificate

Nr.: **85153799** 01 / 1
 Rev.: **0**

Seite / page: 1 von / of 2
 Datum / date: 2015 10 12

Zertifiziert nach / certified to ISO 9001, ISO/TS 16949, ENAS 9100, ISO 14001, NADCAP

Auftraggeber / customer: Alro Steel Corporation 3100 E. High Street JACKSON MI 49204-0927 USA	Bestell Nr. / order no.: 11222683 Datum / date: 2015 03 20
Warenempfänger / consignee: Alro Steel Corporation 5859 Alro Park Drive POTTERVILLE MI 48876 USA	Auftragsbest. Nr. / order confirm no.: 690545 Datum / date: 2015 03 23
	Lieferschein Nr. / delivery note: 85153799 Datum / date: 2015 10 30

Produkt / product: Form / form: Plate, stretched Werkstoff / material: 7075 Zustand / temper: T651 Dim. / dim.: [inch]: 0,625x48,50x144,50 Kundenartikel Nr. / cust. article no.: 28511000	Bedingungen / terms: Technische Lieferbedingungen / techn. spec.: AMS-QQ-A-250/12 Rev. A; 2013-12 ASTM B 209 - 14 AMS 4045K, 12.2010 Sondervorschrift / special terms: not US tested
--	---

AB-Pos. ord.-item	BNr/Los/Lot/Los Lo/No./Part	Guss-Nr. cast no.	Werkstoff material	Kollo packno.	Gewicht netto weight net	Stk pcs
01	71897/01/0C V	01/0071097/5	7075	6905450001	3608,907 lbs	8

Chemische Zusammensetzung (% Gewichtsanteile) / Chemical composition (% weight proportion (OES))

Guss-Nr. / cast no.	material	Si	Fe	Cu	Mn	Mg	Cr	Zn	Ti	Ti+Zr	Others
		Each	Each								
01/0071097/5	7075	-	-	1,2	-	2,1	0,18	5,1	-	-	-
	spec. min.	-	-	1,2	-	2,1	0,18	5,1	-	-	-
	spec. max.	0,40	0,50	2,0	0,30	2,9	0,28	6,1	0,20	0,25	0,05
	actual	0,06	0,12	1,4	0,05	2,5	0,18	5,7	0,04	0,05	0,02
	Others Total										
	spec. min.	-									
	spec. max.	0,15									
	actual	0,03									

BNr/Los Lo/No.	Zustand temper	Richtung direction	Tests	UTS [ksi]	YS [ksi]	A2 ^o [%]
				spec. min. 78,0	68,0	7
				spec. max. -	-	-
71897/01	T651	LT	5 from	84,0	73,8	10
71897/01	T651	LT	to	85,1	74,7	12

Sonstige Prüfungen / other tests:
 Maßkontrolle: OK. / Dimensional Check: OK.

AMAG rolling GmbH, Postfach 32, A-5282 Ranshofen, Österreich - www.amag.at
 AMAG rolling GmbH, P.O. Box 32, A-5282 Ranshofen, Austria - www.amag.at

ALRO STEEL/METAL



RT08184438

NOV 09 2015



Abnahmeprüfzeugnis 3.1 (EN 10204)
Inspection certificate - mill certificate

Nr.: 85153799 01 / 1
Rev.: 0

Seite / page: 2 von / of 2
Datum / date: 2015 10 12

Zertifiziert nach / certified to ISO 9001, ISO/TS 16949, ENAS 9100, ISO 14001, NADCAP

Sonstige Prüfungen / other tests

Oberfläche: OK. / Surface Inspection: OK.

Material wurde gewalzt und gefertigt in Österreich
Material is rolled and processed in Austria

Es wird bestätigt, dass die Lieferung geprüft wurde und den Vereinbarungen bei der Bestellung entspricht.
We hereby certify that the material described above has been tested and complies with the terms of the order contract.

Werkstoffverständiger / factory specialist

Josef Klampfer

E-Mail / e-mail

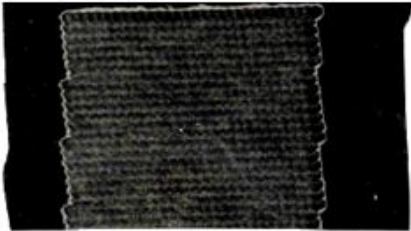
joesef.klampfer@amag.at

Herstellortand: Österreich / goods origin: The goods are of Austrian origin.
Maschinell erstellt - Gültig ohne Unterschrift / Automated - valid without being signed.

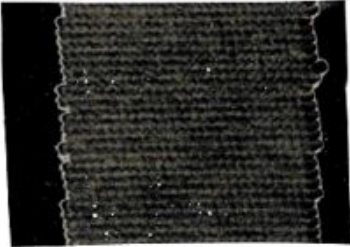
AMAG rolling GmbH, Postfach 32, A-5282 Ranshofen, Österreich - www.amag.at
AMAG rolling GmbH, P.O. Box 32, A-5282 Ranshofen, Austria - www.amag.at

Appendix C. Ablative Tape of Single Application of
Circular Spot Laser Peening Process

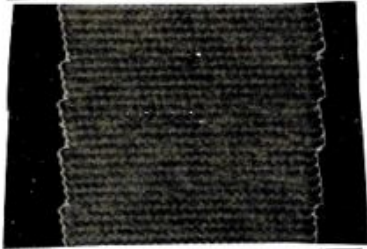
Application 1
(Sequence numbers below)



1



2

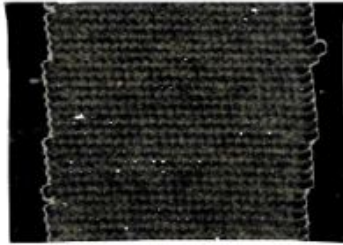


3

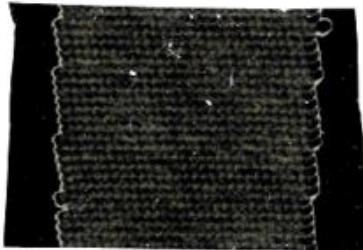


4

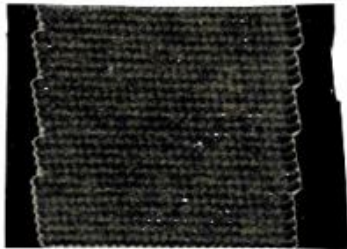
Application 2
(Sequence numbers below)



1



2



3



4

Appendix D. Specimen Machining and Numbering

Indicator	Process description
*	Cutting start
→	Edge obtained through EDM cutting
—	Edge obtained through previous EDM cutting
- - - - -	Rough Edge

Plate	Sample	Direction of cutting
1	1	
1	2	
1	3	
1	4	
1	5	
2	1	
2	2	
2	3	
2	4	
2	5	

3	1	
3	2	
3	3	
3	4	
3	5	
4	1	
4	2	
4	3	
4	4	
4	5	
5	1	
5	2	
5	3	
5	4	
5	5	

Bibliography

- [1] J. R. A. Everett *et al.*, “The effects of shot and laser peening on fatigue life and crack growth in 2024 aluminum alloy and 4340 steel,” *NASA Technical Manual, TM-2001-210843*, 2001.
- [2] U. AFLCMC/EZ, “In-service inspection flaw assumptions for metallic structures,” *Structures Bulletin*, vol. EN-SB-08-012, no. Rev. C, May 2013.
- [3] S. J. Findley and N. Harrison, “Why aircraft fail,” *Material Today*, vol. 5, no. 11, pp. 18–25, 2002.
- [4] (2015, June) F16 durability testing. [Online]. Available: [4.http://www.lockheedmartin.com/us/news/press-releases/2015/june/F16-durability-testing.html](http://www.lockheedmartin.com/us/news/press-releases/2015/june/F16-durability-testing.html)
- [5] (2016, February) Air force prolongs the life of the venerable b-52. [Online]. Available: <https://www.airforcetimes.com/story/military/2016/02/22/air-force-prolongs-life-venerable-b-52/80570810/>
- [6] (2016, March) Lockheed f-35 service life extended to 2070. [Online]. Available: <https://www.flightglobal.com/news/articles/lockheed-f-35-service-life-extended-to-2070-423536/>
- [7] A. Gujba and M. Medraj, “Laser peening process and its impact on material properties in comparison with shot peening and ultrasonic impact peening,” *Materials*, vol. 7, pp. 7925–7974, 2014.
- [8] T. Anderson, *Fracture Mechanics: Fundamentals and Applications*. Florence, KY: Taylor and Francis, 2005.

- [9] W. F. Hosford, *Mechanical Behavior of Materials*. Cambridge, MA: Cambridge University Press, 2005.
- [10] V. E. K. R. G. Forman and R. M. Engle, “Numerical analysis of crack propagation in cyclic-loaded structures,” *Journal of Basic Engineering*, vol. 89.3, p. 459, 1967.
- [11] J. Weertman, “Rate of growth of fatigue cracks calculated from the theory of infinitesimal dislocations distributed on a plane,” *International Journal of Fracture Mechanics*, vol. 2.2, pp. 460–467, 1966.
- [12] M. Klesnil and P. Lukas, “Influence of strength and stress history on growth and stabilisation of fatigue cracks,” *Engineering Fracture Mechanics*, vol. 4, pp. 77–92, 1972.
- [13] P. A. R. K. R.J. Donahue, H.M. Clark and A. McEvily, “Crack opening displacement and the rate of fatigue crack growth,” *International Journal of Fracture Mechanics*, vol. 8, pp. 209–219, 1972.
- [14] A. McEvily, *On Closure in Fatigue Crack Growth, ASTM STP 982*. Philadelphia, PA: American Society for Testing and Materials, 1988.
- [15] K. Walker, *The Effect of Stress Ratio During Crack Propagation and Fatigue for 2024-T3 and 7075-T6 Aluminum, ASTM STP 462*. Philadelphia, PA: American Society for Testing and Materials, 1970.
- [16] K. Heindlhofer, *Evaluation of Residual Stress*. New York, NY: McGraw-Hill, 1948.
- [17] (2017, January) Residual stress. [Online]. Available: <https://www.residualstress.org>

- [18] (2017, January) Hole drilling method. [Online]. Available: <http://hill-engineering.com/hole-drilling-method>
- [19] G. Schajer, *Practical Residual Stress Measurement Methods*. Chichester, West Sussex, UK: Wiley, 2013.
- [20] R. Prakash and R. Sunder, “Crack closure stress estimation by decodable marker banding techniques and comparison of results with electron fractographic technique,” *Proceedings of the Institution of Mechanical Engineers, Part L: Journal of Materials: Design and Applications*, vol. 221.2, pp. 53–62, 2007.
- [21] K. Ding and L. Ye, *Laser Shock Peening: Performance and Process Simulation*. Cambridge, MA: Woodhead Publishing, 2006.
- [22] (2017, January) Laserpeen process. [Online]. Available: <http://www.lspstechnologies.com/brochures/LaserPeen2016.pdf>
- [23] A. Dewald and M. Hill, “Eigenstrain-based model for prediction of laser peening residual stresses in arbitrary three-dimensional bodies. part 1: model description,” *The Journal of Strain Analysis for Engineering Design*, vol. 44, pp. 1–11, 2009.
- [24] A. Turnbull and E. D. L. Rios, “The effect of grain size on fatigue crack growth in an aluminium magnesium alloy,” *Fatigue and Fracture of Engineering Materials and Structures*, vol. 18, no. 11, pp. 1355–1366, 1995.
- [25] R. G. Budynas and J. K. Nisbett, *Shigley’s Mechanical Engineering Design*, 9th ed. New York, NY: McGraw-Hill, 2011.
- [26] (2017, January) Fractography. [Online]. Available: https://www.fose1.plymouth.ac.uk/fatiguefracture/tutorials/FailureAnalysis/Fractography/Fractography_Resource.htm

[27] M. Moore and W. Evans, *SAE Transactions*, vol. 66, pp. 340–345, 1958.

[28] J. Newman *et al.*, *International Journal of Fatigue*, vol. 62, pp. 133–143, 2012.

REPORT DOCUMENTATION PAGE

Form Approved
OMB No. 0704-0188

The public reporting burden for this collection of information is estimated to average 1 hour per response, including the time for reviewing instructions, searching existing data sources, gathering and maintaining the data needed, and completing and reviewing the collection of information. Send comments regarding this burden estimate or any other aspect of this collection of information, including suggestions for reducing this burden to Department of Defense, Washington Headquarters Services, Directorate for Information Operations and Reports (0704-0188), 1215 Jefferson Davis Highway, Suite 1204, Arlington, VA 22202-4302. Respondents should be aware that notwithstanding any other provision of law, no person shall be subject to any penalty for failing to comply with a collection of information if it does not display a currently valid OMB control number. **PLEASE DO NOT RETURN YOUR FORM TO THE ABOVE ADDRESS.**

1. REPORT DATE (DD-MM-YYYY) 3 March 2017	2. REPORT TYPE Master's Thesis	3. DATES COVERED (From — To) Sept 2015 — 3 March 2017
--	--	---

4. TITLE AND SUBTITLE FATIGUE EFFECTS OF LASER SHOCK PEENING MINIMALLY DETECTABLE PARTIAL-THROUGH THICKNESS SURFACE CRACKS	5a. CONTRACT NUMBER 5b. GRANT NUMBER 5c. PROGRAM ELEMENT NUMBER
--	--

6. AUTHOR(S) Eisensmith, David L. A., Captain	5d. PROJECT NUMBER JON 5e. TASK NUMBER 5f. WORK UNIT NUMBER
---	---

7. PERFORMING ORGANIZATION NAME(S) AND ADDRESS(ES) Air Force Institute of Technology Graduate School of Engineering and Management (AFIT/EN) 2950 Hobson Way WPAFB OH 45433-7765	8. PERFORMING ORGANIZATION REPORT NUMBER AFIT-ENY-MS-16-M-259
---	---

9. SPONSORING / MONITORING AGENCY NAME(S) AND ADDRESS(ES) AFRL/RQVS Att: Dr. Kristina Langer 2790 D Street WPAFB OH 45433 Email: kristina.langer@us.af.mil	10. SPONSOR/MONITOR'S ACRONYM(S) AFRL/RQ 11. SPONSOR/MONITOR'S REPORT NUMBER(S)
--	---

12. DISTRIBUTION / AVAILABILITY STATEMENT
DISTRIBUTION STATEMENT A:
APPROVED FOR PUBLIC RELEASE; DISTRIBUTION UNLIMITED.

13. SUPPLEMENTARY NOTES

14. ABSTRACT
“Laser Shock Peening (LSP) has evolved as a viable alternative to other surface treatments (shot peening, burnishing, etc.) which induce beneficial residual stress into structural components. Fatigue life improvements have been recognized by the aerospace industry. Aerospace engineers are inherently risk adverse due to component failures having potentially catastrophic consequences. With fatigue causing an estimated 55% of aircraft structural component failure, fatigue life benefits of LSP cannot be neglected. Aircraft service life extensions compound fatigue issue, especially for non-economically feasible replace components. In-service components may have surface flaws below current inspection limits. Aerospace engineers are concerned with LSP application over an existing crack causing unintended detrimental consequences. To address this concern, two differing types of LSP (circular and square spot shapes) were applied over a partial-through thickness surface fatigue crack of 0.25” (6.35 mm), in 7075-T651 aluminum. The crack length is the minimal detection limit of surface scanning eddy current. Specimens were fatigued under constant amplitude cyclic loading. Baseline specimens fatigue limit was 49, 048 cycles. Peened specimens survived to run-out exhibiting no crack growth when examined with an optical microscope, utilizing marker banding techniques. The result is more than 2000% increase in fatigue life.” —David L. A. Eisensmith, Capt, USAF

15. SUBJECT TERMS

16. SECURITY CLASSIFICATION OF:			17. LIMITATION OF ABSTRACT	18. NUMBER OF PAGES	19a. NAME OF RESPONSIBLE PERSON	
a. REPORT	b. ABSTRACT	c. THIS PAGE			Dr. A. Palazotto, AFIT/ENY	
U	U	U	UU	118	19b. TELEPHONE NUMBER (include area code) (937) 255-3636, x4599; anthony.palazotto@afit.edu	